CHARACTERIZING THE MECHANISM OF NANOCRYSTALLINE ANATASE TO RUTILE PHASE TRANSFORMATION

A DISSERTATION
SUBMITTED TO THE FACULTY OF THE GRADUATE SCHOOL
OF THE UNIVERSITY OF MINNESOTA
BY

KAIRAT SABYROV

IN PARTIAL FULFILLMENT OF THE REQUIREMENTS
FOR THE DEGREE OF
DOCTOR OF PHILOSOPHY

R. LEE PENN, ADVISOR

OCTOBER, 2014

Acknowledgements

First, I would like to thank my advisor, teacher, and mentor, Prof. R. Lee Penn, for her constant support, guidance, advice, motivation, and teachings. I have learned a lot in science and in life since I joined this great research group. Second, I would like to thank my lovely wife for her love, caring, and support, and for the positive energy she always gives. After I married her my happiness and success tripled. Third, I would like to thank my parents and siblings for their help and encouragement, and for the opportunity they gave me to reach my goals and the right path in this life. I would also like to thank past and present members of the Penn research group for creating a friendly, vibrant, and fun environment in lab, for creative research ideas and for sharing awesome food during our group meetings and parties. I also want to thank my friends originally from Turkey and Central Asia for their support and help, and for wonderful activities they organize. Finally, a special thanks to my committee members, especially to Prof. Andreas Stein for his support.

Thank you!

Dedication

THIS DISSERTATION IS DEDICATED TO
THE HONOR AND MEMORY OF

MY FATHER
BERDIGUL SABYROV
(1954 – 2013)

AND

MY MOTHER
BEYSHEKAN DUYSHOBEKOVA
(1954 – 2008)

ЖАТКАН ЖЕРИҢИЗДЕР ЖАЙЛУУ БОЛСУН!

Table of Contents

List of Tables

List of Figures

List of Abbreviations

2D	Two-dimensional
AFM	Atomic force microscopy
CM	Combined model
Cryo-TEM	Cryogenic transmission electron microscopy
DLS	Dynamic light scattering
DP	Dissolution-precipitation
GoF	Goodness of fit
HPLC	High-performance liquid chromatography
HRTEM	High-resolution electron transmission microscopy
ICDD	International Centre for Diffraction Data
IN	Interface-nucleation
MRSEC	Materials Research Science and Engineering Centers
NSF	National Science Foundation
OA	Oriented attachment
OR	Ostwald ripening

PDF	Powder diffraction file
Rwp	R-weighted profile
SAED	Selected area electron diffraction
STM	Surface tunneling microscopy
TEM	Transmission electron microscopy
UV-Vis	Ultraviolet-visible spectroscopy
XRD	X-ray diffraction

Chapter 1: Interface-Mediated Phase Transformation in Nanocrystalline Particles*

Introduction

Phase transformations of solid state materials are central processes in a broad range of environments, including geochemical, biological, and synthetic materials systems.[1-3] Despite decades of innovative research into the mechanisms of phase transformations, detailed understanding of how phase transformations are initiated and propagate through a material is often lacking. Many materials can exist in more than one polymorph, and the different polymorphs can have quite disparate properties, which means that controlling phase transformations can provide a route by which materials of desired properties can be produced.

Crystalline materials grow and phase transform to minimize their total free energy. The main driving force for crystal growth is the contribution to the total free energy by surface area, whereas the phase transformation is driven by the difference in the total free energies of the phases.[4,5] Ultimately, the stabilization of crystalline materials is achieved though the interplay between the two driving forces. In the case of anatase and rutile, anatase has the lower surface free energy but higher bulk free energy whereas rutile has the higher surface free

* A report on this research project is submitted for publication.
Sabyrov, K. and Penn, R. L. *CrystEngComm*, **(under review)**.

energy but lower bulk free energy. Thus, in a system containing pure anatase initially, it was proposed that anatase nanocrystals grow until a “critical” size, after which they transform to rutile.[6,7] The transformation to rutile results in a decrease in the total free energy because the bulk free energy becomes the more important energy term once the size of the anatase particles exceeds the “critical” size.[8,9] Once a heterogeneous mixture of rutile and anatase exists, continued production of the more stable phase, rutile, proceeds by both phase transformation (i.e., solid-state transformation of anatase to rutile) and crystal growth (i.e., growth of existing rutile at the expense of anatase).[10]

Phase transformations are typically accompanied by crystal growth. Crystalline particles typically grow by two major mechanisms: addition of molecular scale species and particle-mediated growth. In addition by molecular scale species, larger crystalline particles grow at the expense of the smaller or more soluble ones.[4,11,12] In the case of a single phase, it is the difference in free energy due to a difference in radii of curvature, or the Gibbs-Thomson effect, that drives the dissolution of the smaller crystals and re-precipitation onto larger ones.

In particle-mediated crystal growth, primary particles serve as building blocks rather than as sources of molecular scale nutrients. Oriented attachment (OA) is a special case of particle-mediated growth in which primary nanocrystalline particles assemble and attach to form new secondary single crystals.[3,13,14] This crystal growth mechanism involves two important intermediates. In the first, primary particles are loosely aggregated via interaction

forces, including van der Waals and Coulombic forces.[15] The primary particles can undergo rearrangements through Brownian motion, which, if the primary particles achieve crystallographic registry with respect to each other, leads to the second intermediate. The defining feature of this intermediate is the lack of direct contact between the primary building block crystallites.[16,17] The formation of this intermediate is hypothesized to be reversible.[17] Depending on the reaction conditions, the intermediate structure can subsequently transform to a secondary single crystalline particle once species residing in the gaps between primary crystallites have been eliminated or incorporated into the crystal.

Similar to particle growth, phase transformations of inorganic materials can occur via dissolution-precipitation as well as particle-mediated mechanisms, or so called interface-nucleation.[10,18-21] The dissolution of one phase and re-precipitation onto another is primarily driven by the higher thermodynamic stability of the latter.[8,9] This process is accompanied by coarsening, or Ostwald ripening, of crystals of the same phase.[6] The kinetics of each process depends on reaction conditions and types of materials present. For hydrothermally treated nanocrystalline anatase, the energy barrier for particle growth is lower than the barrier for transformation to rutile as observed in numerous studies.[6,7,22]

In interface-nucleation, phase transformation occurs at particle-particle interfaces and defects formed by particle aggregation as proposed by Penn *et al*. and Zhang *et al*.[7,14,22,23] Even though the atomic scale mechanism of the transformation from anatase to rutile has yet to be fully elucidated, numerous

studies and observations have demonstrated that particle aggregation induces phase transformation.[14,17,22,24-26] The goal of this article is to review recent research studies focused on aggregation induced phase transformation.

Size dependent stability of nanocrystals

With the evolution of nanoscience and nanotechnology, unexpected size dependent properties and behaviors have emerged. In fact, numerous research studies have demonstrated that phase transformation kinetics of inorganic materials strongly depend on initial crystallite domain size,[6,20,27,28] which means that the kinetics of phase transformation are tied closely to the kinetics of crystal growth. For example, Ding *et al*. observed that anatase particles with smaller grain sizes grew and transformed more rapidly than those with larger grain sizes in air and at temperatures between 675 °C and 775 °C.[29] Powder X-ray diffraction (XRD) was used as a primary tool to quantify the phase content and average crystallite size of the particles. They concluded that the higher interfacial energy stemming from the higher surface area of the smaller grained particles was the main driving factor for the increased growth and phase transformation rates observed.

Gribb *et al*. performed similar experiments, and their data tracking average crystallite size, size distribution, and phase content (by powder XRD) over time were consistent with the results of Ding *et al*. in that smaller anatase transformed faster than larger anatase. Interestingly, the average size of the product rutile was many times larger than the average size of the anatase, even after only a

small amount of rutile had formed.[6] In addition to quantification of the samples by powder XRD, the authors used transmission electron microscopy (TEM) to determine the size distributions of anatase and rutile in the samples. The observation that average size of rutile is so much larger than the average size of anatase is consistent with results obtained by others investigating the anatase to rutile phase transformation, both in air[28,29] and aqueous media[21,27]. Kumar *et al*. argues that rutile has a critical size above which it is the most thermodynamically stable and that the critical size is larger than the average particle size of the primary crystallites of anatase.[30]

However, Gribb *et al*. demonstrated a significant overlap between the anatase and rutile size distributions (Figure 1.1). They proposed a mechanism by which anatase nanocrystals first coarsen to a certain size, a “critical” size, and then transform to rutile due to lower free energy of rutile at larger size. That is to say, the “critical” size is the size at which both anatase and rutile have the same total free energy. They observed a bimodal anatase size distribution with a small difference between the average size of anatase nanocrystals represented by the second peak and the average size of rutile nanocrystals at the early stages of transformation. This is consistent with the hypothesis that once an anatase crystal reaches the critical size, it transforms to rutile. However, this seems to contradict the observation of faster transformation kinetics with smaller anatase crystals. Nevertheless, according to the authors it is not a contradiction since the free energy change for the transformation is not a rate-determining step at small

crystallite sizes. What remains lacking, however, is a detailed mechanism for how the phase transformation is initiated.

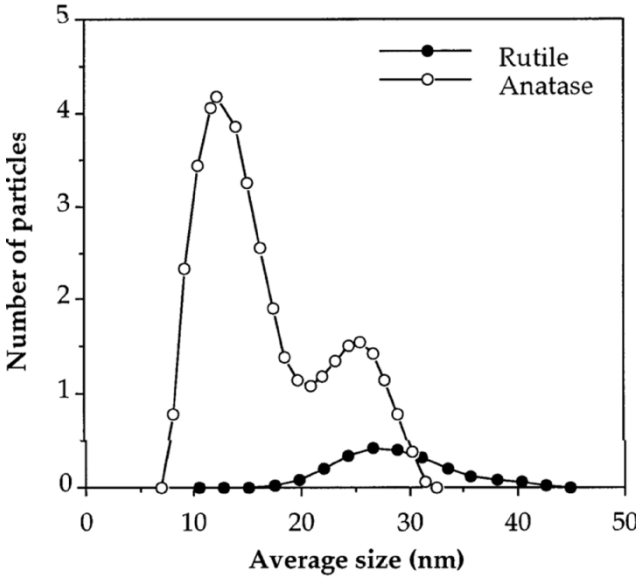

Figure 1.1 Size distributions of anatase and rutile nanoparticles in the sample treated at 525 °C for 1.2 h. Approximately 9.6% of the sample is rutile. The calculations were performed using Warren-Averbach analysis. Reprinted with permission from reference 6.

Aggregation-mediated nucleation

Detailed studies of the microstructure of the hydrothermally processed TiO_2 nanoparticles led to new insights into the mechanism of phase transformation. Penn *et al*. proposed an atomic scale mechanism by which small amounts of the product phase forms at particle-particle interfaces, such as twin boundaries, which can form by oriented attachment.[14,22] Using high-resolution transmission electron microscopy (HRTEM), in combination with crystallographic considerations, the authors concluded that anatase twin boundaries possess structural elements common to both rutile and brookite. Depending on the

reaction conditions, these structural elements could facilitate nucleation and subsequent phase transformation. The authors showed that the anatase {112} twin interface is composed of a one unit cell wide strip of brookite, which could act as a nucleus for further brookite growth at the expense of anatase. Indeed, intergrowths of brookite at anatase twin boundaries are commonly observed in hydrothermally processed anatase samples (e.g., Figure 1.2).

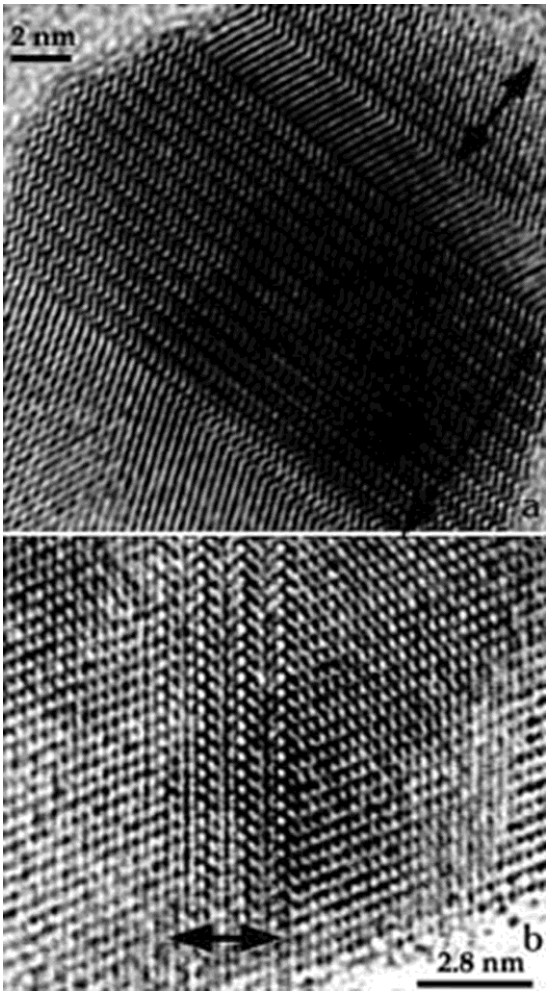

Figure 1.2 HRTEM images of anatase viewed down [131] and brookite down [011]. The boundary is anatase and (100) brookite. (a) Domains of brookite (indicated by arrows) separated by anatase in twinned orientation; (b) three unit cell-wide strip of brookite in anatase. Reprinted with permission from reference 14.

Furthermore, the authors showed that the anatase twin boundary contains structural elements common to rutile. For rutile to nucleate and grow from that twin boundary, only 7 of the 24 Ti-O bonds per unit cell need be ruptured and cooperative displacement of the remaining Ti and O need occur at the boundary. Such interfaces are expected to result in decreased activation barriers for rutile nucleation and, thus, contribute significantly to the observed higher transformation rates in nanocrystalline materials compared to coarsely crystalline particles. Recently, Zhou *et al*. used molecular simulation techniques to investigate the anatase to rutile transformation in TiO_2 nanocrystals.[25] Their findings are consistent with the mechanism described above. The authors observed the formation of anatase {112} twins at the interfaces of nanocrystal aggregates. Consistent with the experimental observations, stable rutile nuclei with {101} facets were produced among the anatase {112} twins.

Quantifying the kinetics of transformation

Macroscopic modelling enables quantitative analysis of the kinetics of phase transformation and particle growth. A kinetic model for aggregation induced phase transformation, or interface-nucleation, was developed by Zhang *et al*. to characterize the process and obtain deeper understanding of its atomic scale mechanism:[19]

$$\ln\left[\frac{1}{(1-\alpha)(D_0/D_t)^3}-1\right]=\ln k+\frac{m-1}{m}\ln t$$

where α is the weight fraction of nanoparticles transformed at time t, k is the transformation rate constant, and D_0 and D_t are the average diameters of the transforming nanocrystals at time $t = 0$ and time t, respectively. The exponent m representing the grain growth behavior generally has values between 2 and 4.

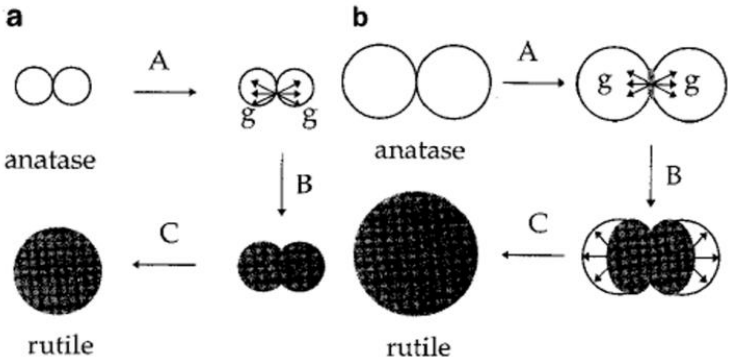

Figure 1.3 Diagram showing the proposed steps of the phase transformation of nanocrystalline anatase particles over shorter reaction times (a) and over longer reaction times (b). The *g* is the nucleus growth rate. Reprinted with permission from reference 19.

The model was derived based on the experimental studies by Penn *et al*., in which particle-particle contacts or defects generated by oriented aggregation were proposed to facilitate phase transformation. The dependence of the transformation rate constant on particle size was incorporated into the kinetic equation by assuming the process as second order with respect to the numbers of transforming nanocrystals. Figure 1.3 presents a diagram illustrating the steps of the proposed mechanism for the anatase to rutile phase transformation, in which rutile nucleates at the interface between two anatase nanocrystals and grows by consuming the nanocrystals simultaneously. Moreover, according to this mechanism, larger rutile forms at later reaction times due to increased size of

the anatase nanocrystals, which also grow over time.

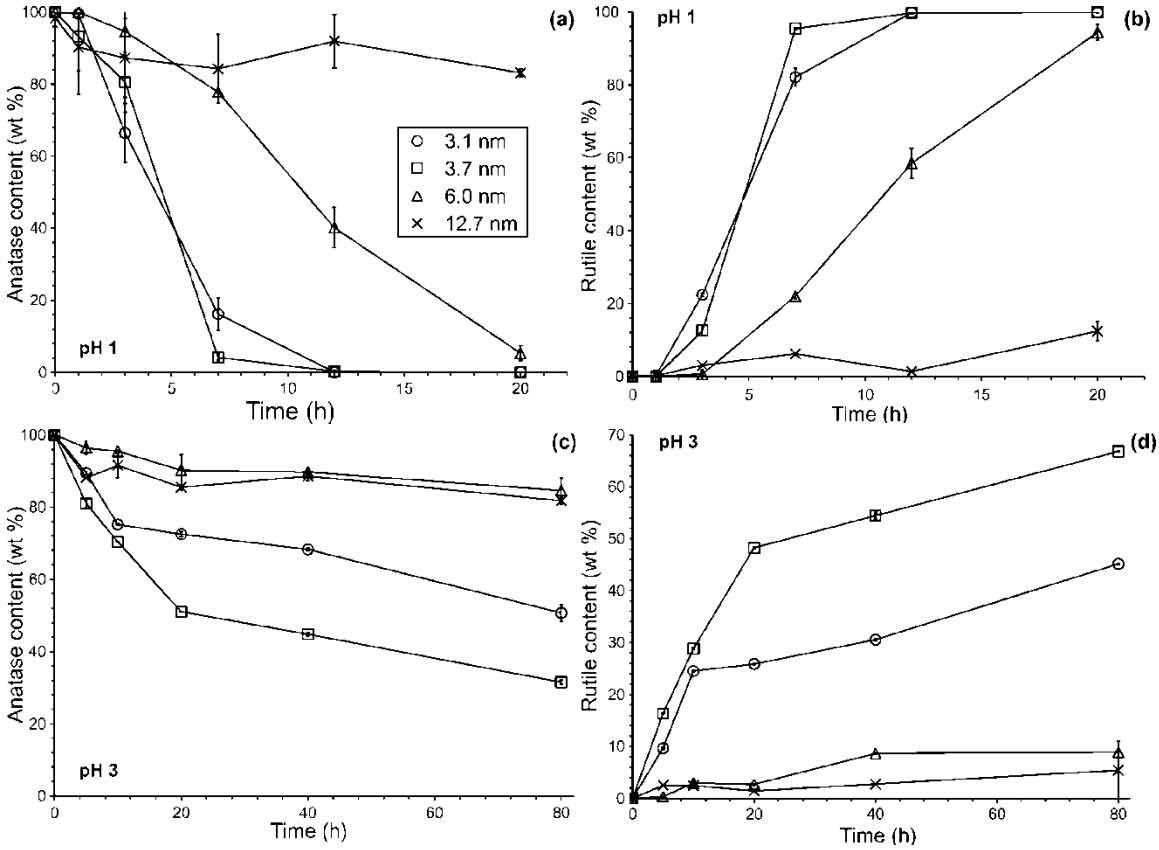

Figure 1.4 Plots showing the anatase content (a, c) and rutile content (b, d) as a function of aging time for samples hydrothermally aged at 250 °C and pH 1 (panels a and b) or pH 3 (panels c and d). Reprinted with permission from reference 27. Copyright 2012 American Chemical Society.

The authors used the Arrhenius equation to further analyze data tracking the anatase to rutile phase transformation and quantified the dependence of activation energy and pre-exponential factor on particle size. For the anatase samples treated in air at temperatures between 480 °C and 580 °C, the activation energy varied slightly with particle size whereas the pre-exponential factor was inversely proportional to particle size to approximately the fourth power. The large pre-exponential factor obtained for small nanocrystals was attributed

primarily to the high concentration of particle-particle contacts, which would result in a high concentration of nucleation sites per unit volume.[28]

Recently, Sabyrov *et al*. explored the effect of particle size on the mechanism of the anatase to rutile phase transformation in hydrothermally processed samples.[10,27] Their results were consistent with previous results demonstrating faster transformation rates in samples with smaller anatase crystallites (Figure 1.4). Several factors might contribute to more rapid transformation of smaller anatase. Samples of smaller nanocrystals might contain more particle-particle contacts and, thus, nucleation sites, such as the twin boundaries produced by oriented attachment. Indeed, their results showed that smaller nanocrystals have higher rates of growth by oriented attachment as compared to larger ones, presumably due to more interactions between nanocrystals in the suspension.[31-33] Furthermore, once rutile nucleates, growth at the expense of smaller anatase crystallites might be faster than growth at the expense of larger anatase crystallites due to the comparatively lower stability of the smaller anatase. This phenomenon, often referred to as Gibbs-Thomson effect, might be a dominant factor in rutile growth under conditions of significant titania solubility.

The kinetics of the anatase to rutile phase transformation is expected to be sensitive to reaction conditions. Indeed, using macroscopic modeling as a primary tool, Sabyrov *et al*. showed that anatase to rutile phase transformation proceeds via a combination of both interface-nucleation (IN) and dissolution-

precipitation (DP) under hydrothermal conditions.[10] IN involves the nucleation and growth of rutile nanocrystals from the interfaces formed between anatase crystals and is dominant at the early stages of the process, when the anatase nanocrystals are smallest in size. At later stages, anatase nanocrystals are substantially larger and the transformation is dominated by the dissolution of anatase and precipitation onto existing rutile crystals. The interplay between these two growth mechanisms is dictated by experimental parameters affecting particle-particle interactions and the solubility of the phases present. Important parameters include pH, solvent, ionic strength, and aging temperature. For instance, decreasing the pH of the aqueous suspension, from pH 3.0 to 1.0, results in a switch from IN as the dominant mechanism to DP, as described by the kinetic models. At intermediate pH values (pH 2.2) both mechanisms contributed substantively to the phase transformation.

A more general kinetic model enables the quantitative description of the simultaneous contributions of IN and DP to phase transformation:[34]

$$\frac{(D_t / D_0)^3}{(1-\alpha)} - 1 = \left(1 + \frac{k_{in} N_0}{k_{dp}}\right)(e^{k_{dp} t} - 1)$$

where the variables common with the interface-nucleation model represent those same parameters. In addition, N_0 represents initial number of particles in anatase sample, and k_{dp} and k_{in} are the rate constants for DP and IN, respectively. Note that the parameters of the left-hand-side of the equation (D_t, D_0, and α) are

experimentally quantifiable. Figure 1.5 presents plots obtained by applying the equation for the anatase to rutile transformation at pHs 1.0, 2.2, and 3.0 at a temperature of 250 °C. Excellent fits obtained at all three different conditions indicate that the model can be used to characterize the contributions of IN and DP to the phase transformation. Rearrangement enables a robust description and quantification of the overall contribution by each mechanism under hydrothermal conditions.

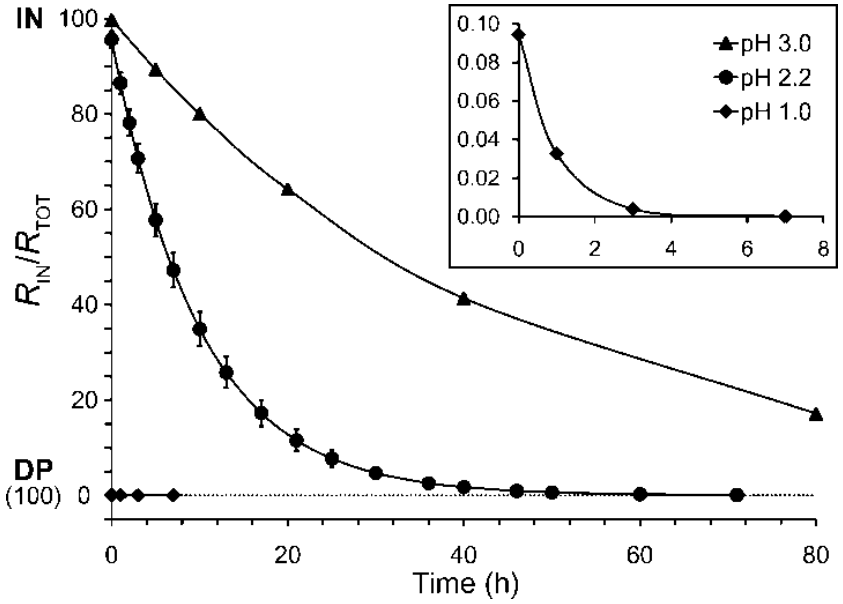

Figure 1.5 The plot presents the amount of anatase (in terms of mass) transformed to rutile by IN relative to the amount transformed by DP as a function of time.

However, depending on conditions, continued rutile production can either involve new rutile particles or growth of already existing rutile particles. Importantly, the model can detect small contributions to the phase transformation by IN, even under conditions strongly favoring dissolution and precipitation. In

fact, Sabyrov *et al*. also used TEM as a correlative method to characterize the sample in which the overall contribution to the phase transformation, by mass, was below one part in one thousand even at the earliest stages. They observed crystals with morphologies and microstructures consistent with oriented attachment, which would be expected if IN played a significant, albeit a small, role in the production of rutile. They concluded that rutile crystallites were formed by IN but that subsequent growth of those crystallites, at the expense of anatase, resulted in fast gains in rutile mass and losses in anatase mass.

Characterization

Materials characterization is a critical step in elucidating the mechanisms of fundamental processes like phase transformation and crystal growth. Research is often limited by the availability of characterization methods as well as what is even possible using state-of-the-art instrumentation. As better characterization tools are designed to investigate the processes, deeper insights into the mechanisms will be gained. Early studies of phase transformation and crystal growth benefitted primarily from diffraction techniques, such as XRD and electron diffraction. Today, a wide variety of characterization methods and state-of-the-art instrumentation are available to examine materials at the atomic and molecular scales.

Combining methods that enable direct examination of individual particles at the atomic scale, such as transmission electron microscopy (HRTEM and cryo-TEM)[17,22,24] and scanning probe microscopy (AFM and STM),[35,36] with

methods that yield an average result for a population of particles can serve to better understand mechanisms of the processes. Techniques like XRD,[29,37] ultra-violet-visible (UV-Vis)spectroscopy[38,39] and Raman[40] spectroscopy, among others, provide representative sampling, but obtaining size and morphology distribution as well as quantifying irregular morphologies of the particles can be impossible. Together with these techniques, HRTEM can serve to characterize microstructural evolution, size distribution, crystallinity, and morphology of particles as a function of time.[10,14] In addition, methods that enable *in situ* characterization are particularly useful for the analysis of particle growth, aggregation, and phase transformation as they can provide information about particle-particle interactions in liquid media.[41]

Cryo-TEM has been effectively used to directly image nanoparticles contained in their native environment.[17,42,43] Samples are prepared by vitrifying, or rapidly cooling, a thin film of suspension in a cryogen. Three dimensional arrangements of the particles are preserved in the vitrified suspension. Successful sample preparation and characterization prevent artifacts and potential modifications to the sample. As a consequence, cryo-TEM enables accurate analysis of particle dynamics in suspension and facilitates the elucidation of mechanisms of particle aggregation.

Cryo-TEM was successfully used by Sabyrov *et al*., for the first time, to demonstrate the effect of particle aggregation on transformation of nanocrystalline anatase to rutile.[27] They observed that anatase nanocrystals with

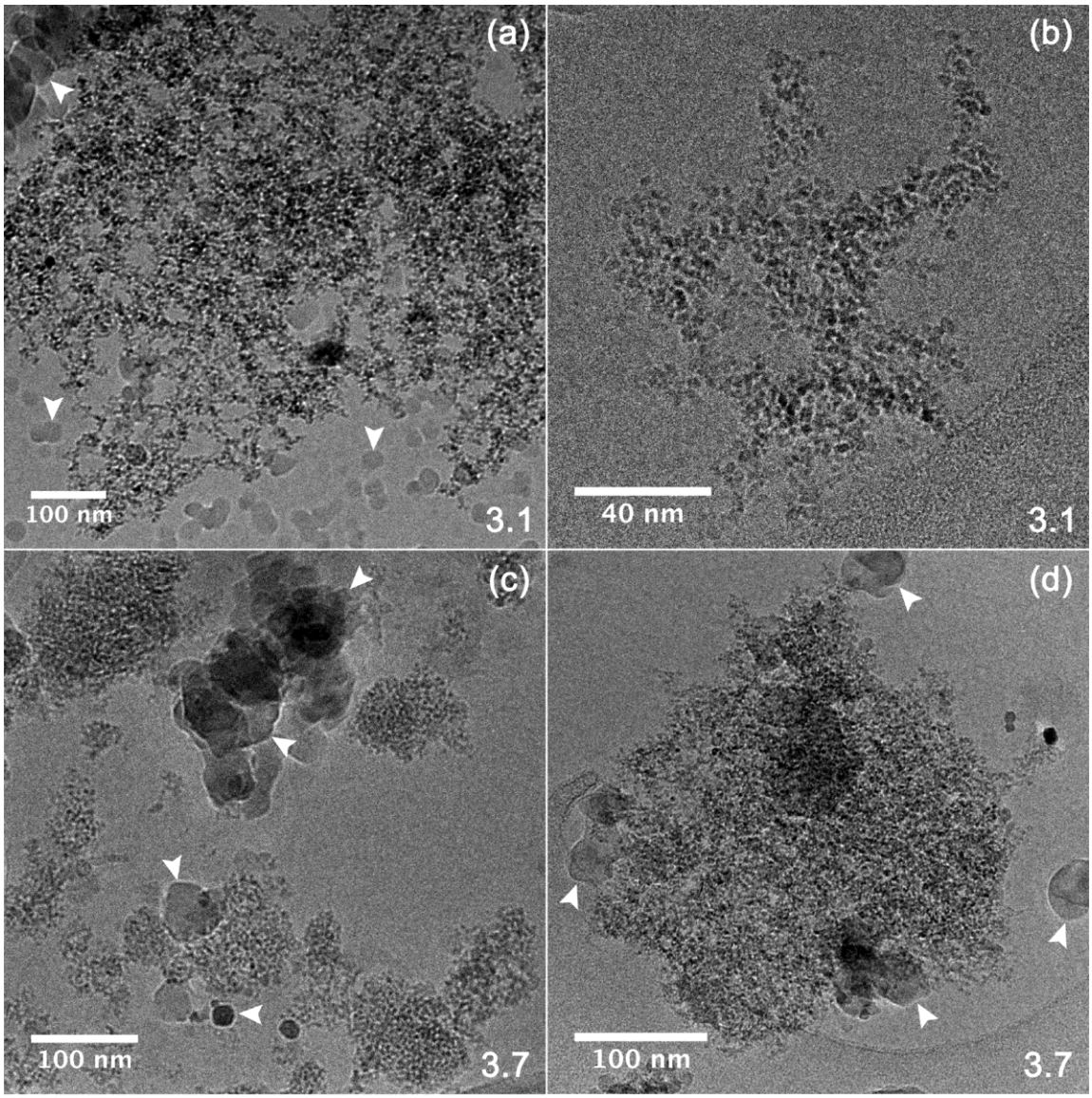

Figure 1.6 The figure presents cryo-TEM images of suspensions at pH 3: (a, b) 3.1-nm particles, (c, d) 3.7-nm particles. White arrows show frost that formed during vitrification. The numbers shown in the lower right corners of the micrographs give the average size of the nanoparticles. Reprinted with permission from reference 27. Copyright 2012 American Chemical Society.

average crystallite size of ~3.7 nm transformed more quickly than did anatase nanocrystals with average crystallite size of ~3.1 nm, which was unexpected. They further observed no change in transformation rate as a function of mass

loading, which was consistent either with phase transformation dominated by DP or extensive aggregation. Fits using macroscopic modeling were not consistent with the former; therefore, they employed cryo-TEM characterization. The data revealed that suspensions prepared with the ~3.7 nm anatase particles contained more compact and dense aggregates, whereas the suspensions of ~3.1 nm anatase contained more open aggregates (Figure 1.6). Aggregates were characterized semi-quantitatively by analyzing numerous cryo-TEM images and determining the 2D packing density of each aggregate imaged. The average 2D packing density for the more densely packed aggregates was ~0.6 and for the less densely packed aggregates was ~0.1 (details of the calculation can be found in chapter 2). Particles with the more dense aggregation state have a higher frequency of particle-particle contacts. Thus, the authors concluded that there were more interfaces that could facilitate rutile nucleation in the more dense aggregates, which led to the increased transformation rate for the slightly larger particles.

Solubility appears to play the most critical role in determining the dominant mechanism by which rutile is produced. In a second cryo-TEM study, Sabyrov *et al*. examined the products of the anatase to rutile phase transformation under mild solvothermal conditions in which titania solubility was very low.[44] Cryo-TEM and TEM images of samples before and after low temperature aging (~2 days at 35 °C followed by ~2 days at 55 °C) demonstrate that the product rutile crystals are substantially larger than the anatase and that the rutile crystals are

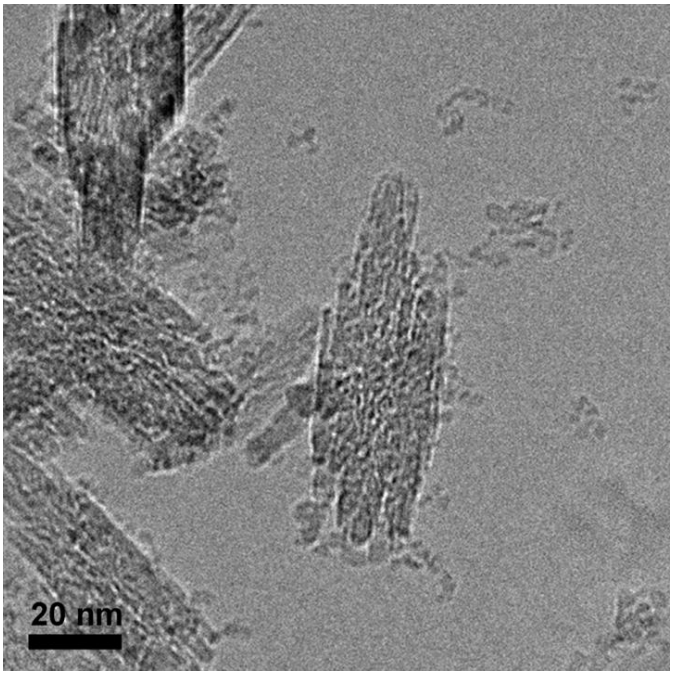

Figure 1.7 Cryo-TEM image of nanoporous rutile in the sample aged for 1 day at ~23 °C, 2 days at ~35 °C, and 2 days at ~55 °C.

mesoporous and exhibit features consistent with formation involving a particle-mediated mechanism (Figure 1.7). The authors concluded that the low solubility conditions enabled preservation of the relics of a particle-mediated mechanism. That is to say, without substantial titanium dioxide solubility, additional rutile growth by DP did not occur, which would have filled in the mesopores and smoothened out crystal facets. In fact, the difference between the appearance of rutile from conditions of higher solubility versus lower solubility is stark. Rutile crystals from higher solubility experiments are smoothly faceted crystals, and the only notable relic of a particle-mediated mechanism is the rutile twin boundary. In contrast, the rutile crystals from the lower solubility experiments are quite irregular, although they are elongated along the same crystallographic direction.

Thus, one can conclude that low solubility so strongly favors particle-mediated crystal growth and IN that retention of porous structures as well as other irregular features becomes possible. This approach could be used to prepare phases with controlled microstructures and porosity.

What cannot be discerned from these sets of images with whether rutile phase transformation occurred before or after an aggregation step. However, results presented heretofore and elsewhere are consistent with the aggregation step preceding the phase transformation step. That is to say, the more stable phase is initially formed via IN. Experiments tracking the aggregation state, phase composition, crystal growth, and morphology with time would most certainly provide the detail required to elucidate when the phase transformation occurs.

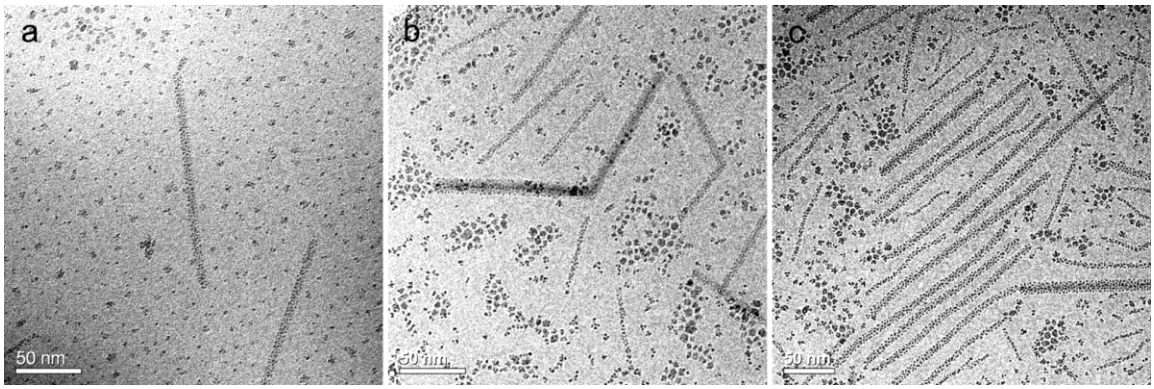

Figure 1.8 Cryo-TEM images of goethite mesocrystals after (a) 5 days, (b) 10 days, (c) 24 days of aging at 80 °C. Reprinted with permission from reference 17. Copyright 2010 American Chemical Society.

Similarly, two recent studies with iron (oxy)hydroxides demonstrate the potential for cryo-TEM to elucidate the mechanism of aggregation induced phase transformation. Ferrihydrite nanocrystals dispersed in slightly acidic aqueous

media (pH 4) transformed to goethite nanorods under mild hydrothermal aging.[17] Initially isolated nanoclusters containing a few to several hundred ferrihydrite particles spontaneously assembled to form thin and long structures composed of crystallographically oriented, but spatially separated, primary particles (Figure 1.8).

High-resolution cryo-TEM studies demonstrated that the thin and long structures are composed of crystalline goethite nanocrystals, and that the elongation direction is parallel to the *c* crystallographic axis. As time progresses, those assemblies of goethite particles converted into single-crystalline goethite nanorods. Similarly, smaller akaganeite nanoparticles aggregated and phase transformed to micron-sized hematite spindles.[24] Small hematite nanoparticles, comparable in size to akaganeite nanocrystals, were not detected leading to a conclusion that hematite forms during aggregation of akaganeite nanocrystal as presented in Figure 1.9. The authors concluded that particle-mediated crystal growth of metastable phase facilitates the formation of the more stable secondary phase.

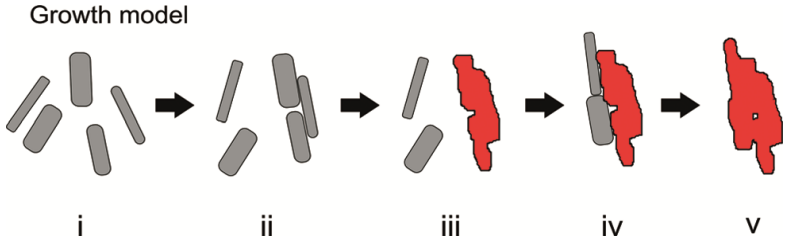

Figure 1.9 Akaganeite particles (grey rectangles, i) aggregate (ii) and transform to hematite spindles (red structures, iii). After the “incubation period” (i–iii), the hematite spindles grow more rapidly through aggregation of akaganeite particles (iv) followed by phase transformation of akaganeite to hematite (v). Reprinted with permission from reference 24 - published by The Royal Society of Chemistry.

Summary and outlook

As more advanced instruments and techniques are developed, deeper insights into the mechanisms of the process are expected. Data collected using XRD are essential in modelling and quantifying the kinetics of the processes, whereas HRTEM enables sub-nanometer scale characterization of materials. Cryo-TEM is unique in addressing the aggregation state of the particles in liquid media. Correlative methods such as UV-Vis, DLS, and Raman spectroscopy can be used to test whether TEM results describe the sample in a representative fashion.

Combination of the experimental and theoretical techniques is critical in exploring the mechanisms of phase transformation and crystal growth. Macroscopic modelling together with newly invented state-of-the-art instruments such as *in situ* fluid cell TEM or synchrotron-based X-ray spectroscopy techniques might provide unprecedented insights into the mechanisms of the phenomena. The obtained results might lead to better control over phase transformation and crystal growth to produce materials with desired properties.

Chapter 2: Size-Dependent Anatase to Rutile Phase Transformation and Particle Growth*

Introduction

The greatest degree of control over size-dependent properties of nanoparticles can be achieved through controlling the early stages of growth; that is, when their size is in the nano size regime.[1-4] After nucleation, inorganic nanoparticles grow via two major mechanisms: coarsening and aggregation.[5,6] Coarsening, or Ostwald ripening (OR), is the growth process by which smaller particles dissolve due to thermodynamic instability and larger particles continue to grow by consuming dissolved species in solution. In other words, larger particles grow at the expense of smaller ones.[7-9] Alternatively, secondary particles can be produced by aggregation of primary particles. In oriented aggregation mechanism, primary particles first aggregate, then align crystallographically to form mesocrystals. Primary particles in mesocrystals are separate units that are not in direct contact with each other. However, these primary crystallites are in crystallographic registry. Subsequently, mesocrystals transform to secondary crystalline particles or oriented aggregates.[10-12] Controlling these mechanisms may lead to materials with optimized properties.[13] Understanding the relationship between growth mechanisms and

* Reprinted with permission from Sabyrov, K., Burrows, N. D. and Penn, R. L. *Chemistry of Materials* **2012**, *25,* 1408-1415. Copyright 2012 American Chemical Society.

the physical and chemical properties of the product material is crucial to designing novel nanostructures.

In our work, TiO_2 was used as a model system, because of its potential use in many applications, including energy and environmental applications.[14-16] Anatase, rutile, and brookite are three important polymorphs of TiO_2. Each phase has unique properties. For example, it has been shown that anatase has the lowest surface free energy whereas rutile has the lowest bulk free energy.[17,18] As a result, nanoparticulate TiO_2 usually occurs in the anatase phase.[19] Based on previous experimental work, a "critical size" of ~10–15 nm was proposed, above which rutile is expected to be the dominant phase.[17] However, consistent evidence for such a critical size is lacking.

Nucleation, growth, and phase transformation between the titania polymorphs have been extensively investigated with the purpose of designing novel titania nanostructures with useful properties. However, uncovering how these processes occur in solution is challenging, because the hydrolysis of precursors and nucleation of particles are fast, experimental techniques to characterize reaction intermediates are lacking, and these processes are highly sensitive to small variations in reaction conditions.

Previously, it was shown that the anatase-to-rutile transition is highly size-dependent in air and at high temperatures (~600 °C).[20,21] However, particles may behave in a different manner when they are treated in aqueous media, where the

diffusion and collision of particles, adsorption of ions and water molecules on the particle surfaces, and electrostatic and dispersion forces are crucial.[9] In this work, we present data demonstrating the size dependence of anatase-to-rutile phase transformation rates and particle growth in an aqueous medium.

Experimental section

Synthesis

Anatase samples were synthesized using a sol–gel method similar to that developed by Gribb and Banfield in 1997, in which the titanium isopropoxide is hydrolyzed under acidic conditions.[22] A slightly modified version of that was employed by Isley *et al*. and yielded 100% anatase.[23] Here, 12.5 mL of titanium isopropoxide (Aldrich) and 125 mL isopropanol were mixed (Fisher, HPLC grade), using an ice bath to maintain the temperature near 0 °C. A nitric acid (Mallinckrodt) solution with a pH of −0.6 was used as a catalyst and added dropwise with vigorous and continuous mixing over a period of 3 h. The final Ti:H_2O ratio was 1:100 for all samples. The obtained white suspension then was heated to boiling and allowed to reflux for 24 h. After reflux, suspensions were dialyzed (Spectra/Por) against Milli-Q water (Millipore Corporation) to remove ions and byproducts of the synthesis. The water was changed ∼15 times over the course of 10–15 days. After dialysis, the pH of the suspensions ranged from pH 4.0 to pH 4.7. The ionic strength of the medium during synthesis was changed to tune the nanoparticle sizes using $NaNO_3$ and NaCl. Table 2.1

summarizes the average sizes, synthesis conditions, and types and concentrations of salts used to adjust ionic strength for each sample. To synthesize the largest particles, the sample was placed into the Teflon liner of a Parr Instrument autoclave bomb and aged for 48 h in an oven at 200 °C, in addition to adjusting ionic strength during refluxing.

Hydrothermal processing

Aqueous suspensions were hydrothermally treated, and the anatase-to-rutile phase transformation was monitored by X-ray diffraction (XRD). First, 3 mL of the original dialyzed suspensions were diluted with 5 mL of Milli-Q water and adjusted to pH 1 or 3, using nitric acid. Then, each was placed into a Teflon liner of a Parr Instrument acid-digestion, autoclave bomb and aged for 1–80 h at 250 °C. The bombs were removed from the oven and allowed to cool to room temperature. The pH values were measured again after the aging process and no significant pH deviations (±0.3) were observed.

Table 2.1 Summary of experimental conditions for the synthesis of anatase nanoparticles with different average sizes.[a]

Size (nm)	Initial synthesis (~3 °C)	Reflux (~83 °C)	Hydrothermal aging (~200 °C)
3.1	2M $NaNO_3$	no salt	no aging
3.7	no salt	no salt	no aging
6.0	no salt	2.5M NaCl	no aging
12.7	no salt	2.5M $NaNO_3$	aging for 48 h

[a]The sizes were determined from peak broadening using the Scherrer equation.

Characterization

XRD was used to characterize phase composition and particle size. For these analyses, several drops of the resulting suspension were placed onto a zero-background, quartz slide and allowed to dry in air. Diffraction patterns were collected using a PANalytical X'Pert Pro diffractometer equipped with a high-speed X'Celerator detector and a Co Kα radiation source. The patterns were collected over a 2θ range of 24°–62°. Previously, this shorter range was compared to a range of 24°–110° and was shown to be sufficient for Rietveld refinement.[24] The scanning mode was continuous, with an effective step size of 0.016° and an effective dwell time of 765 s. A 0.5° divergent slit and a 1° anti scattering slit were used for all measurements. The diffraction patterns were compared to International Centre for Diffraction Data (ICDD) powder diffraction files for anatase, rutile, and brookite.

Using the X'Pert High Score Plus software, quantitative phase compositions were determined by Rietveld refinement.[25] This refinement technique is used to quantify phase composition by simulating a theoretical line profile until it matches the experimental profile. Refinements were performed as described previously by Isley and Penn.[24] The parameters refined were zero shift (° 2θ); scale factor; preferred orientation; W, U, and V profile parameters; unit-cell parameters; and peak shapes; other parameters were fixed, such as thermal parameters, fractional atomic coordinates, roughness parameters, the extinction, and porosity. To evaluate the quality of the fits, goodness of fit (GoF), and R-

weighted profile (Rwp) values were monitored. In this study, the GoF values ranged from 1.4 to 18.1, whereas Rwp ranged from 1.5 to 5.6. Typically, the refinements were considered successful if GoF ≤ 3 or no improvement was observed over multiple refinement iterations.[26] Finally, the average size of nanocrystals was determined from peak broadening, using the Scherrer equation.[27] The peaks used were (101) and (110) for anatase and rutile, respectively.

Suspensions of anatase nanoparticles were characterized using dynamic light scattering (DLS) to measure aggregate sizes at pH 1 and pH 3 just before hydrothermal processing. Samples were prepared by adjusting the pH of the original suspension with nitric acid at room temperature and placing 3 mL of suspension into a cuvette. Before measurements, the suspension in the cuvette was shaken several times by hand. The suspensions were characterized using the Zeta Pals (Zeta potential analyzer, Brookhaven) equipped with HeNe laser with a wavelength of 632.8 nm. The angle of incident laser with respect to detector position was 90°. Three runs were carried out for each sample at 25 °C, and the number-based mean values and standard deviations were calculated.

Cryogenic transmission electron microscopy (cryo-TEM) enables almost *in situ* characterization.[11,28] For cryo-TEM, samples were prepared by first diluting nanoparticle suspensions with Milli-Q water and depositing a small quantity of the sample solution onto a TEM copper grid with lacey carbon film (200 mesh Cu

grid, SPI supplies). The grid then was blotted with a filter paper using a Vitrobot Mark IV (FEI Company) under 100% relative humidity. The blotted grid was then plunged into liquid ethane in order to vitrify the suspension. Finally, the grid was cryogenically transferred to the cryo-TEM holder, which was then inserted into the microscope while still maintaining cryogenic conditions. In vitrified samples, the crystallization of water does not occur, because of the rapid temperature decrease. In cryo-TEM analysis, low-dose imaging conditions were employed to minimize sample damage.

Two-dimensional (2D) packing densities were calculated using 2D cryo-TEM images of the samples. The ratio of the projected area of the densest part of the aggregate to the projected area of the entire aggregate was calculated using ImageJ.[29] Approximately 10–20 cryo-TEM images were processed for each sample and mean values were used to compare the compactness of the aggregates. However, it should be noted that this method is semi quantitative and provides only a rough estimate of the packing densities.

Results and discussion

All four samples are initially composed of anatase, with no evidence of other phases detected (see Figure 2.1). The average sizes, as determined using X-ray line broadening analysis, range from 3.1 nm to 12.7 nm and are summarized in Table 2.1.

During hydrothermal treatment at 250 °C, the rate of anatase-to-rutile transformation generally increased as the initial anatase nanoparticle size decreased. Figure 2.2a shows the change in anatase content after 20 h of hydrothermal processing (250 °C, pH 1), and Figure 2.2b shows the change in rutile content. Samples with initial average anatase sizes of 3.1 and 3.7 nm transformed more rapidly than those with 6.0 and 12.7 nm. After 12 h of aging, samples prepared using the 3.1- and 3.7-nm particles were 100% rutile, whereas the 6.0- and 12.7-nm samples were ~40% and ~10% rutile, respectively. Thus, it can be concluded that the rate of transformation generally increases as the initial crystallite size decreases.

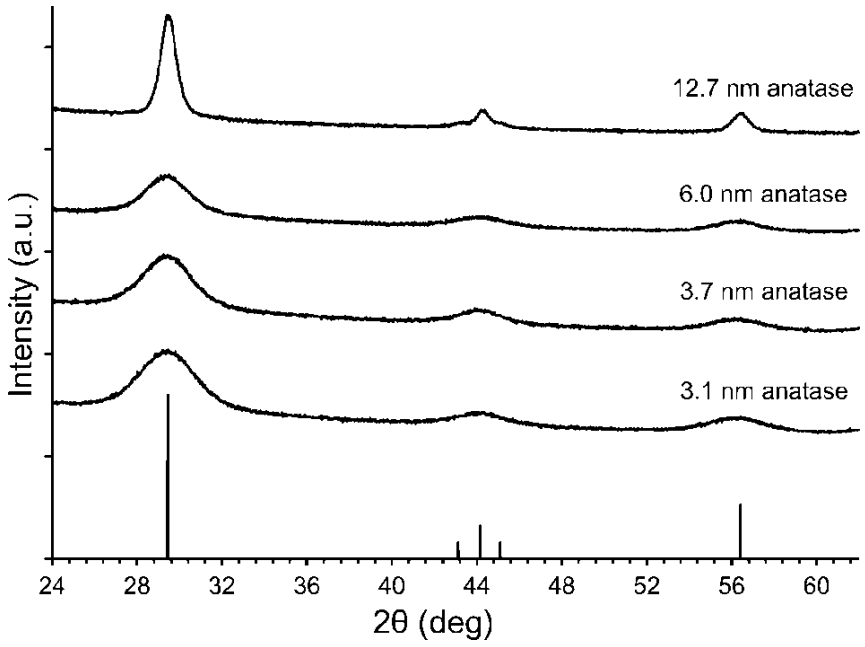

Figure 2.1 XRD patterns of pure anatase nanoparticles before aging. Data for anatase (ICDD PDF Card No. 01-073-1764) are shown as a stick pattern.

Zhang and Banfield treated dry anatase powder at high temperatures (<600 °C) in air and showed that the anatase-to-rutile phase transformation takes place via an interface nucleation mechanism and that the transformation was size-dependent. According to their results, the activation energy for the transformation increased slightly while the pre-exponential factor increased dramatically with decreasing particle size. As a result, the transformation rate constant increased as the particle size decreased. They attributed this observation to the concentration of particle–particle contacts. Smaller particles had a higher number of particle–particle contacts per unit volume, giving rise to a higher pre-exponential factor.[20] According to the results obtained in our work, the anatase-to-rutile transformation is similarly size-dependent. However, the results thus far do not elucidate whether the transformation is initiated at particle–particle contacts or whether other factors, such as solubility or ion and water adsorption, play important roles.[9]

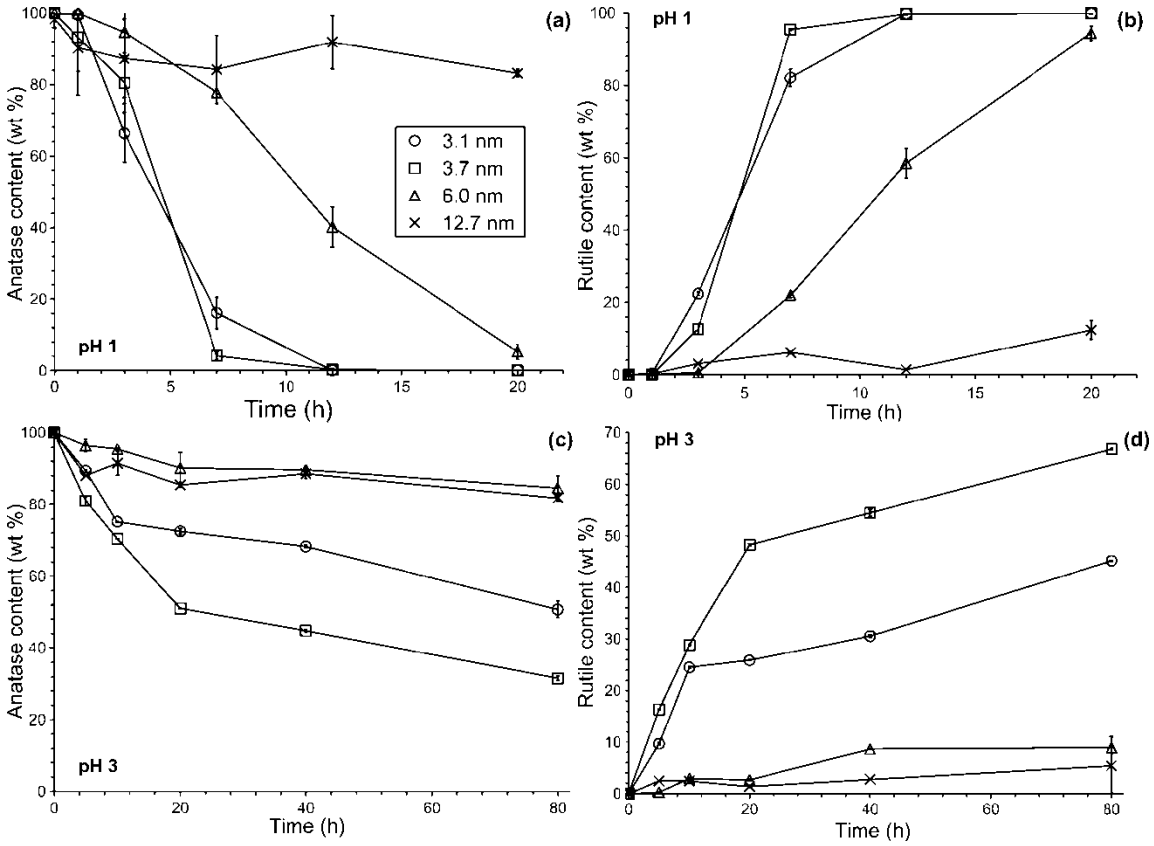

Figure 2.2 Plots showing the anatase content (a, c) and rutile content (b, d) for samples aged at 250 °C and pH 1 (panels a and b) or pH 3 (panels c and d). Error bars represent the standard deviation calculated from multiple refinements performed for each sample. [Note: In all figures in this paper, error bars represent the standard deviation calculated in the same way. Connecting lines serve to help guide the eye, unless otherwise stated.]

At pH 3, for which data are shown in Figures 2.2c and 2.2d, the anatase-to-rutile phase transformation is comparatively slow but still generally size-dependent. Even after 80 h of hydrothermal treatment, the maximum conversion observed was only ~65%. At this pH, the solubility of anatase is orders of magnitude lower than at pH 1.[30-32] Therefore, a decrease in the transformation rate is expected if the dissolution-precipitation mechanism plays an important role in the anatase-to-rutile phase transformation.

The phase transformation data were fit using conventional kinetic models[33,34] and the model developed by Zhang and Banfield.[35] However, the fits were poor as nonlinearity was observed in all cases. A new model was developed in which it was assumed that the phase transformation takes place via dissolution of anatase nanoparticles and precipitation of rutile (Equation 1). This model was used to fit the data, and the fits were good for transformation under the most acidic (i.e., pH 1) conditions.

$$TiO_2\ (anatase) \leftrightharpoons dissolved\ species \leftrightharpoons TiO_2\ (rutile) \quad (1)$$

First, the rate of dissolution (R_d) is assumed to be first order, with respect to the concentration of active surface sites (C_s) of anatase nanoparticles:[36]

$$R_d = k_d C_s \quad (2)$$

where k_d is a rate constant for the dissolution of anatase. It is assumed that the dissolution of an anatase nanoparticle is fast enough that the concentration of active surface sites (C_s) is proportional to the number of anatase nanoparticles (N). This allows the rate to be expressed in terms of the number of anatase nanoparticles:

$$R_d = k_d' N \quad (3)$$

The rate of rutile formation (R_r) can be derived from the rate of dissolution if steady-state approximation is applied to Equation 1. This approximation is plausible since concentration of the dissolved species is small and constant

throughout the transformation, because of the low solubility of TiO_2 under these conditions.[31,32] Thus, the rate of rutile formation can be expressed using a first-order rate law, with respect to the number of anatase nanoparticles (*N*):

$$R_r = -\frac{\mathrm{d}N}{\mathrm{d}t} = \mathrm{k_r} N \tag{4}$$

where k_r is a rate constant of rutile formation. The integrated form of this rate equation is:

$$\ln\left(\frac{N_t}{N_o}\right) = -\mathrm{k_r} t \tag{5}$$

where N_0 and N_t are the numbers of anatase nanoparticles at time $t = 0$ and time t, respectively. The above expression cannot be used in its current form, because the number of nanoparticles cannot be experimentally identified. Nevertheless, the ratio of the number of anatase nanoparticles at time *t* to initial number can be expressed in terms of weight fraction and size of nanoparticles. If α is the weight fraction of anatase nanoparticles transformed at time *t*, then:

$$\alpha = 1 - \frac{m_t}{m_o} \tag{6}$$

where m_0 is the initial mass of anatase nanoparticles and m_t is the mass at time *t*. Here, the ratio of the mass of anatase nanoparticles at time *t* to its initial mass is proportional to the ratio of size cubed and number of anatase particles if the

change in the density is assumed to be negligible with the change in nanoparticle size:

$$\alpha = 1 - \left(\frac{D_t}{D_o}\right)^3 \frac{N_t}{N_o} \tag{7}$$

where D_0 and D_t are the average diameters of anatase nanoparticles at time $t = 0$ and time t, respectively. By rearranging Equation 7 and plugging into Equation 9, the final form is derived:

$$\ln\left[(1-\alpha)\left(\frac{D_o}{D_t}\right)^3\right] = -k_r t \tag{8}$$

Figure 2.3 shows the kinetic plots based on Equation 8, which describes the dissolution-precipitation mechanism. The equation was used to fit the data obtained from the transformation of anatase nanoparticles with different initial sizes except 12.7-nm particles. The transformation of 12.7-nm particles was negligible, making it impossible to apply the equation. Figures 2.3a and 2.3b show the kinetic plots for the transformation at pH 1 and pH 3, respectively. Excellent fits of the equation for the data at pH 1, as indicated by R^2 values, are consistent with the dissolution-precipitation mechanism dominating at pH 1. However, the equation does not produce a good fit for the data from the pH 3 experiments. This suggests that the anatase-to-rutile transformation does not take place solely via the dissolution-precipitation mechanism. It is possible that

an aggregative mechanism is contributing to the anatase-to-rutile transformation at pH 3.[37]

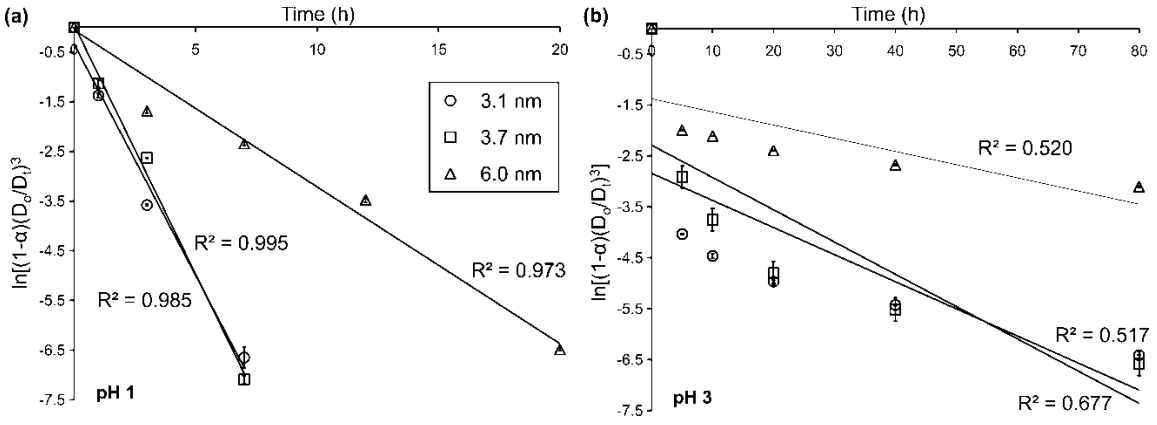

Figure 2.3 Plots presenting the experimental data and kinetic plots, based on Equation 8: (a) fit of the data obtained at pH 1, and (b) fit of the data obtained at pH 3. R^2 values are shown to indicate how well the data points fit the equation.

To further elucidate the mechanisms operating at each of the pHs, particle size was monitored as a function of time. Under acidic conditions, coarsening is expected to dominate, because the solubility of titania, as well as some other oxides, increases as the acidity of the medium increases, and coarsening depends on solubility.[5,31,32,38] Figure 2.4 presents data tracking the size of both anatase and rutile nanoparticles, as a function of hydrothermal treatment time at 250 °C and pH 1 (see Figures 2.4a and 2.4b) and pH 3 (see Figures 2.4c and 2.4d). The trend of anatase nanoparticle growth was similar to the transformation trend; the particle growth rate is dependent upon the initial anatase particle size. After 7 h of hydrothermal processing, the samples with 3.1- and 3.7-nm particles had completely transformed to rutile, and, thus, it was no

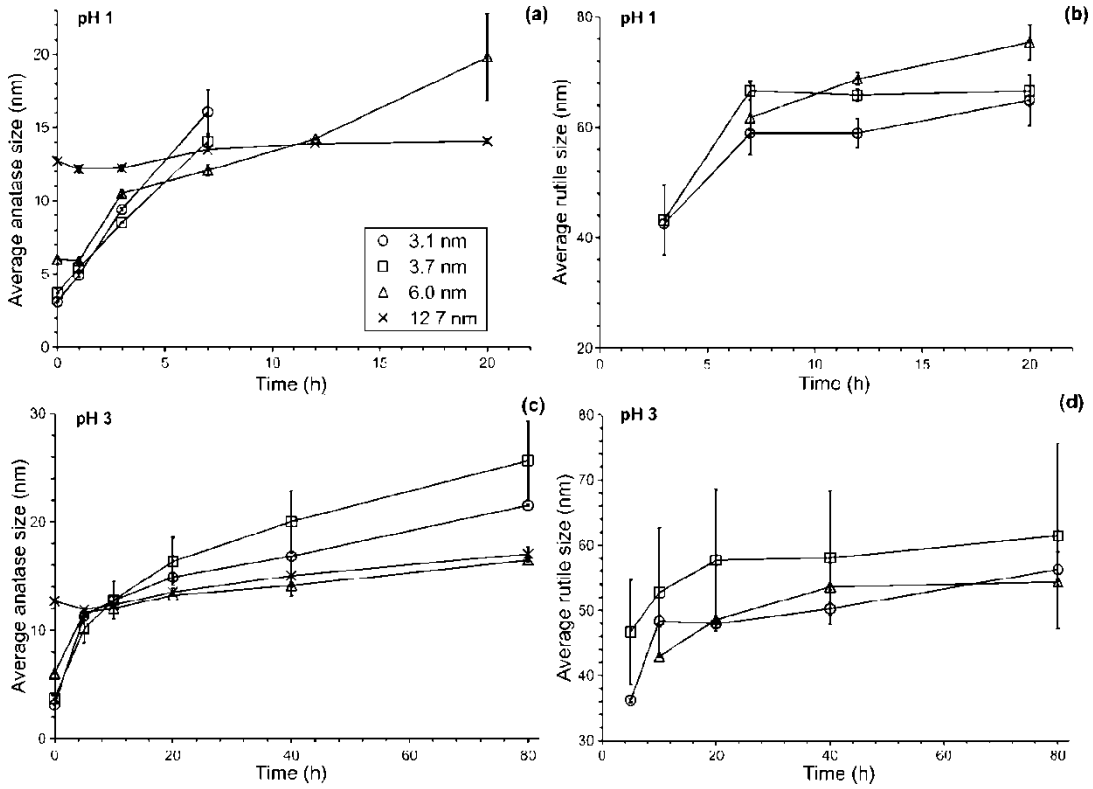

Figure 2.4 Figures present the change of average sizes of (a, c) anatase particles and (b, d) rutile particles with aging time. Panels a and b show the results obtained at pH 1, and panels c and d show the results obtained at pH 3.

longer possible to track anatase growth (Figure 2.4a). The sample containing 12.7-nm particles showed only a slight increase in anatase size throughout the aging process, which was similar to its transformation behavior. In addition, the growth of rutile nanoparticles with time was monitored (see Figures 2.4b and 2.4d). In the plot, the average sizes of only three samples are presented, because the rutile content in the aged 12.7-nm samples never exceeded a trace amount. The three samples showed similar growth trends. However, in the same suspension, the rutile nanoparticles were always much bigger than the corresponding anatase nanoparticles.

If an aggregative growth mechanism is important at pH 3, as was shown by Isley *et al*.,[39] 2008, then one might predict that the particle growth rate should increase with increased particle number concentration. To test this, suspensions containing 3.7-nm particles, with concentration values of 3.12, 4.50, 6.25, and 31.25 mg/mL, were used. Figure 2.5 shows the change in phase composition and particle size with time at pH 3 for experiments using the 3.7-nm anatase sample. From these data, it is evident that particle concentration does not affect the phase transformation rate nor the anatase and rutile growth rates. According to the kinetic studies shown in Figure 2.3, it was concluded that, at pH 3, the anatase-to-rutile transformation does not follow dissolution-precipitation mechanism alone. However, the data shown in Figure 2.5 are not consistent with a growth mechanism involving aggregation.

Some clues can be found in examining the data employing the 3.7- and 3.1-nm anatase particles. The suspension containing 3.7-nm particles transformed more rapidly, compared with the suspension containing 3.1-nm particles, which was not expected (Figure 2.2). One explanation could involve impurities such as brookite, which could increase solubility or act as nucleation sites for rutile.[6,21,37] However, no brookite was detected in the 3.7- and 3.1-nm samples (Figure 2.1), although the limit of detection via XRD is ca. 1 wt %.

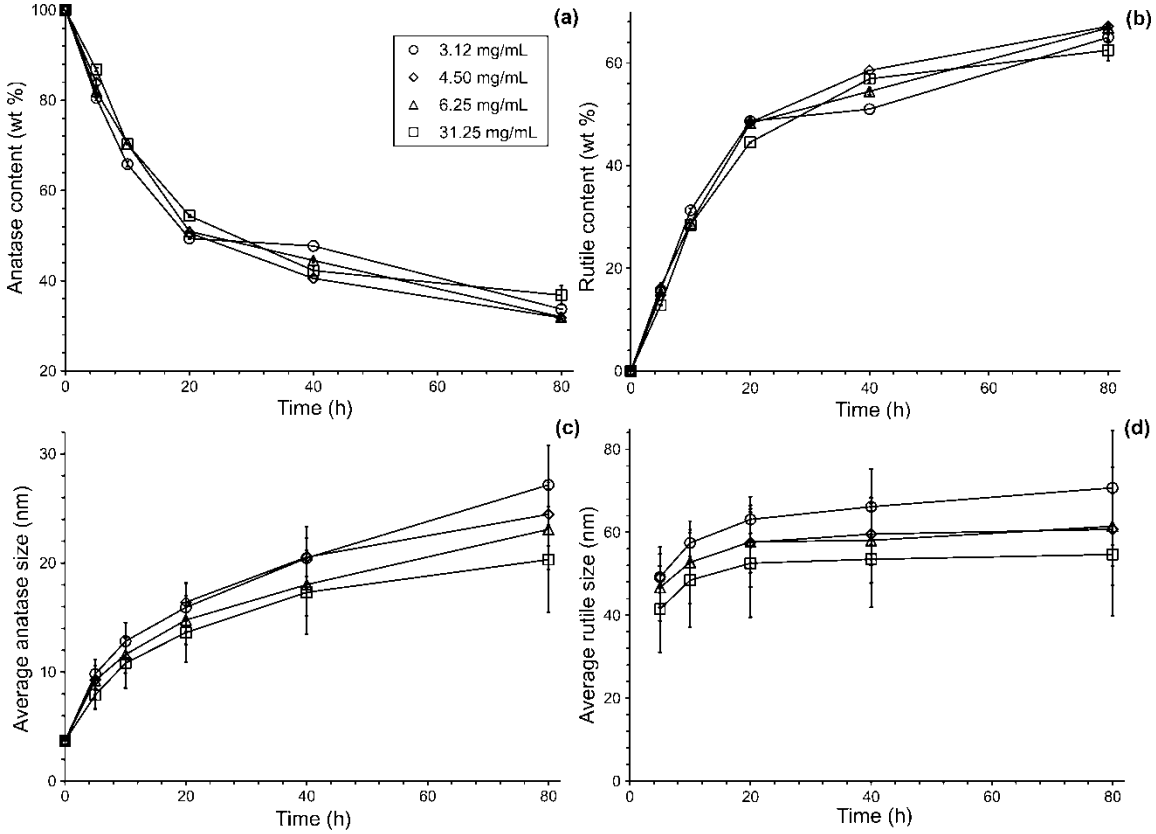

Figure 2.5 The change in (a, b) phase contents and (c, d) average sizes of anatase (panels a and c) and rutile (panels b and d). The figure describes the results when 3.7-nm anatase particles with different concentrations were aged hydrothermally at 250 °C and pH 3.

Table 2.2 presents the average sizes of aggregates in the suspensions at pH 1 or 3, as determined using dynamic light scattering (DLS). The average aggregate sizes differ significantly and range from ~100 nm to a few micrometers. There is no clear trend of increasing or decreasing aggregate size with changing crystallite size. In addition, the average aggregate sizes of the same samples at pH 1 were similar to those at pH 3. Therefore, it is unlikely that the overall decrease in transformation rate with decreasing acidity is due to a simple change in aggregate size. However, those measurements were

performed at room temperature, and these measurements do not yield information about aggregate density.

Increased compactness of aggregates could substantially increase the effective concentration of particle–particle contacts, and this would be expected to increase the rate of phase transformation.[37,40] For example, it was experimentally shown that more compact aggregates of titania nanocrystals tended to transform faster when dry powders were aged at ~600 °C, because they had more particle–particle contacts, and, therefore, they had a greater probability of producing nucleation sites for the rutile phase.[41]

Table 2.2 Average aggregate sizes (nm) of anatase nanocrystals in the suspensions characterized by dynamic light scattering (DLS) at pH 1 and pH 3 before aging.[a]

	3.1-nm particle aggregates	3.7-nm particle aggregates	6.0-nm particle aggregates	12.7-nm particle aggregates
pH = 1	$1.0\times10^{3} \pm 0.3\times10^{3}$	$1.8\times10^{2} \pm 0.1\times10^{2}$	$7.2\times10^{2} \pm 0.2\times10^{2}$	$0.9\times10^{2} \pm 1.2\times10^{1}$
pH = 3	$3.5\times10^{3} \pm 0.2\times10^{3}$	$1.7\times10^{2} \pm 0.2\times10^{2}$	$6.2\times10^{2} \pm 1.2\times10^{2}$	$1.0\times10^{2} \pm 0.3\times10^{1}$

[a]The number-based average was used for all suspension characterizations

Cryo-TEM can reveal the size and nature of aggregates in their native environment. Unlike dry transmission electron microscopy (TEM), cryo-TEM can

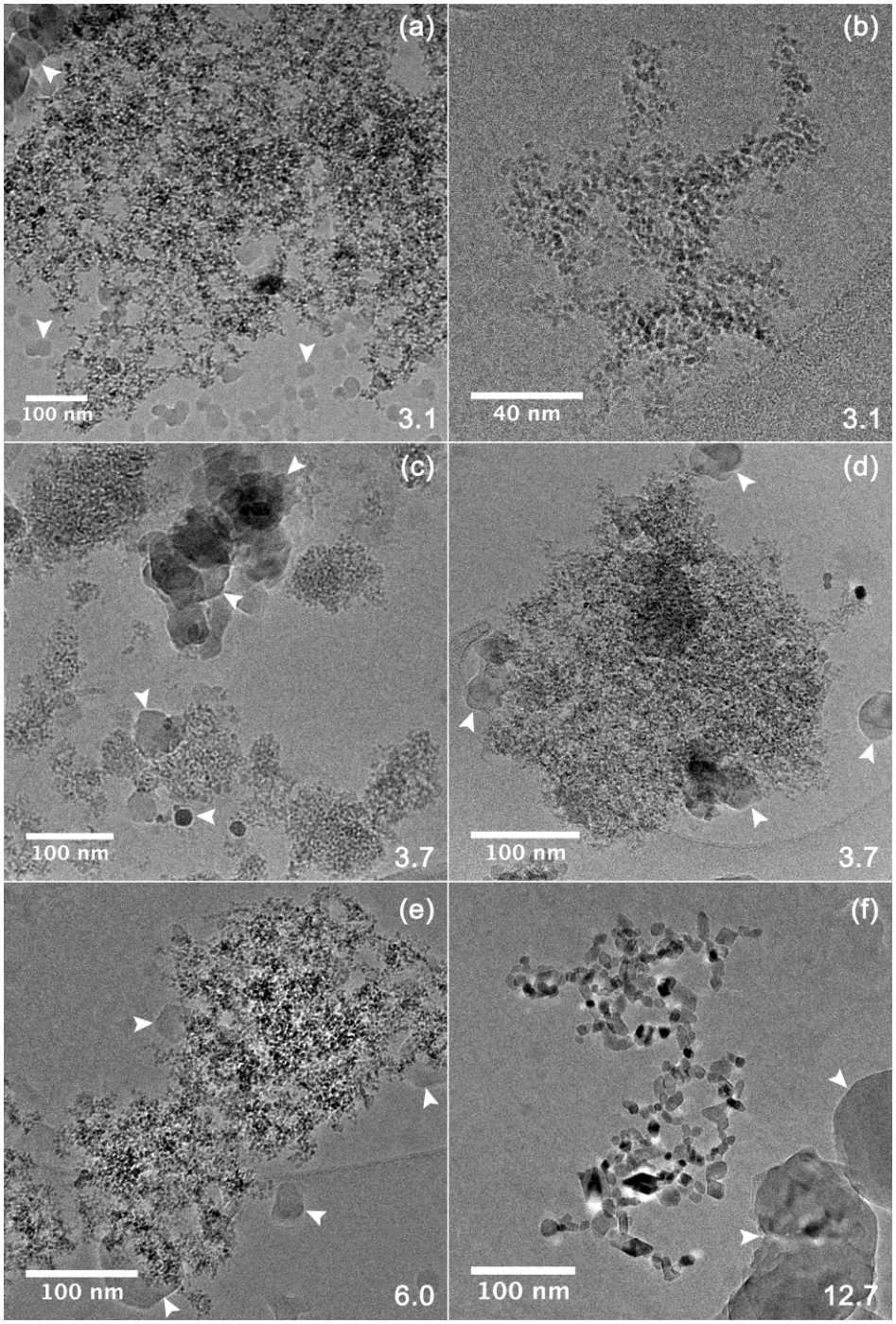

Figure 2.6 The figure presents cryo-TEM images of suspensions at pH 3: (a, b) 3.1-nm particles, (c, d) 3.7-nm particles, (e) 6.0-nm particles, and (f) 12.7-nm particles. White arrows show frost that formed during vitrification. The numbers shown in the lower right corners of the micrographs give the average size of the nanoparticles.

be used to directly image particles in suspension, enabling distinction between compact and loosely aggregated particles in a suspension. Figure 2.6 shows cryo-TEM images of suspensions containing the 3.1-, 3.7-, 6.0-, and 12.7-nm anatase crystals. The aggregates of 3.1-nm crystals shown in Figures 2.6a and 2.6b generally had more open, fractal-like structures, whereas aggregates composed of 3.7-nm crystals (Figures 2.6c and 2.6d) had denser and compact structures. In order to semi quantitatively characterize compactness, packing densities of the aggregates were determined using the two-dimensional (2D) cryo-TEM images of each sample. The aggregates of 3.7-nm crystals had a 2D packing density of 0.60, while the aggregates composed of 3.1-nm crystals had a 2D packing density of only 0.13, clearly indicating that the former was significantly more compact than the latter. The observed compactness of the aggregates composed of 3.7-nm crystals is consistent with the faster transformation, compared to aggregates of 3.1-nm crystals. Figures 2.6e and 2.6f show the structures of the aggregates composed of 6.0 and 12.7 nm crystals, respectively. The 2D packing densities of 6.0 and 12.7 nm particles are 0.29 and 0.25, respectively. As indicated by their packing densities, these nanoparticles have similar aggregation states, even though their sizes are different. Therefore, the difference in transformation rates might be solely due to the difference in primary particle size.

Thus, we conclude that the compactness of the aggregation leads to more particle–particle contacts: the 3.7-nm particles transform faster than the 3.1-nm

particles, because of this fundamental difference. This conclusion is still consistent with the results regarding mass loading - the aggregation state of the particles precluded the possibility of significant changes in particle-particle collisions with changes in mass loading. As a result, the particle concentration did not affect the transformation.

Finally, the number and types of defects in the 3.7-nm crystals might also affect the transformation. These particles may include defects or may have different nanocrystal microstructures, because the synthesis conditions of 3.7-nm particles were slightly different than the synthesis conditions of 3.1-nm particles, as shown in Table 2.1. Defects increase the solubility due to higher strain, and higher solubility leads to faster transformation via dissolution-precipitation mechanism.[42] However, defects can also act as nucleation sites for the other phases such as brookite and rutile. For example, Penn and Banfield showed that twin interfaces of anatase nanoparticles have brookite and rutile structural elements, which might reduce the anatase-to-rutile transformation activation energy.[6,37] Nevertheless, further investigation is needed to evaluate the effect of defect concentration and microstructure on phase transformation.

Conclusions

Pure anatase nanocrystals with different initial sizes were hydrothermally processed at 250 °C and pH 1 or pH 3, and the observed anatase-to-rutile phase transformation and particle growth rates were observed to be size-dependent.

The overall decrease in phase transformation and growth rates with decreasing acidity of the suspensions was presumably due to the decrease in solubility of the particles. At pH 1, the primary mechanism driving both particle growth and phase transformation is likely dissolution-precipitation. However, at pH 3, the data are consistent with an aggregative mechanism or a combination of the two. In addition, particle concentration did not affect the transformation and the particle growth rates at pH 3, but it is concluded that the aggregation state of the particles precluded the possibility of significant changes in particle-particle collisions with changes in mass loading. The results obtained in this work contribute to a deeper understanding of phase transformation and particle growth.

Acknowledgments

We thank the University of Minnesota, the National Science Foundation (No. NSF-0957696), and the Nanostructural Materials and Processes Program at the University of Minnesota for financial support. Parts of this work were carried out in the Characterization Facility at the University of Minnesota, which is a member of the NSF-funded Materials Research Facilities Network (www.mrfn.org) via the MRSEC program.

Chapter 3: Two-Step Phase Transformation of Anatase to Rutile in Aqueous Suspension*

Introduction

The thermodynamic stability of nanocrystalline materials often changes with crystallite size due to the relative contributions of the bulk and interfacial free energies to the total free energy as a function of size.[1-7] Since the contribution of the interfacial free energy to the total free energy increases with decreasing crystallite size, it can be an important determinant at nanometer scale dimensions. As a consequence, the phase with the lowest interfacial free energy is the most stable phase for fine nanocrystals. However, nanocrystals can phase transform once they reach a size at which the bulk energy becomes the more important energy term. This is due to the increased role of bulk free energy and decreased role of interfacial free energy as crystallite size increases. For example, TiO_2 nanocrystals with sizes below ~15 nm usually occur in the anatase form and transform to rutile as they grow because rutile has lower bulk free energy as compared to anatase, which has the lower interfacial free energy.[3,8,9]

Depending on reaction conditions, anatase nanocrystals may transform to rutile by dissolution-precipitation, interface-nucleation, or a combination of both.[6,7,10,11] It has been experimentally shown that the dissolution-precipitation

* Reprinted with permission from Sabyrov, K., Adamson, V. and Penn, R. L. *CrystEngComm* **2014**, *16,* 1488-1495. Published by The Royal Society of Chemistry.

transformation begins with the growth of fine anatase nanocrystals in suspension.[6] Presumably, once they reach a critical size, they start dissolving due to thermodynamic instability, and the more stable phase, rutile, nucleates homogeneously from the solution and coarsens at the expense of anatase nanocrystals until all the anatase nanocrystals are consumed. In this mechanism, the rate of transformation is dependent on the relative solubilities of anatase and rutile. Subsequently, the rate depends on factors affecting solubility, such as crystallite size, aggregation state, aging temperature, pH of the suspension, ionic strength, and type of solvent. For example, our previous work demonstrated that, at sufficiently acidic conditions, the anatase to rutile phase transformation kinetics fit well to a mathematical model describing the dissolution-precipitation mechanism, and the rate was highly dependent on anatase nanocrystal size.[6]

At the other end of the spectrum is the interface-nucleation mechanism, by which rutile heterogeneously nucleates atanatase nanocrystal interfaces and subsequently grows at a constant rate by solid-state transformation.[10,11] The rate of the transformation is significantly affected by initial anatase size and aggregation state (*e.g.*, the compactness of the aggregated nanocrystals) because smaller nanocrystals and more aggregated nanoparticles may have a higher frequency of particle-particle contacts that can act as nucleation sites for rutile.[6,12,13] Such an interface-nucleation mechanism was suggested by Zhang and Banfield based on the results obtained by treating dry anatase nanocrystals in air at 465 °C – 525 °C.[11] Moreover, Penn and Banfield showed the nucleation

of rutile at anatase twin boundaries when anatase nanocrystals were hydrothermally treated at low pH at 250 °C for just a few hours.[14]

Most anatase to rutile phase transformation experiments have been carried out by heating dry anatase samples at high temperature in air.[5,11,12,15] Depending on reaction conditions, anatase nanocrystals have been shown to transform to rutile via interface nucleation, surface nucleation, and bulk nucleation.[10,11] However, the transformation mechanism of anatase nanocrystals treated in aqueous suspension is unclear due to a large number of factors affecting the transformation including particle growth, aggregation state, surface hydration, and solubility.

In this work the effects of initial crystallite size and aging temperature on the anatase to rutile phase transformation were characterized to better understand the anatase to rutile transformation mechanism in aqueous suspension. The particle size and aging temperature were systematically changed while reaction parameters, such as pH and ionic strength, particle concentration, and type of solvent were fixed. X-ray diffraction (XRD) was used to monitor average anatase and rutile crystallite sizes as well as the phase composition of samples, and high-resolution transmission electron microscopy was (HRTEM) used to characterize the morphology and microstructure of the nanocrystals. Finally, the anatase to rutile phase transformation kinetic data were fit to mathematical models describing the dissolution-precipitation and interface-nucleation mechanisms. Results demonstrate that interfacial nucleation plays an

important role in the anatase to rutile phase transformation in acidic aqueous suspensions.

Experimental methods

Synthesis

Anatase nanoparticles were synthesized via a modified sol–gel method.[16] Briefly, 12.5 mL of titanium isopropoxide (Aldrich) was dissolved in 125 mL isopropanol (Fisher, HPLC grade) and cooled using an ice bath (~3 °C).The titanium isopropoxide precursor was hydrolyzed using a nitric acid (Mallinckrodt) solution (pH -0.6). The nitric acid solution was added dropwise with addition rate of 1 drop/10 s with continuous stirring. The ratio of 1:100 for Ti:H_2O was used in all sample syntheses. The suspension then was refluxed for 24 h at ~83 °C using a cold-water condenser to prevent concentration. Finally, the obtained milky white suspension was dialyzed (Spectra/Por) against Milli-Q (Millipore Corporation) water for 10–15 days. The water of the dialysis was changed several times per day. The goal of the dialysis step was to remove any water soluble impurities and to avoid washing and drying step which usually changes the aggregation state of the newly synthesized nanoparticles.[17,18] A salt solution was added to change the particle size of the final anatase product by changing the ionic strength of the solution during synthesis. For the synthesis of 3.1 nm anatase, 2 M $NaNO_3$ solution was added during hydrolysis of titanium isopropoxide, and 2.5 M NaCl solution was added during reflux for the synthesis

of 6.0 nm anatase. For 3.7 nm anatase, pure water was added during hydrolysis step.

Hydrothermal processing

The pH values (at room temperature) of the original dialyzed suspensions were adjusted to 1.0 using nitric acid. Then, 8 mL of the suspensions were placed into a 23 mL Teflon liner of a Parr Instrument autoclave bomb and aged in oven for 1–75 h at 200 °C, 225 °C, and 250 °C. After aging, bombs were removed from the oven and allowed to cool to room temperature. The room temperature pH values of the suspensions were 1.0±0.3 after treatment.

Characterization

All samples in this work were characterized by powder XRD to measure the change in phase composition and particle size as the samples were hydrothermally processed. The samples were prepared by drying several drops of the resulting aqueous suspensions on a zero-background quartz slide. The XRD patterns were collected over 24°–62° 2θ range using PANalytical X'Pert Pro diffractometer equipped with a high-speed X'Celerator and Co Kα radiation source. The scanning was continuous with an effective dwell time of 765 s and step size of 0.016°. A 1° antiscattering slit and a 0.5° divergent slit were used in all measurements.

For quantitative analyses of phase composition and particle size Rietveld refinements were performed as described by Isley and Penn.[19,20] X'Pert High

Score Plus software was used in the refinements to simulate a theoretical line profile until it matches the experimental profile. The only parameters refined were zero shift (° 2θ), scale factor, preferred orientation, W, U and V profile parameters and unit cell parameters. The other parameters were fixed such as peak shapes, thermal parameters, fractional atomic coordinates, roughness parameters, the extinction, and porosity. The simulations were carried out until minimum possible values for goodness-of-fit (GoF) and R weighted profile (Rwp) were obtained. Finally, Scherrer equation was used to determine the average size of the nanoparticles from peak broadening.[21] Average anatase and rutile sizes were calculated from the full widths at half maximum of the anatase (101) and rutile (110) peaks after correcting for instrumental broadening. The error bars were determined by analyzing two repetitions of Rietveld refinement on the same sample.

Hydrothermally treated suspensions were further characterized by transmission electron microscopy (TEM) and high-resolution transmission electron microscopy (HRTEM) to analyze the morphology and microstructure of the resulting nanocrystals. The suspensions were first diluted with Milli-Q water and a drop of the suspension was placed and dried on a TEM copper grid with a holey carbon film (200 mesh Cu grid, SPI supplies).

Results and discussion

Hydrothermal treatment of 3.1 nm anatase at 200 °C and pH 1 results in anatase crystal growth as well as phase transformation to rutile (Figure 3.1a). No

other phases, including brookite, were detected. The average crystallite size of the first detected rutile (72 nm at 15 h) was *ca*. 7 times larger by size and nearly 400 times larger by volume than the average anatase crystallite size (10 nm at 15 h) at that same time. The total rutile content at this point was *ca*. 18%. Figure 3.1b is a plot of the average anatase and rutile crystallite sizes as a function of aging time as determined from the XRD patterns shown in Figure 3.1a. In all aged samples, average rutile size was substantially larger than the average anatase size (supporting information, Figure A.1).

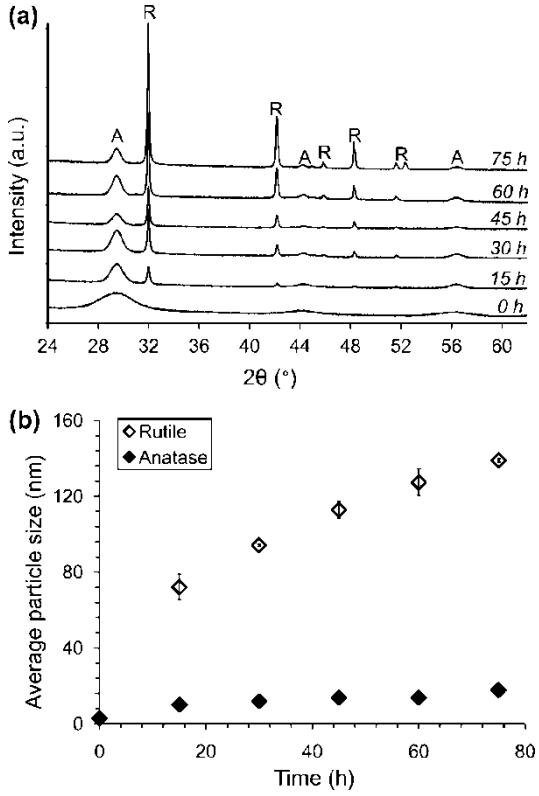

Figure 3.1 (a) XRD patterns of anatase samples hydrothermally treated at 200 °C, an initial room temperature pH of 1, and an initial anatase crystallite size of 3.1 nm. Material was sampled at the specified times. Only anatase and rutile were detected, and peaks for anatase and rutile are labeled with A and R, respectively. (b) The average anatase and rutile sizes as a function of aging time as determined from the XRD patterns shown in (a).

The data obtained from the TEM characterization of the samples support the results obtained from XRD characterization. Figure 3.2 shows TEM and HRTEM (inset) images of the 3.1 nm anatase sample after hydrothermal treatment for 45 h at 200 °C. Smaller nanocrystals with different shapes, including the truncated bi-pyramidal shape, are anatase, as identified by lattice fringe measurements. The lattice fringes apparent in the HRTEM image shown in the inset of Figure 3.2a are consistent with the {101} of anatase. The lattice fringes of the larger nanocrystals, such as shown in Figure 3.2b, match the d-spacing for the {110} of rutile.

The observation that rutile is substantially larger in size than anatase at all time points (Figure 3.1b) is consistent with the lower total free energy of rutile as compared to anatase once a critical anatase crystal size has been reached. In particular, once rutile nucleates, rapid growth of rutile is expected to lead to a substantial drop in total bulk and interfacial free energies. After reaching the critical size, anatase phase transforms to rutile leading to a lower total bulk free energy due to the lower bulk energy of rutile. The total interfacial free energy also decreases as anatase transforms to rutile due to the dramatic decrease in total surface area as larger rutile nanoparticles grow at the expense of smaller anatase nanoparticles. Thus, once comparatively large rutile is present, anatase crystallites will be substantially more soluble than rutile, both due to the larger bulk energy and comparatively small size of the anatase present. From the perspective of the dissolution and precipitation mechanism, a large disparity in

solubility for the small anatase versus the large rutile crystals would be expected to lead to rapid growth of rutile at the expense of anatase. Thus, little growth of anatase would also be expected. Indeed, this is observed in the experimental kinetic data.

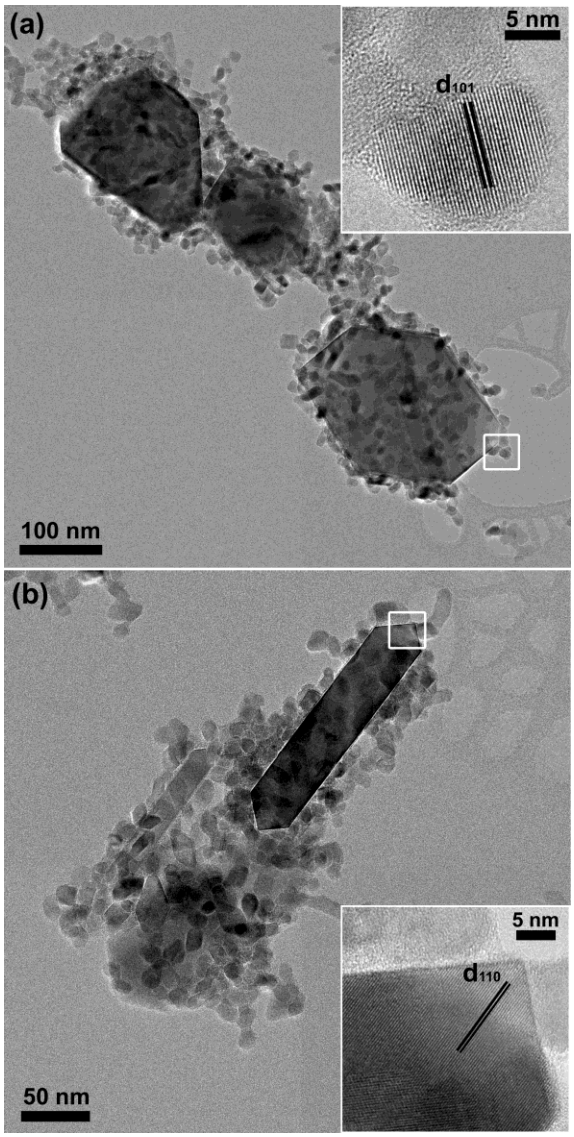

Figure 3.2 TEM and HRTEM images of the sample aged at 200 °C for 45 h. Smaller and larger nanocrystals were identified as anatase and rutile, respectively. HRTEM images of anatase and rutile nanocrystals in the inset of (a) and (b), respectively. Insets show the images of the region labeled with white boxes.

Further analysis of the phase transformation data reveal that the initial anatase nanocrystallite size and aging temperature affect the transformation significantly. Figure 3.3 presents the change in anatase and rutile contents as a function of aging time for the samples initially containing 3.1 nm, 3.7 nm and 6.0 nm anatase particles. The rate of phase transformation from anatase to rutile was slowest for the sample with the largest initial anatase average size (6.0 nm). According to the plot, 3.1 nm and 3.7 nm particles showed similar transformation rates. The effect of aging temperature for all three samples was consistent; the transformation rates increased with increasing temperature.

A dissolution-precipitation model, which was developed in our previous work, was used to fit the data points obtained in this work:[6]

$$\ln\left[(1-\alpha)\left(\frac{D_0}{D_t}\right)^3\right] = -kt \qquad (1)$$

where α is the weight fraction of the anatase nanoparticles transformed (or weight fraction of rutile nanoparticles formed) at time *t*, *k* is the transformation rate constant, and D_0 and D_t are the average diameters of anatase nanoparticles at time $t = 0$ and time *t*, respectively. Figure 3.4a, 3.4b, and 3.4c show the plots obtained from application of the model to the transformation data from the 3.1 nm, 3.7 nm, and 6.0 nm anatase nanoparticles, respectively.

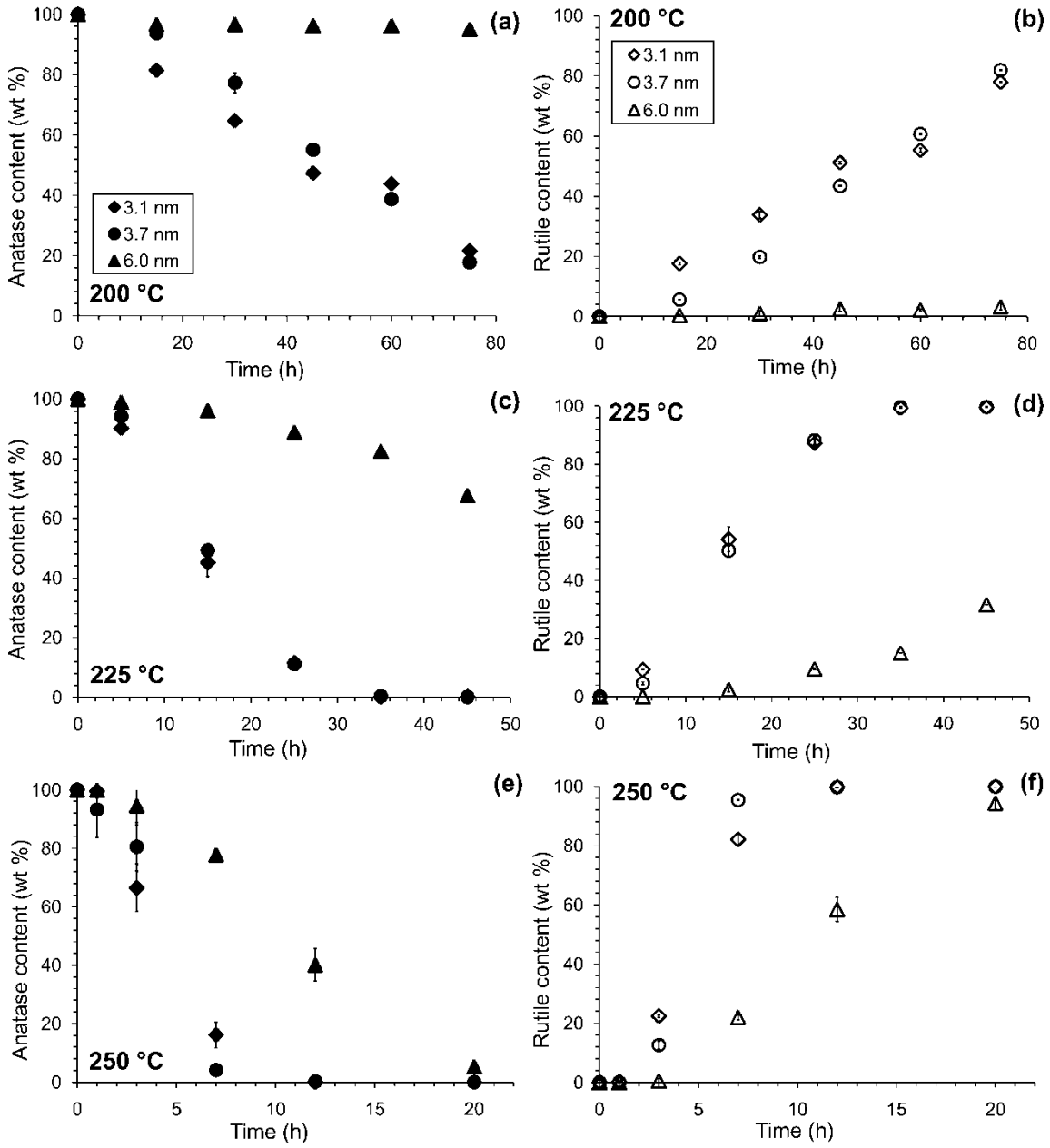

Figure 3.3 Figures present the change in phase content of the samples aged at 200 °C (a and b), 225 °C (c and d), and 250 °C (e and f) for different time periods. pH 1 was used in all suspensions.

For all samples, the data were fit fairly well by the model for the experiments at 250 °C, as indicated by the coefficients of determination (R^2). However, the fits were poor at lower temperatures as the data points at early

times deviated substantially from the model. In addition, the model produced better fits for data from experiments using the smaller initial anatase particle sizes (3.1 and 3.7 nm) than for the larger ones (6.0 nm). In Figure 3.4d, the coefficient of determination was plotted against aging temperature for all samples to highlight the progressively poorer fit as a function of decreasing temperature and increasing size.

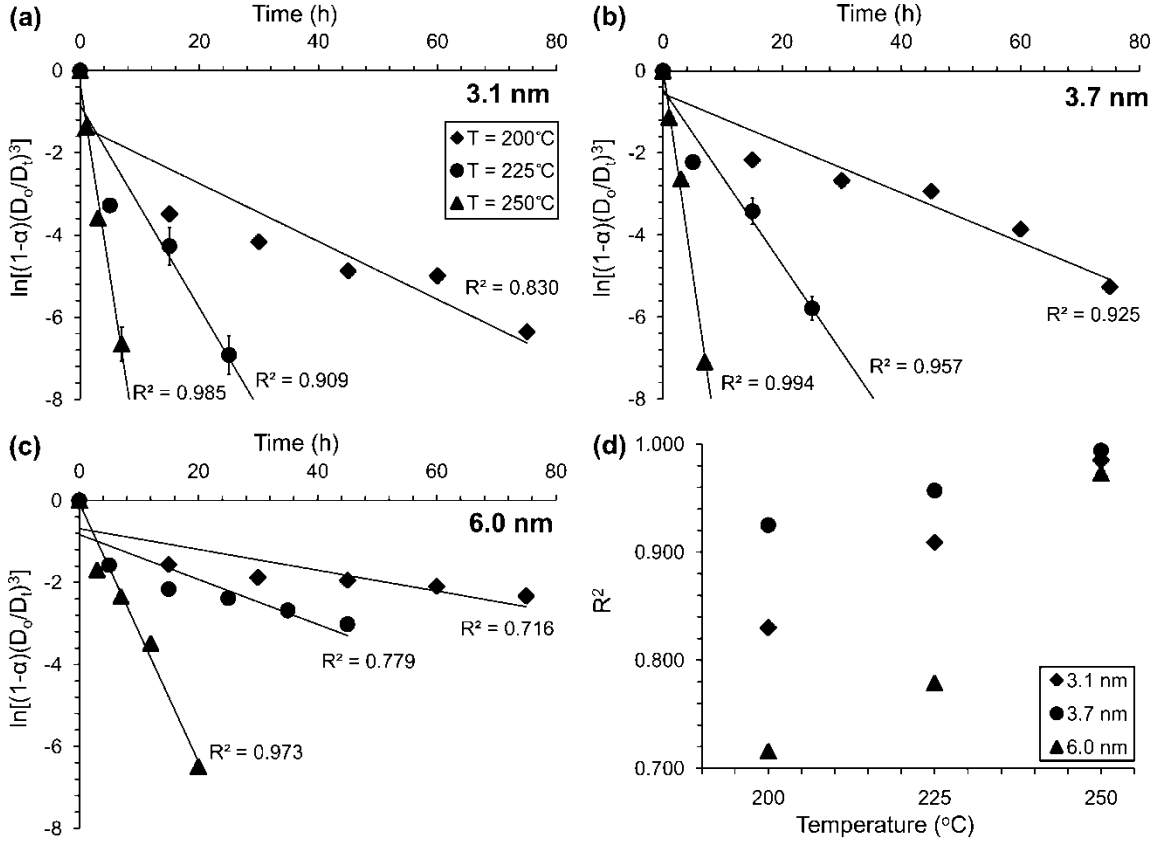

Figure 3.4 The plots obtained by applying Equation 1 to the transformation of 3.1 nm (a), 3.7 nm (b), and 6.0 nm (c) anatase nanoparticles aged at 200 °C, 225 °C, and 250 °C. Coefficients of determination (R^2) are shown to indicate how well the data points fit the equation. (d) R^2 values (obtained from panels a, b and c) as a function of transformation temperature.

The deviations observed in the application of the dissolution-precipitation model to the transformation data suggest that this model does not holistically

describe the fundamental mechanisms driving the phase transformation. The good fits obtained using the dissolution-precipitation model for experiments performed at 250 °C may indicate that the dissolution-precipitation mechanism is the dominant one at this temperature. This would be consistent with the higher solubility of titania at higher temperatures. Furthermore, as discussed above, the comparatively higher solubility of anatase nanocrystals would be expected to lead to rapid growth of rutile nanoparticles at the expense of anatase.[2,8] At lower aging temperatures, however, the observed, significant deviations from the model may indicate that the contribution to crystal growth by the dissolution-precipitation mechanism has decreased, perhaps due to the lower solubility of anatase nanoparticles. If an aggregative mechanism were at play, it could become more apparent at the lower temperatures.

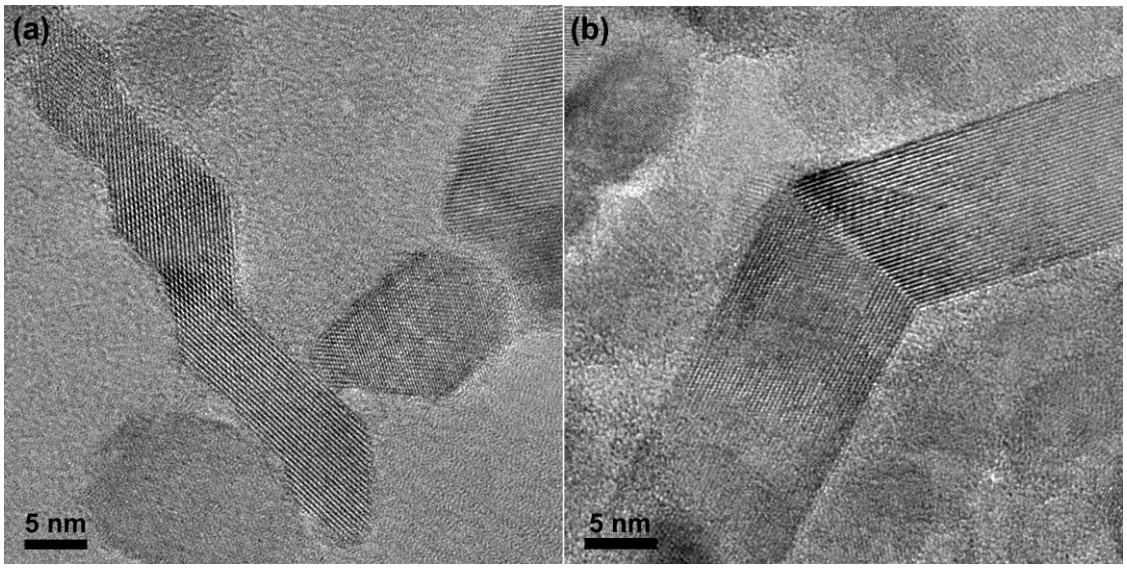

Figure 3.5 HRTEM images of the sample aged at 200 °C for 45 h. The image of a single crystalline anatase formed from oriented aggregation of several primary nanocrystals (a). The image of a twinned rutile nanocrystal (b). The angular relationship between the two arms of the rutile twin is close to that expected for anatase twinned across the {112} face.

The morphology and microstructure of the aged materials were examined using HRTEM as it can provide detailed information about the transformation mechanisms.[14,22] Anatase nanocrystals from the sample aged for 45 h at 200 °C were commonly observed to have morphologies indicative of crystal growth by oriented aggregation (Figure 3.5a). Figure 3.5b shows HRTEM image of twinned rutile nanocrystal in the same sample. Images like those shown in Figure 3.5a serve to highlight a second crystal growth mechanism that is clearly operating in these samples. Thus, models for the phase transformation kinetics must include growth by oriented aggregation. In addition, the rutile twins observed in this work are consistent with those observed by Penn and Banfield, in which they described the nucleation of rutile from anatase {112} twin boundaries.[14]

The growth of 3.1 nm anatase nanoparticles by oriented aggregation and the presence of twinned rutile nanocrystals in the same sample suggest that a competing mechanism might be interface-nucleation. Anatase twin boundaries, which can be formed by oriented aggregation, can act as nucleation sites for rutile by decreasing the energy barrier for nucleation of rutile.[14] Specifically, as anatase twin boundaries contain structural elements common to rutile, nucleation occurs by displacement of only one half of the titanium cations. Further rutile growth involves the breakage of only 7 of 24 Ti-O bonds per unit cell. Subsequently, the adjacent anatase octahedra would be destabilized, which would lead to a reduced activation energy for the phase transformation and, thus, rapid progression of the transformation into the bulk material. Twinned rutile

nanocrystals, such as shown in Figure 3.5b, might be products of the transformation by the same mechanism in which rutile nanocrystals have preserved the parent anatase twin morphology.[14]

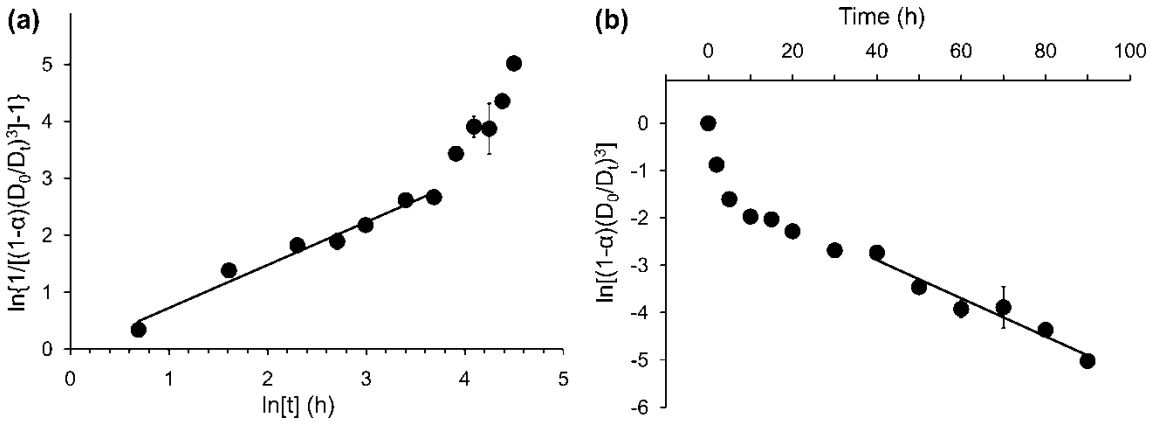

Figure 3.6 Plots obtained by application of interface-nucleation and dissolution-precipitation models to the transformation of 3.7 nm anatase at 200 °C and pH 1. (a) Plot of the left-hand side of Equation 2 vs. ln[t] (natural logarithm of time) and (b) the left-hand side of the Equation 1 vs. t (time). Linear regression was applied to the portion of the data obtained before (a) and after (b) 40 h of aging. The grain growth exponent (m) derived from the slope of the regression line obtained using interface-nucleation model is 4.2.

The interface-nucleation model, which was developed by Zhang and Banfield, was applied to the transformation of 3.7 nm anatase sample aged at 200 °C and pH 1:[11]

$$\ln\left[\frac{1}{(1-\alpha)(D_0/D_t)^3}-1\right]=\ln k+\left(\frac{m-1}{m}\right)\ln t \qquad (2)$$

where the variables common with Equation 1 represent those same parameters, and *m* is the grain growth exponent, which represents the grain growth behaviour of the nanocrystals and usually falls between 2 – 4.[23] For this work, 3.7 nm anatase sample aged at 200 °C was selected because it had substantial

deviation from the dissolution-precipitation model and evidence of crystal growth by oriented aggregation. The plots presented in Figure 3.6a and 3.6b were obtained by the application of interface-nucleation (Equation 2) and dissolution-precipitation (Equation 1) models, respectively. For both models linearity of the plots is expected if the models describe the transformation mechanism. The interface-nucleation model was applicable for the experimental data obtained before 40 h of aging, whereas dissolution-precipitation model described well the portion of the data after 40 h.

According to the results, anatase nanocrystals aged in acidic aqueous solution at elevated temperature exhibit a two-step phase transformation. At the early stages of the transformation, interface-nucleation is the dominant mechanism. At these stages, the rate of the interface-nucleation is assumed to be substantially higher than the rate of the dissolution-precipitation. An increase in aggregation, and thus particle-particle contacts, is expected with decreasing particle size, which would result in an increase in the number of nucleation sites. In addition, particle growth by oriented aggregation has been shown to affect the transformation kinetics significantly.[14] It has been experimentally shown that the kinetics of particle growth by oriented aggregation highly depend on crystallite size and that the contribution to crystal growth is at its maximum during the early stages of aging, *i.e*., when the nanocrystals are at their smallest.[24-28] In this project, the crystal growth by oriented aggregation might occur via intra-aggregate rearrangement of the anatase nanoparticles as they were

hydrothermally treated. Before treatment, the anatase nanoparticles were shown to be highly aggregated using cryogenic transmission electron microscopy.[6] In addition, evidence for crystal growth by oriented aggregation has been observed for highly flocculated iron oxide nanoparticles in aqueous suspension.[25]

At later stages, crystal growth by oriented aggregation appears to slow dramatically, which is consistent with the larger average crystal size. According to the proposed two-step model, the frequency of new rutile nucleation would drop off substantially, presumably due to the negligible frequency of interface-nucleation. In fact, once interface-nucleation slowed dramatically, the increase in the number concentration of rutile crystals was observed to slow as well. The number concentration of rutile was estimated using the known mass loading of titania in the aqueous suspension, the weight fraction of rutile (α) derived by Rietveld refinement of the XRD pattern, and the average volume of rutile nanocrystals. The average volume was calculated using the average nanocrystal size determined by Scherrer equation and assuming rutile nanocrystals as spheres. According to the estimate, the number concentration of rutile levelled off after ~40 h of aging, suggesting a substantial decrease in the frequency of nucleation of new rutile (supporting information, Figure A.2). Thus, it can be concluded that during the second stage of growth, the increase in total rutile content primarily results from dissolution of the more soluble and smaller anatase particles and precipitation onto the larger and already existing rutile crystals.

The good fit for the interface-nucleation model at the early stages of

transformation strongly suggest that rutile nucleates at particle-particle interfaces. However, after nucleation rutile can grow by solid-state transformation, dissolution-precipitation, or both depending on the aging conditions as observed in the present and in previous work.[14] Even under high temperature hydrothermal conditions, at which nanoparticles have comparatively high solubility and predominantly transform by dissolution-precipitation, nucleation of rutile might take place at the particle interfaces. In fact, examination of HRTEM images of samples aged at 250 °C demonstrates that crystal growth by oriented aggregation occurs under those conditions. In this case, the effect of the nucleation event cannot be seen in the application of the dissolution-precipitation model because the net gain in rutile content via nucleation is small as compared to the net gain in rutile content via precipitation of material onto existing rutile crystals. Indeed, the absence of rutile nanoparticles with sizes similar to the anatase crystals and observations of partially transformed nanoparticles in the samples suggests rapid coarsening of rutile as compared to the frequency of rutile nucleation.

A significant increase in the rutile production rate by dissolution-precipitation at later stages, at which rutile nanocrystals are substantially larger than anatase nanocrystals, is in line with the higher solubility of anatase crystallites as compared to the larger rutile. Similar phenomena were observed in the growth of iron oxide nanoparticles in aqueous suspension. Using *in situ* TEM liquid cell, it was observed that small (<5 nm) but stable iron oxide nanoparticles

dissolve when they encounter large iron oxide nanoparticles.[29] Similarly, comparatively small anatase nanoparticles may be attracted to large rutile nanoparticles and phase transform by rapid and local dissolution and precipitation. In addition to the difference in free energies of anatase and rutile, the curvature dependence of the free energy is likely a primary driving factor for the dissolution of smaller anatase nanocrystals in the vicinity of larger rutile nanocrystals.

Conclusions

Particle size and aging temperature have substantial effects on the transformation mechanism of anatase nanoparticles aged in acidic solution (pH 1). At sufficiently high temperatures, the kinetics of the phase transformation of small anatase nanoparticles to rutile are dominated by the dissolution-precipitation mechanism, presumably due to the higher solubility of the anatase nanoparticles. At lower aging temperatures, the phase transformation kinetics are well described by a two-step phase transformation. The early stages of the transformation are dominated by interface-nucleation as evidenced by excellent fit of the model to the experimental data. However, at later stages, the dominant mechanism is dissolution-precipitation. These results are consistent with the idea that the interface-nucleation occurring at interfaces produced by oriented aggregation decreases with increasing particle size.

Acknowledgements

We acknowledge financial support from the University of Minnesota, the National Science Foundation (No. NSF-0957696), and the Nanostructural Materials and Processes Program at the University of Minnesota. We also thank the Characterization Facility at the University of Minnesota, the member of the NSF-funded Materials Research Facilities Network (www.mrfn.org).

Chapter 4: A Kinetic Model for Two-Step Phase Transformation of Hydrothermally Treated Nanocrystalline Anatase*

Introduction

Hybrid nanostructures may exhibit novel properties ensuing from atomic-scale interactions at interfaces and synergistic effects of the phases present. For example, numerous studies have demonstrated that mixed-phase samples of anatase and rutile possess higher catalytic activity than anatase or rutile alone due to increased separation of photoexcited charge carriers in the mixture.[1,2] The main driving force for enhanced charge transfer is the energetic alignment of band edges of the individual polymorphs. Band alignment of anatase and rutile occurs due to close electronic interactions at the interfaces between the phases. Engineering nanoarchitectures with clean and abundant interfaces of a specific type is a major challenge facing materials scientists developing inorganic semiconductor-based photocatalysts. Controlling the anatase to rutile phase transformation could lead to the purposeful preparation of materials with novel properties.

Fitting experimental data using mathematical modeling has led to substantial insights into the mechanisms of phase transformation.[3-6] Zhang and

* A report on this research project is submitted for publication.
Sabyrov, K. and Penn, R. L. *Chemistry of Materials*, **(under review)**.

Banfield developed an interface-nucleation (IN) model to characterize the phase transformation of nanocrystalline anatase heated (465–525 °C) in air:[7]

$$\ln\left[\frac{1}{(1-\alpha)(D_0/D_t)^3}-1\right]=\ln[k_{in}N_0]+\ln t \qquad (1)$$

where α is the weight fraction of anatase nanoparticles transformed at time t, k_{in} is the transformation rate constant for IN, N_0 represent initial number of particles in anatase sample, and D_0 and D_t are the average diameters of anatase nanocrystallites at time $t = 0$ and time t, respectively. Zhang and Banfield extracted important mechanistic information by applying the model to experimental data. Transformation kinetics were found to strongly depend on anatase crystallite size and aging temperature, with the transformation second order with respect to the number of anatase particles present.

The transformation mechanism was further elucidated by quantifying the dependence of activation energy and the pre-exponential factor on crystallite size.[8] While activation energy varied only slightly with particle size, the pre-exponential factor was inversely proportional to particle size to approximately the fourth power. The larger pre-exponential factor for the small nanocrystals was attributed to a higher number of particle-particle contacts per unit volume. Thus, the probability for rutile nucleation is higher for smaller as compared to larger nanocrystals. Furthermore, a transformation mechanism second order with respect to the number of anatase particles is consistent with nucleation involving two primary anatase particles. Finally, the activation energy was found to be much lower than the activation energy values reported in the literature. The

apparent difference in the activation energy values is consistent with the IN model, which includes the effect of surface area on the transformation mechanism.

These results are consistent with previous work in which an atomic scale mechanism was proposed for nucleation of rutile.[9] According to Penn and Banfield, the nucleation could be facilitated by the structural elements present at anatase twin boundaries. Anatase {112} twins have one-half their octahedra arranged in a rutile-like structure. These rutile structural elements were hypothesized to trigger the anatase to rutile phase transformation and serve as sites for rutile nucleation. As a consequence, smaller anatase nanocrystals might lead to higher rutile nucleation and growth rates due to higher frequency of twin boundaries for the same total mass.

In our previous work, the phase transformation kinetics of hydrothermally treated nanocrystalline anatase was explored using a mathematical model to fit experimental results.[3] Nanocrystalline anatase was revealed to transform to rutile predominantly via dissolution-precipitation (DP) mechanism in acidic aqueous solutions at 250 °C. We derived a kinetic model assuming rapid dissolution of anatase nanocrystals and re-precipitation onto rutile under acidic hydrothermal conditions:

$$\ln\left[(1-\alpha)\left(\frac{D_0}{D_t}\right)^3\right] = -k_{dp}t \qquad (2)$$

where the variables common with Equation 1 represent those same parameters and k_{dp} is the rate constant for DP. The kinetic model fit the experimental data well only at the most acidic conditions (pH 1, 250 °C), confirming the importance of TiO_2 nanocrystal solubility in the transformation. However, significant deviations between the kinetic model and the experimental data were observed at aging conditions at which TiO_2 nanocrystals have lower solubility (i.e., pH 3.0 at 250 °C), indicating another mechanism could be contributing to the overall transformation. By applying the corresponding mathematical models to the experimental data, the authors concluded that IN competed with DP.[4]

Indeed, under these hydrothermal conditions, nanocrystalline anatase transforms to rutile via a two-step mechanism: IN followed by DP.[4] At the early stages, IN dominates the transformation, presumably due to smaller size of anatase nanocrystals. Smaller anatase nanocrystals grow more rapidly by oriented aggregation, thus generating more interfaces and potential nucleation sites for rutile. At later stages, the contribution of IN decreases dramatically as nanocrystal size increases, leading to increased contribution to the overall production of rutile by DP. This observation was further confirmed by the study on the change in number concentration of rutile crystals as a function of aging time.[4] As the weight fraction of rutile steadily increased, no concurrent increase in the number concentration of rutile crystallites was observed. This observation is

consistent with later rutile production by monomer-by-monomer growth of rutile at the expense of anatase as opposed to the formation of new rutile particles by IN. Here, we describe a general kinetic model derived by combining the IN and DP models. Experimental data tracking both the phase composition as well as the average sizes of anatase and rutile nanocrystals were analyzed using the combined model (CM) as well as each individual kinetic model. The combined kinetic model describes the two-step anatase to rutile transformation well. Furthermore, the CM was shown to fit the transformation data well at all conditions explored in this work and enabled quantification of the relative contributions to rutile production by IN and DP over time. Importantly, the relative contribution to overall rutile production by each of the two mechanisms can be quantified, providing detailed insight into the major control parameters for the anatase to rutile phase transformation under solvothermal conditions. Generally speaking, the contribution to the overall phase transformation by DP increases with increasing solubility. However, results demonstrate the importance of IN under all conditions explored. Results are expected to lead to improved control over the phase transformation.

Experimental section

Synthesis

The experimental data for the anatase to rutile phase transformation at pH 1.0 and 3.0 (250 °C) were obtained from our previous work.[3] For the investigation

of the transformation at pH 2.2 and 250 °C anatase samples were freshly prepared via a sol-gel method that has been previously published.[3,4] Briefly, 12.5 mL of titanium isopropoxide (Aldrich) was mixed with 125 mL isopropanol (Fisher, HPLC grade) and the mixture was cooled in an ice bath (~3 °C) for ~30 minutes under constant magnetic stirring. The nitric acid (Mallinckrodt) solution (4 M or pH −0.6) was used as a catalyst to hydrolyze titanium isopropoxide. The acid solution was added dropwise using a burette at a rate of 1 drop/10 seconds with continuous stirring (a ratio of 1:100 for Ti:H_2O was used). The obtained clear solution was refluxed at ~83 °C (boiling point of isopropanol) for ~ 1 day. A cold-water condenser was used to prevent concentration of the sample. After 30 minutes of refluxing the clear solution/suspension changed to milky white suspension, which might indicate the precipitation of anatase nanocrystals or aggregation of dispersed primary anatase nanocrystals. Then the obtained white suspension was dialyzed (Spectra/Por) against Milli-Q (Millipore Corporation) water for 10–15 days to remove any water soluble impurities and avoid the washing and drying step.

Hydrothermal processing

To prepare samples for hydrothermal treatment, the pH of each dialyzed suspension was adjusted to 1.0, 2.2, and 3.0 using nitric acid. Then, the acidified suspensions were placed into a 23 mL Teflon liner of a Parr Instrument autoclave bomb and placed into a pre-heated oven held at 250 °C and aged for 1–90 hours. The autoclave bombs were naturally cooled to room temperature before

characterization. At room temperature, insignificant pH deviations were observed (±0.3).

Characterization

The samples were characterized by powder X-ray diffraction (XRD). Several drops of the hydrothermally treated suspensions were placed directly onto zero-background quartz slides and allowed to dry in air at room temperature. XRD patterns were collected using PANalytical X'Pert Pro diffractometer equipped with a high-speed X'Celerator and Co K*α* radiation source. Continuous scanning was used to collect the XRD patterns, and the dwell time and step size used were 765 seconds and 0.016°, respectively. In all measurements a 1° antiscattering and a 0.5° divergent slits were used.

Rietveld refinement was performed using X'Pert High Score Plus software to quantify average crystallite domain size and phase composition of each sample. The parameters were simulated until the theoretical line profile matches the experimental line profile, and the quality of the fits were monitored by goodness-of-fit (GoF) and R weighted profile (Rwp) values. The refined parameters were zero shift (° 2θ), scale factor, preferred orientation, W, U and V profile parameters and unit cell parameters. Peak shapes, thermal parameters, fractional atomic coordinates, roughness parameters, the extinction, and porosity were fixed. ° 2θ and the full widths at half maximum values were extracted from the simulated line profile to calculate average crystallite size of the sample using

Scherrer equation.[10] The peaks used for anatase and rutile size determination were (101) and (110), respectively.

Hydrothermally treated samples were also characterized by high-resolution transmission electron microscope (HRTEM) for the analysis of microstructure and morphology of the nanocrystals. Suspensions were diluted ~10 times with Milli-Q water and a small drop of the diluted suspension was deposited onto a transmission electron microscopy (TEM) copper grid coated with a holey carbon film (200 mesh grid, SPI supplies). Then, the drop on the grid was allowed to dry at room temperature and in air.

Results and discussion

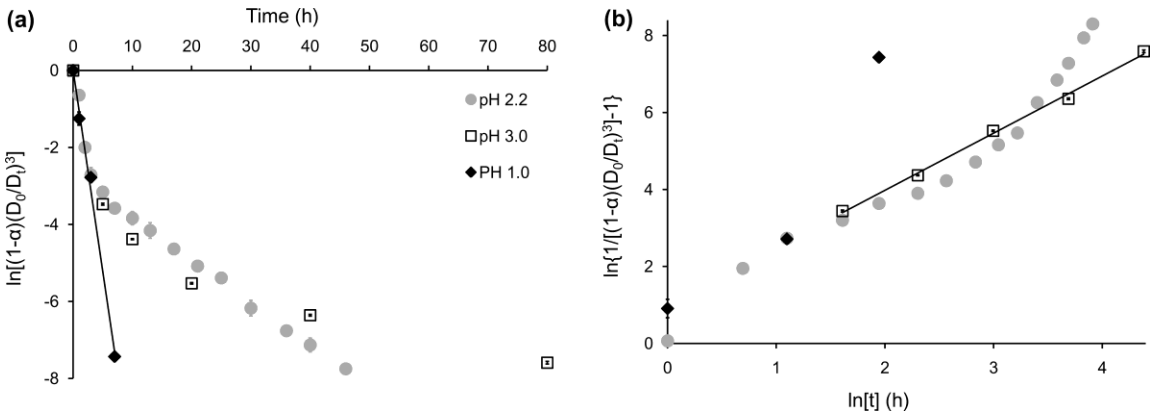

Figure 4.1 Plots obtained by applying (a) dissolution-precipitation (DP) and (b) interface-nucleation (IN) models to the experimental data obtained from the hydrothermal treatment of suspensions at pH 1.0 (dark, closed diamonds)3, pH 2.2 (grey, closed circles), and pH 3.0 (open squares). The straight lines represent linear fit of the corresponding equations to the experimental data.

Excellent fits using the DP model (Equation 1) were obtained for experimental data collected from samples hydrothermally treated at pH 1.0 and

250 °C, and excellent fits were obtained using the IN model (Equation 2) for experimental data from experiments performed at pH 3.0 and 250 °C, as presented in Figure 4.1. However, neither model produced adequate fits for data tracking the transformation at the intermediate pH of 2.2, as shown by the lack of a linear trend in the plots shown in Figures 4.1a (DP model) and 4.1b (IN model). These results highlight the need for a new kinetic model.

The DP and IN models were combined to derive a more general kinetic model that enables quantitative assessment of the contribution to the rate of phase transformation by each mechanism. As DP and IN are first and second order with respect to number of anatase particles (*N*), respectively,[3,7] and the rate determining step for both mechanisms is the nucleation of rutile,[11] the overall transformation rate can be expressed in terms of *N* according to the relation:

$$-\frac{dN}{dt} = k_{dp}N + k_{in}N^2 \qquad (3)$$

where k_{dp} and k_{in} are transformation constants for DP and IN, respectively. As Equation 3 has the same mathematical form as the kinetic equation used by Zhang and Banfield to characterize simultaneous transformation of nanocrystalline anatase samples treated at elevated temperatures in air, and as the same fundamental assumptions are valid, the final form of the CM is the same as their kinetic model:[5]

$$\ln\left[\frac{k_{dp}}{(1-\alpha)}\left(\frac{D_t}{D_0}\right)^3 + k_{in}N_0\right] = k_{dp}t + \ln(k_{dp} + k_{in}N_0) \qquad (4)$$

which can be rearranged to facilitate analysis of the experimental data:

$$\frac{(D_t / D_0)^3}{(1-\alpha)} - 1 = \left(1 + \frac{k_{in} N_0}{k_{dp}}\right)(e^{k_{dp} t} - 1) \quad (5)$$

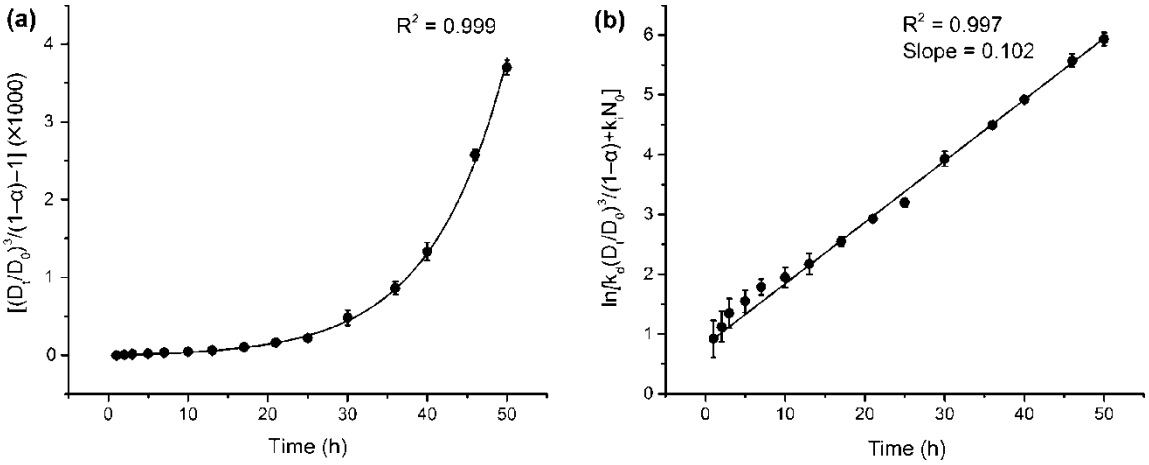

Figure 4.2 Plots presenting the application of the CM to the experimental data obtained at pH 2.2.The plot obtained by performing non-linear curve fitting method using the right-hand side of the Equation 5 on the experimental data points calculated using the left-hand side of the same equation (a). Linear relationship between the data points calculated using left-hand side of the Equation 4 and time (b). R^2 values are shown to indicate how well the data points were fit by the equations.

Figure 4.2 shows the experimental data collected for samples treated at pH 2.2 and 250 °C with the fit using the CM. The plot in Figure 4.2a presents experimental data resulting from application of the left-hand side of Equation 5 to the experimentally measured parameters as a function of aging time. The transformation rate constants (k_{dp} and $k_{in}N_0$) were then extracted from the plot by fitting the right-hand side of the same equation using non-linear least squares fitting. These constants were then used to examine the applicability of the kinetic model by integrating them into the Equation 4. The plot presented in Figure 4.2b

demonstrates a linear relationship between the left-hand side of the Equation 4 versus time.

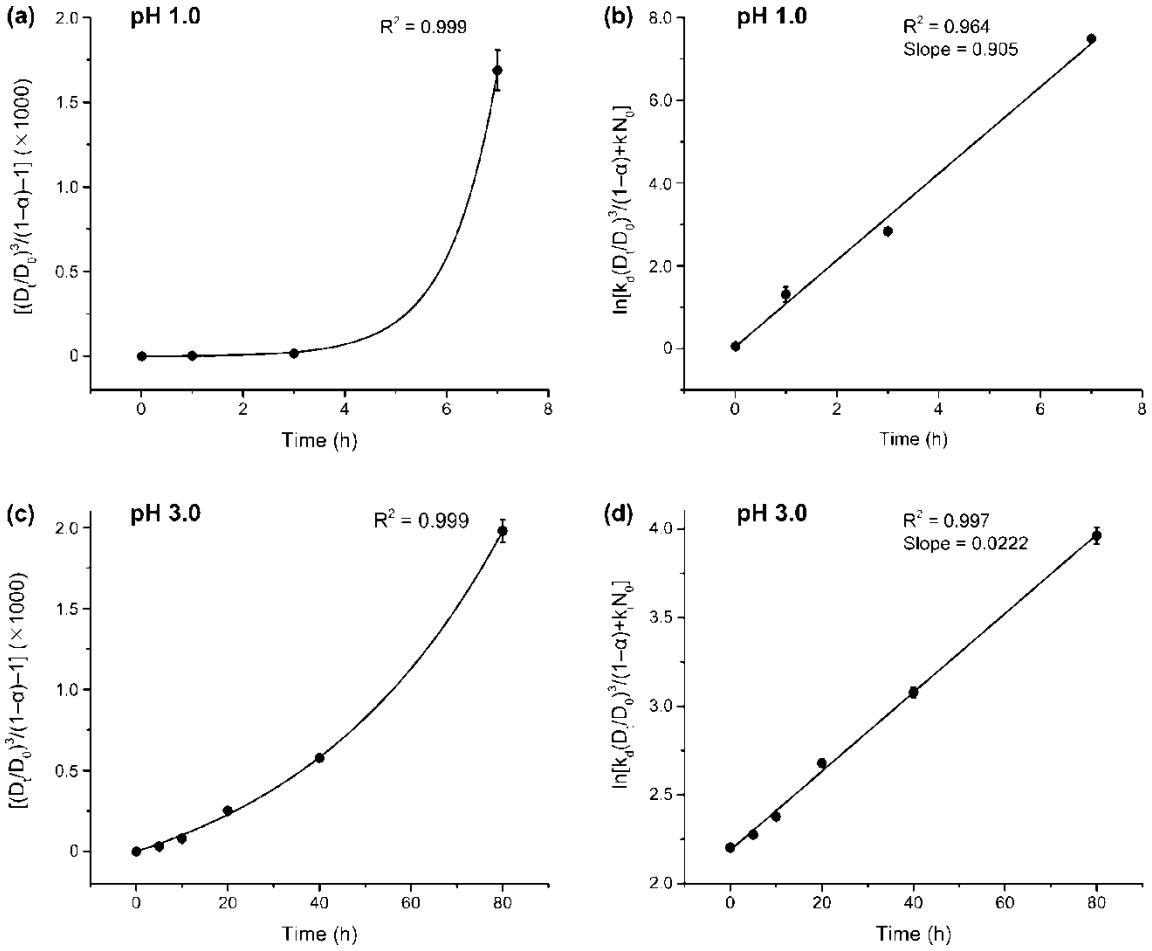

Figure 4.3 Plots demonstrating the application of the combined model at pH 1.0 (a, b) and pH 3.0 (c, d).The data points calculated by operating the left-hand side of the Equation 5 to the experimentally measurable parameters and fitted with right-hand side of the same equation (a, c). The plots showing the linear least squares fit of the data to the left-hand side of the Equation 4 as a function of time (b, d). R^2 values present the degree of the fits.

If the CM describes the kinetics of the phase transformation well, then it should also describe the data well for experiments at the lower and higher pHs employed. Thus, CM was used to fit experimental data from experiments performed at pH 1.0 and 3.0. At pH 1.0, the best fit between the model and the

data was obtained for positive and small values of $k_{in}N_0$ ($0 < k_{in}N_0 << 1$) as presented Figure 4.3a and 4.3b. Otherwise, the non-linear fitting simulation does not converge to give meaningful values for transformation constants. At pH 3.0, the model fit the data well without any boundary conditions, as shown Figures 4.3c and 4.3d. Furthermore, CM model fit the data well for the anatase to rutile phase transformation at the lower aging temperature of 200 °C as well, as shown in Figure B.2.

Table 4.1. Transformation rate constants obtained from the application of three different kinetic models.

	k_{dp} (h^{-1})		$k_{in}N_0$ (h^{-1})	
pH	DP	CM	IN	CM
1.0	1.05 ± 0.00	1.06 ± 0.01	–	$0 < k_iN_0 << 1$
2.2	–	0.101 ± 0.008	–	2.38 ± 0.78
3.0	–	0.0220 ± 0.0004	2.75 ± 0.03	9.04 ± 0.12

Table 4.1 summarizes the values for the transformation rate constants obtained from the application of the combined as well as individual kinetic models as described above. According to the data presented in Table 4.1, the values for k_{dp} decrease while $k_{in}N_0$ increases consistently with increasing pH, indicating a decreasing contribution to the production of rutile by DP. Furthermore, the relative contribution to the transformation by each mechanism evolves with time, as presented in Figure 4.4. The relative contribution by each mechanism was

calculated by determining the ratio of the rate by IN (R_{IN}) to the total rate (R_{TOT}) by way of equation (6):

$$\frac{R_{IN}}{R_{TOT}} = \frac{k_{in}N_0 \cdot e^{-k_{dp}t}}{(k_{in}N_0 + k_{dp})} \cdot 100 \qquad (6)$$

IN is dominant at the very early stages of transformation, both at pH 2.2 and 3.0, and the contribution by IN decreases exponentially with time. However, at pH 1.0 the dominant mechanism is DP, although some contribution by IN is detected and the change in the contribution to the overall transformation rate by IN is shown in the inset of Figure 4.4.

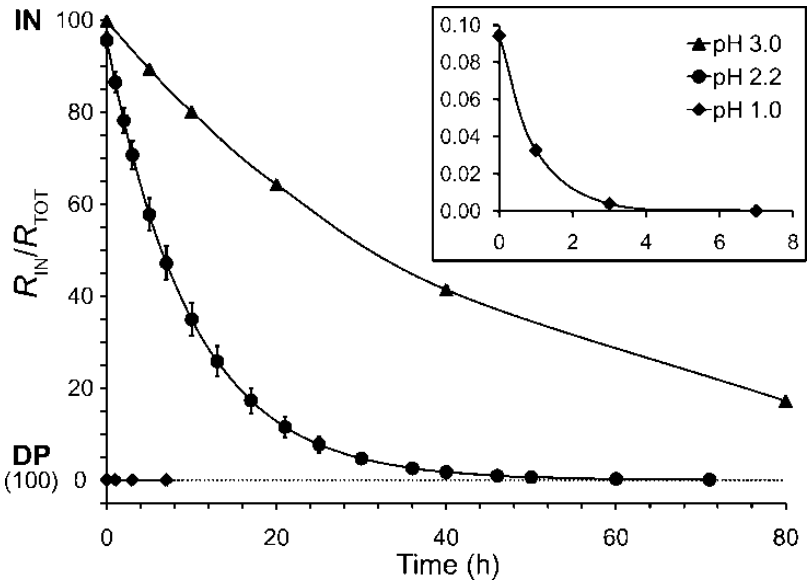

Figure 4.4 The plot presents the amount of anatase (in terms of mass) transformed to rutile by IN relative to the amount transformed by DP as a function of processing time.

These results demonstrate that CM enables a robust assessment of the contribution by DP and IN at different hydrothermal conditions. At very acidic conditions (pH 1.0), the transformation takes place predominantly via dissolution

of anatase and re-precipitation of rutile, and the contribution of IN mechanism is very small, as seen in Figure 4.4 (and inset). At the less acidic conditions (pH 2.2 and 3.0), at which TiO_2 has lower solubility, nanocrystalline anatase transforms to rutile via both IN and DP. IN dominates the early stages of the transformation, whereas DP dominates the later stages.

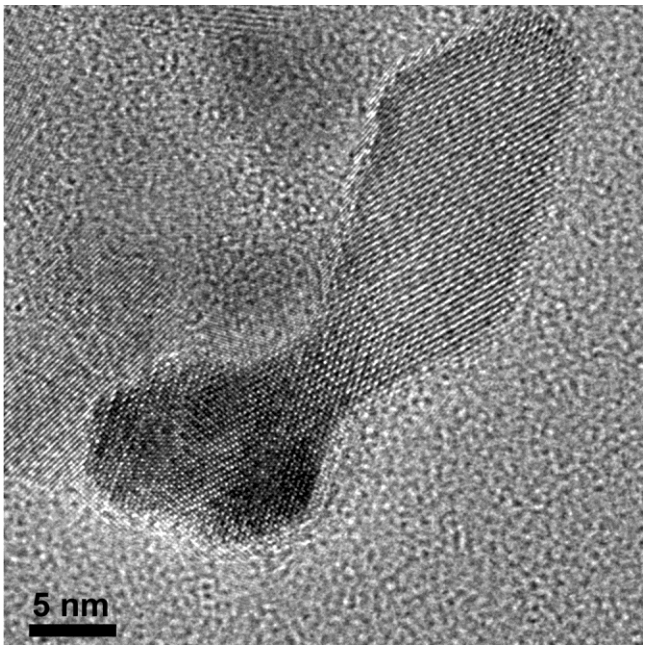

Figure 4.5 HRTEM image of anatase nanocrystal that was treated for 45 hours at pH 1.0 and 200 °C. The morphology of the nanocrystal is indicative of crystal growth by oriented aggregation.

Direct imaging of the particles is consistent with the results obtained by macroscopic modeling of the phase transformation. Anatase nanocrystals with morphologies indicative of particle growth by oriented aggregation mechanism were frequently observed in all our samples. For example, Figure 4.5 presents HRTEM image of the sample hydrothermally treated for 45 hours at pH 1.0. The frequent observation of nanocrystals with features consistent with growth by

oriented aggregation is consistent with the importance of aggregative mechanisms in the growth and phase transformation even under the conditions of high titania solubility.

Indeed, particle-particle interactions and oriented attachment might be the main mechanism by which rutile nucleates via IN at the early stages. At these stages, the crystallite domain size is small and the rate of the oriented attachment is high as demonstrated previously.[12-16] Furthermore, the fact that IN is dominant at the early stages of transformation is consistent with the work in which the change in number concentration of rutile particles as a function of aging time was illustrated.[4] Even though the mass fraction of rutile increased steadily the number concentration of rutile nanocrystals reached plateau at certain aging time. This might be an indication that IN dominated the transformation only until certain aging time resulting in the production of new rutile. Then, nucleated rutile further grew predominantly by dissolution of anatase nanocrystals and re-precipitation onto rutile, which had no effect on rutile particle concentration.

Conclusions

A new kinetic model derived by combining IN and DP models enables quantitative analysis of the kinetics of nanocrystalline anatase to rutile phase transformation. Generally speaking, the overall contribution to the phase transformation by IN is at its greatest at the earliest stages, regardless of titania solubility. As the transformation progresses, and the particle size of both

anatase and rutile increase, the contribution by IN decreases and DP increases. For low titania solubility (pH 3.0 suspensions), hydrothermally treated anatase nanocrystals transform to rutile primarily by IN, while the transformation is dominated by DP when titania is more soluble (pH 1.0). However, even under conditions of higher titania solubility, results are consistent with IN playing a crucial role in producing the initial rutile crystallites, which subsequently grow by DP. The results obtained in this work enable deeper understanding of the mechanism and better control over phase transformation to produce materials with desired properties.

Acknowledgements

We thank University of Minnesota, the Nanostructural Materials and Processes Program at the University of Minnesota, and National Science Foundation (NSF-0957696) for their financial support. We acknowledge Characterization Facility at the University of Minnesota, a member of the NSF-funded Materials Research Facilities Network (www.mrfn.org) via the MRSEC program. KS would also like to acknowledge helpful discussion with Hengzhong Zhang at the Department of Earth and Planetary Science, University of California at Berkeley.

Chapter 5: Synthesis of Porous Rutile Nanocrystals under Mild Conditions*

Introduction

Phase transformation of inorganic materials is an important fundamental process by which crystalline particles lower the total free energy. The route to achieving the lowest energy state is governed by solubility, crystallite size, and aggregation state.[1-3] Under conditions of high solubility, nanocrystals predominantly transform by dissolution-precipitation, which involves the growth of the more stable phase at the expense of less stable.[4] The phenomenon is driven primarily by decreasing the total free energy. This is a consequence of the interplay between surface free energy and bulk free energy. For example, nanoparticulate TiO_2 usually occurs in anatase phase as it has the lowest surface free energy. The total free energy is dictated by the surface free energy due to high surface area per unit mass at smaller size. However, as anatase crystallites grow transformation to rutile occurs as rutile has lower bulk free energy than anatase and the contribution of bulk free energy to the total free energy becomes higher at larger sizes.

The effect of crystallite size on phase transformation kinetics has been observed for numerous systems including anatase to rutile phase

* A report on this research project will be submitted for publication.
Sabyrov, K., Yuwono, V. M. and Penn, R. L. *Crystal Growth & Design*, **(in preparation)**.

transformation.[5-7] The majority of the studies demonstrate that the higher frequency of particle interfaces is the primary cause for faster transformation of smaller crystallites. This is because the nucleation of the second phase might occur at the interfaces and thus determine the rate of the transformation. Indeed, scarcity of partly reacted crystals and absence of multiply twinned rutile in the processed anatase sample, indicate a rate law based on slow nucleation and rapid growth.[7,8] Furthermore, the kinetic models derived based on these experimental observations describe the experimental data well and enable quantitative analysis of the relationship between the kinetics of the transformation and particle size.[5,7] For example, the pre-exponential factor, which is proportional to the vibrational frequency of the atoms attempting the transformation, was demonstrated to be highly size dependent. Authors attributed large frequency factor obtained for small crystallites to the high concentration of particle-particle contacts per unit volume.

The mechanism for aggregation induced nucleation and growth was proposed by Penn *et al*.[8,9] Particle interfaces and defects produced during growth by oriented attachment might act as nucleation sites for the secondary phase. For example, anatase twins were demonstrated to possess structural elements common to rutile. The hypothesis was that the structural similarity at the boundary might serve to facilitate the nucleation and subsequent transformation from anatase to rutile. For this to happen at the {112} anatase twin boundary, only 7 out of 24 Ti-O bonds per unit cell need be ruptured. High-resolution

transmission electron microscope (HRTEM) image of anatase twin containing three unit cell wide strip of rutile at the boundary stands as a strong evidence for aggregation-mediated phase transformation (Figure 5.1).

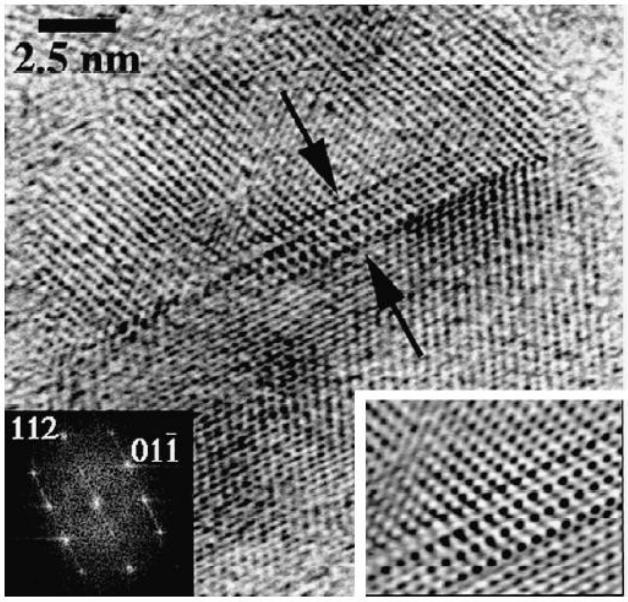

Figure 5.1 Rutile nucleus (indicated by arrows) at the {112} anatase twin surface (viewed down [131] anatase). Inset (lower right) shows rotationally filtered image of the interface.[8] Reproduced with permission from reference 8.

In this work, cryogenic transmission electron microscope (cryo-TEM) was used as a primary technique to study the role of aggregation in the anatase to rutile phase transformation under hydrothermal conditions. Cryo-TEM enables characterization of nanoparticles and their aggregates in the suspension by vitrifying a thin layer of suspension and imaging under TEM. Unfortunately, the suspension must be cooled to ambient conditions prior to sample preparation, but the goal is to directly examine the aggregation state of the particles while still suspended in the liquid medium. The technique has been used to image

aggregates and assemblies of nanocrystals, providing unprecedented insights into crystal growth by oriented attachment.[10,11]

Experimental section

For our experiments, highly dispersed and stable suspensions of anatase nanocrystals were prepared using sol-gel method.[12] For the synthesis 6.25 mL of titanium isopropoxide (Aldrich) was dissolved in 62.5 mL of isopropanol (Fisher, HPLC grade) and the solution is cooled to ~3 °C in an ice-bath. Then 23.1 mL of 4 M nitric acid (Mallinckrodt) was added dropwise (1 drop per ~10 s) using 25 mL burette to hydrolyze the titanium isopropoxide. The volumes correspond to Ti:H_2O mole ratio of 1:100. Then the final suspension was allowed to warm to room temperature and then aged at room temperature (~23 °C) for 1 day, at ~35 °C for 2 days, and at ~55 °C for 2 days.

Then, suspensions were aged at several temperatures for different time periods, and samples were taken at specified time intervals so as to prepare samples for characterization by X-ray diffraction (XRD), high-resolution transmission electron microscope (HRTEM) and cryo-TEM.

For XRD characterization, several drops of suspension were dried on a zero-background quartz slide and the diffraction patterns collected over a 2θ range of 24°−62° using a PANalytical X'Pert Pro diffractometer equipped with a high-speed X'Celerator detector and a Co Kα radiation source. Rietveld refinement of the patterns was performed using the X'Pert High Score Plus

software to quantify phase composition. The parameters refined were zero shift (° 2θ); scale factor; preferred orientation; W, U, and V profile parameters; unit-cell parameters; and peak shapes; other parameters were fixed, such as thermal parameters, fractional atomic coordinates, roughness parameters, the extinction, and porosity.

For cryo-TEM characterization, the suspension was diluted 4 times with Milli-Q water (Millipore Corporation) and a small quantity of the sample solution was deposited onto a TEM copper grid with lacey carbon film (200 mesh Cu grid, SPI supplies). The grid then was blotted with a filter paper using a Vitrobot Mark IV (FEI Company) under 100% relative humidity. The suspension on the blotted grid was then vitrified by plunging into liquid ethane. Finally, the grid was cryogenically transferred to the cryo-TEM holder, which was then inserted into the microscope while still maintaining cryogenic conditions.Low dose imaging conditions were employed to minimize beam damage to the thin film of vitreous water and the TiO_2 nanocrystals.

In addition to cryo-TEM, HRTEM was used to analyze the morphology and microstructure of the nanoparticles. For that, original suspension was diluted 4 times with Milli-Q water, and a drop of the final suspension was naturally dried on a TEM copper grid with holey carbon film (200 mesh Cu grid, SPI supplies).

Results and discussion

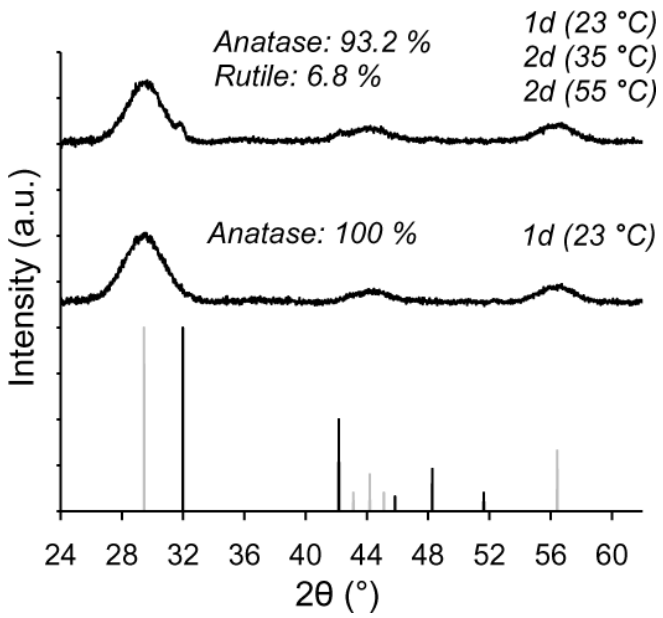

Figure 5.2 XRD patterns of the samples aged for shorter (1 day at ~23 °C) and longer (1 day at ~23 °C, 2 days at ~35 °C, and 2 days at ~55 °C) time periods. Data for anatase (grey) and rutile (black) are shown as a stick pattern.

XRD results (Figure 5.2) demonstrate that rutile does not form after one day of aging at room temperature but does form after the additional aging for 2 days at ~35 °C and 2 days at ~55 °C. Average crystallite sizes of the nanoparticles were determined from XRD peak broadening using Scherrer equation.[13] The average domain size of the anatase particles aged for a shorter time is ~3.4 nm, whereas the sample aged for longer time period contains ~4.3 nm anatase nanocrystals. The crystallite size of the rutile nanoparticles in the sample aged for a longer time was calculated to be ~25 nm. However, it should be noted that the determined size for rutile is not accurate due to small amount of rutile in the sample. Figure 5.3a shows a cryo-TEM image of the sample after

aging for 1 day at room temperature (~23 °C). In general, the nanocrystals are highly dispersed and uniformly distributed throughout the suspension. No dense clusters of nanocrystals or large aggregates are detected, and only anatase is detected by XRD (Figure 5.2). However, after aging the suspension for 2 days at ~35 °C and 2 days at ~55 °C, relatively loose clusters of smaller nanocrystals and larger nanoparticles with mesoporous-like structure are observed. Representative images are shown in Figures 5.3b, 5.3c and 5.3d (higher magnification). The higher magnification cryo-TEM image (Figure 5.3d), which is taken at large defocus, and HRTEM image (Figure 5.4) exhibit latticle fringes that have a spacing consistent with rutile, which confirms that the larger crystals are composed of rutile and not anatase. Furthermore, fast Fourier transform (FFT) of the cryo-TEM image and selected area electron diffraction (SAED) of the larger particle are consistent with single crystalline nature of rutile nanoparticles. TEM observations combined with the XRD results are consistent with smaller anatase and larger single-crystalline rutile nanoparticles.

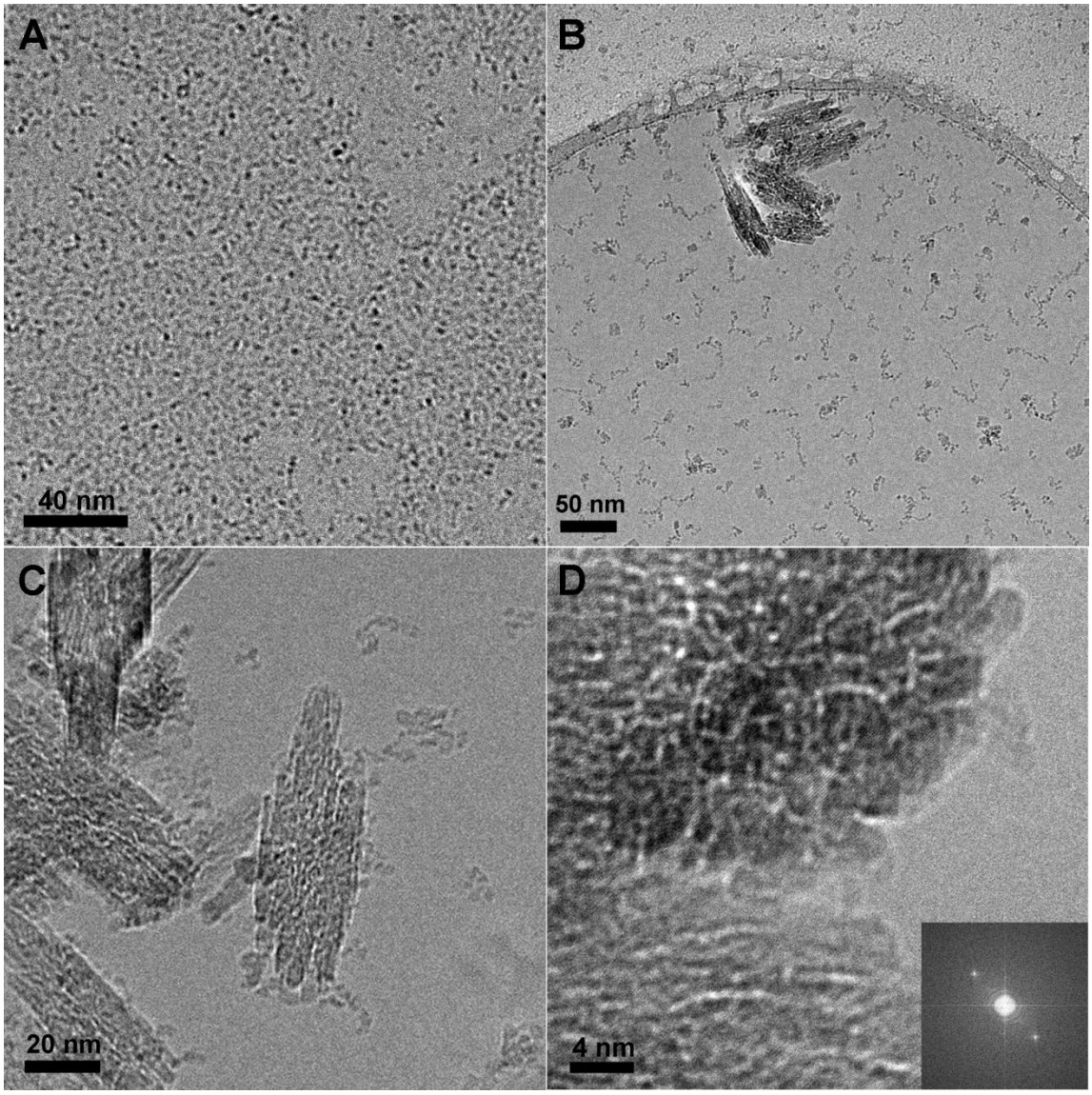

Figure 5.3 Cryo-TEM images of the samples aged for 1 day at ~23 °C (a) and for 1 day at ~23 °C, 2 days at ~35 °C, and 2 days at ~55 °C (b, c and d). The inset in Figure 5.3d shows FFT of the nanoporous rutile.

The relatively uniform dispersion of anatase nanocrystals at room temperature is a strong indication that the particles have high stability against particle aggregation and sedimentation. The stability of the particles might be originating from electrostatic forces. Positive charge and electric potential can

accumulate at the surface of the particles due to protonation of surface hydroxyl groups in acidic medium and cause particle-particle electrostatic repulsion.[14,15]

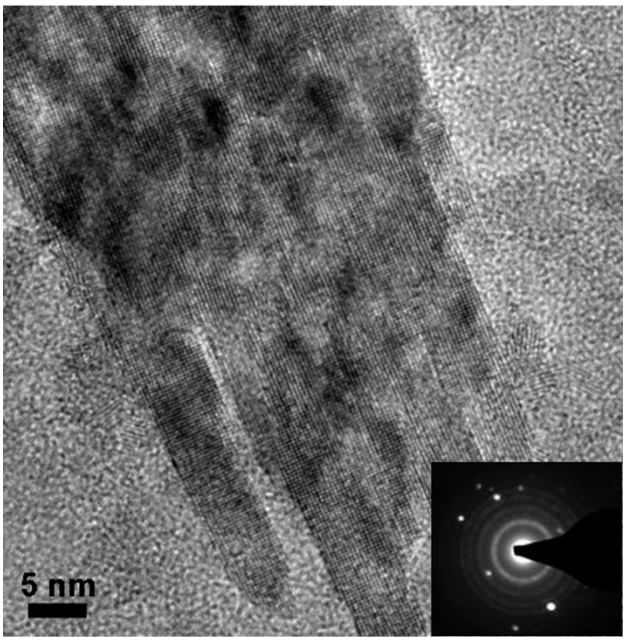

Figure 5.4 HRTEM image of a mesoporous rutile nanocrystal in the sample aged for 1 day at ~23 °C followed by 2 days at ~35 °C and 2 days at ~55 °C. The inset shows SAED of the rutile nanocrystal. The lattice fringes shown in the HRTEM image corresponds to d_{110} of rutile.

The morphological features, such as the mesopores and rounded protrusions of size similar to the primary crystallites, of the larger rutile crystals produced after the extended aging procedure are strong evidence for crystal growth by oriented attachment.[16,17] However, such features do not conclusively demonstrate that the rutile crystals grew by oriented attachment of rutile primary particles. The aggregation state of the anatase crystallites dramatically shifted after the extended aging period, transitioning from a highly dispersed state to an aggregated state in which loose aggregates of ca. 10 – 20 anatase crystallites are observed. This shift in aggregation state is consistent with a drop in particle

stability in the suspension. Coupled with the observed mesoporous microstructure of the rutile crystals, these results are consistent with particle aggregation playing an important role in the formation of the mesoporous rutile crystals.

Two hypotheses can be formulated based on the cryo-TEM images. Firstly, it is possible that anatase crystallites first transform to rutile, with subsequent rutile crystal growth by oriented attachment with other rutile crystallites. However, rutile nanocrystals having sizes similar to those of primary anatase nanocrystals have never been detected. The second, and more likely, hypothesis is that the anatase crystallites aggregate and some contacts produce structural elements that can facilitate the anatase to rutile phase transformation, with the phase transformation quickly propagating throughout the aggregate or the particles.[3,8,9,18] This hypothesis is consistent with previous observations that the first detected rutile (by XRD and TEM) is relatively larger than anatase and has morphologies indicative of aggregation-mediated growth. The lattice fringes spanning the entire particle are clear evidence that the small primary particles composing the larger secondary particle are in crystallographic registry with one another as observed by high-resolution cryo-TEM (Figure 5.3d). Finally, our observations are consistent with recent cryo-TEM studies demonstrating aggregation-mediated phase transformation in iron (oxy)hydroxide nanoparticles.[10,19]

Acknowledgements

We acknowledge the University of Minnesota, the National Science Foundation (No. NSF-0957696), and the Nanostructural Materials and Processes Program at the University of Minnesota for financial support. We also thank Characterization Facility at the University of Minnesota, a member of the NSF-funded Materials Research Facilities Network (www.mrfn.org) via the MRSEC program.

Chapter 6: Summary and Outlook

Summary of thesis

Size dependent anatase to rutile phase transformation

Phase transformation and particle growth are fundamental processes that govern final particle size and morphology, as well as phase composition. At the nanoscale, these processes can be significantly affected by initial particle size. Rates of anatase growth and its transformation to rutile increase with decreasing initial size under hydrothermal conditions at pH 1 and pH 3. Overall, rates are slower at the higher pH. At pH 1, the data fit well to a kinetic model developed based on a dissolution-precipitation mechanism. However, at pH 3, it deviates substantially from the model, indicating that the transformation occurs via a different mechanism or a mixture of dissolution-precipitation and another mechanism, which likely involves aggregation. Finally, the compactness of the aggregates affects the processes significantly. That is, densely aggregated particles show higher transformation and growth rates, compared to loosely aggregated ones.

Two-step anatase to rutile phase transformation

Kinetic data tracking the anatase to rutile phase transformation under acidic, hydrothermal conditions (200 °C, pH 1) are consistent with a two-step

transformation mechanism. Fitting the experimental data using phase transformation models, interface-nucleation dominates the early stages of transformation and dissolution-precipitation dominates at later stages. During the first stage, the rate of transformation by interface-nucleation is consistent with a substantially higher number of nucleation sites, possibly generated by crystal growth by oriented aggregation. Characterization of the hydrothermally treated samples using HRTEM revealed that anatase crystal morphologies indicative of crystal growth by oriented aggregation are common. Furthermore, twinned rutile crystals, which are consistent with transformation of anatase twinned across the {112} to rutile twins by interface-nucleation, were also observed. At later stages, the kinetics of the anatase to rutile transformation are consistent with dissolution-precipitation, and the number concentration of rutile crystallites reaches a plateau. These results are consistent with a decrease in crystal growth by oriented aggregation as the anatase particle size increases and the dissolution of anatase and reprecipitation onto already existing rutile crystals due to the larger bulk energy and comparatively small size of anatase.

A new model to quantify the kinetics of phase transformation

A kinetic model that enables quantitative assessment of the contribution to the rate of phase transformation by dissolution-precipitation (DP) and by interface-nucleation (IN) has been developed. Results demonstrate that, under highly acidic, hydrothermal conditions, anatase phase transforms to rutile

predominantly by DP, presumably due to the comparatively high solubility of TiO_2 at 250 °C and pH 1.0. In contrast, the phase transformation is dominated by IN at pH 3.0, at which the solubility of TiO_2 is substantially lower. Furthermore, kinetic data for the phase transformation at the intermediate pH of 2.2 were fit poorly by the IN and DP models individually but fit well using the new kinetic model. Generally speaking, IN plays a critical role during the early stages of the transformation, regardless of pH, whereas DP dominates the later stages of the transformation. The contribution to the rate of rutile production by DP is the greatest under conditions of higher titania solubility. However, even under conditions of higher titania solubility, results are consistent with IN playing a crucial role in producing the initial rutile crystallites, which subsequently grow by DP. Transmission electron microscopy (TEM) results are consistent with the results obtained by the new model. Thus, new insights into the mechanism of the anatase to rutile phase transformation under hydrothermal conditions are gained, enabling quantitative assessment of the contribution by interface-nucleation.

Production of porous rutile nanocrystals

Control over phase transformation mechanism can be exploited to synthesize nanocrystalline materials with desired properties. In this work, nanocrystalline rutile with complex morphology was produced under mild solvothermal conditions. First, highly dispersed and phase pure anatase nanocrystals were obtained using a sol-gel method. Then, the freshly synthesized anatase sample was treated for 1 day at room temperature, for 2

days at ~35 °C, and for 2 days at ~55 °C to facilitate rutile nucleation and growth. The results are consistent with the hypothesis that defects and particle interfaces produced by oriented aggregation of primary anatase nanocrystals induce rutile nucleation and growth. Indeed, rutile nanocrystals in the processed samples possess features indicative of aggregation-mediated phase transformation as characterized by cryo-TEM and HRTEM. The reaction conditions exploited in this work might favor oriented aggregation, and thus, nucleation of rutile at the particle interfaces. Low solubility of TiO_2 particles under these mild solvothermal conditions might result in the formation of single-crystalline and nanoporous rutile. As the results obtained in this work are consistent with the observations in other systems, our approach might be used as a general method to produce single-crystalline materials with complex morphologies.

Outlook

Even though considerable effort has been put to describe interface-mediated phase transformation, nucleation and subsequent growth of a secondary phase needs to be further explored at the atomic level. Newly invented state-of-the-art instruments such as *in situ* fluid cell TEM or synchrotron-based X-ray spectroscopy techniques together with theoretical methods might provide unprecedented insights into the mechanisms of the phenomena. Molecular level description of the process might lead to better control over the mechanism to produce nanomaterials with novel properties.

Bibliography

Chapter 1: References

1 Offerman, S. E., van Dijk, N. H., Sietsma, J., Grigull, S., Lauridsen, E. M., Margulies, L., Poulsen, H. F., Rekveldt, M. T. and van der Zwaag, S. Grain Nucleation and Growth During Phase Transformations. *Science* **2002**, *298,* 1003-1005.

2 Schwertmann, U. Transformation of Hematite to Goethite in Soils. *Nature* **1971**, *232,* 624-625.

3 Banfield, J. F., Welch, S. A., Zhang, H., Ebert, T. T. and Penn, R. L. Aggregation-based crystal growth and microstructure development in natural iron oxyhydroxide biomineralization products. *Science* **2000**, *289,* 751-754.

4 Voorhees, P. W. The theory of Ostwald ripening. *Journal of Statistical Physics* **1985**, *38,* 231-252.

5 Lifshitz, I. M. and Slyozov, V. V. The kinetics of precipitation from supersaturated solid solutions. *Journal of Physics and Chemistry of Solids* **1961**, *19,* 35-50.

6 Gribb, A. A. and Banfield, J. F. Particle size effects on transformation kinetics and phase stability in nanocrystalline TiO_2. *American Mineralogist* **1997**, *82,* 717-728.

7 Zhang, H. and Banfield, J. F. Understanding Polymorphic Phase Transformation Behavior during Growth of Nanocrystalline Aggregates: Insights from TiO_2. *The Journal of Physical Chemistry B* **2000**, *104,* 3481-3487.

8 Ranade, M., Navrotsky, A., Zhang, H., Banfield, J., Elder, S., Zaban, A., Borse, P., Kulkarni, S., Doran, G. and Whitfield, H. Energetics of nanocrystalline TiO_2. *Proceedings of the National Academy of Sciences* **2002**, *99,* 6476-6481.

9 Levchenko, A. A., Li, G., Boerio-Goates, J., Woodfield, B. F. and Navrotsky, A. TiO_2 stability landscape: Polymorphism, surface energy, and bound water energetics. *Chemistry of Materials* **2006**, *18,* 6324-6332.

10 Sabyrov, K., Adamson, V. and Penn, R. L. Two-step phase transformation of anatase to rutile in aqueous suspension. *CrystEngComm* **2014**, *16,* 1488-1495.

11 Kahlweit, M. Ostwald ripening of precipitates. *Advances in Colloid and Interface Science* **1975**, *5,* 1-35.

12 Wagner, C. Theorie der Alterung von Niederschlägen durch Umlösen (Ostwald-Reifung). *Zeitschrift für Elektrochemie, Berichte der Bunsengesellschaft für Physikalische Chemie* **1961**, *65,* 581-591.

13 Penn, R. L. and Banfield, J. F. Morphology development and crystal growth in nanocrystalline aggregates under hydrothermal conditions:

Insights from titania. *Geochimica et Cosmochimica Acta* **1999**, *63,* 1549-1557.

14 Penn, R. L. and Banfield, J. F. Oriented attachment and growth, twinning, polytypism, and formation of metastable phases: Insights from nanocrystalline TiO_2. *American Mineralogist* **1998**, *83,* 1077-1082.

15 Zhang, H. and Banfield, J. F. Interatomic Coulombic interactions as the driving force for oriented attachment. *CrystEngComm* **2014**, *16,* 1568-1578.

16 Cölfen, H. and Antonietti, M. Mesocrystals: Inorganic Superstructures Made by Highly Parallel Crystallization and Controlled Alignment. *Angewandte Chemie International Edition* **2005**, *44,* 5576-5591.

17 Yuwono, V. M., Burrows, N. D., Soltis, J. A. and Penn, R. L. Oriented aggregation: formation and transformation of mesocrystal intermediates revealed. *Journal of the American Chemical Society* **2010**, *132,* 2163-2165.

18 Zhang, H. and Banfield, J. F. Understanding polymorphic phase transformation behavior during growth of nanocrystalline aggregates: insights from TiO_2. *The Journal of Physical Chemistry B* **2000**, *104,* 3481-3487.

19 Zhang, H. and Banfield, J. F. New kinetic model for the nanocrystalline anatase-to-rutile transformation revealing rate dependence on number of particles. *American Mineralogist* **1999**, *84,* 528-535.

20 Zhang, H. and Banfield, J. F. Phase transformation of nanocrystalline anatase-to-rutile via combined interface and surface nucleation. *Journal of Materials Research* **2000**, *15,* 437-448.

21 Finnegan, M. P., Zhang, H. and Banfield, J. F. Phase stability and transformation in titania nanoparticles in aqueous solutions dominated by surface energy. *The Journal of Physical Chemistry C* **2007**, *111,* 1962-1968.

22 Penn, R. L. and Banfield, J. F. Formation of rutile nuclei at anatase {112} twin interfaces and the phase transformation mechanism in nanocrystalline titania. *American Mineralogist* **1999**, *84,* 871-876.

23 Penn, R. L. and Banfield, J. F. Imperfect oriented attachment: dislocation generation in defect-free nanocrystals. *Science* **1998**, *281,* 969-971.

24 Frandsen, C., Legg, B. A., Comolli, L. R., Zhang, H., Gilbert, B., Johnson, E. and Banfield, J. F. Aggregation-induced growth and transformation of β-FeOOH nanorods to micron-sized α-Fe_2O_3 spindles. *CrystEngComm* **2014**, *16,* 1451-1458.

25 Zhou, Y. and Fichthorn, K. A. Microscopic view of nucleation in the anatase-to-rutile transformation. *The Journal of Physical Chemistry C* **2012**, *116,* 8314-8321.

26 Liu, W., Huang, F., Liao, Y., Zhang, J., Ren, G., Zhuang, Z., Zhen, J., Lin, Z. and Wang, C. Treatment of CrVI-Containing $Mg(OH)_2$ Nanowaste. *Angewandte Chemie International Edition* **2008**, *47,* 5619-5622.

27 Sabyrov, K., Burrows, N. D. and Penn, R. L. Size-dependent anatase to rutile phase transformation and particle growth. *Chemistry of Materials* **2012**, *25,* 1408-1415.

28 Zhang, H. and Banfield, J. F. Size dependence of the kinetic rate constant for phase transformation in TiO_2 nanoparticles. *Chemistry of Materials* **2005**, *17,* 3421-3425.

29 Ding, X.-z. and Liu, X.-h. Grain growth enhanced by anatase-to-rutile transformation in gel-derived nanocrystalline titania powders. *Journal of Alloys and Compounds* **1997**, *248,* 143-145.

30 Kumar, K.-N. P. Growth of rutile crystallites during the initial stage of anatase-to-rutile transformation in pure titania and in titania-alumina nanocomposites. *Scripta Metallurgica et Materialia* **1995**, *32,* 873-877.

31 Lee Penn, R., Tanaka, K. and Erbs, J. Size dependent kinetics of oriented aggregation. *Journal of Crystal Growth* **2007**, *309,* 97-102.

32 Burrows, N. D., Hale, C. R. and Penn, R. L. Effect of ionic strength on the kinetics of crystal growth by oriented aggregation. *Crystal Growth & Design* **2012**, *12,* 4787-4797.

33 Burrows, N. D., Hale, C. R. and Penn, R. L. Effect of pH on the kinetics of crystal growth by oriented aggregation. *Crystal Growth & Design* **2013**, *13,* 3396-3403.

34 Sabyrov, K. and Penn, R. L. A kinetic model for two-step phase transformation of hydrothermal-ly treated nanocrystalline anatase. *Chemistry of Materials* **(under review)**.

35 Yau, S. T. and Vekilov, P. G. Quasi-planar nucleus structure in apoferritin crystallization. *Nature* **2000**, *406,* 494-497.

36 Tao, F. and Salmeron, M. In Situ Studies of Chemistry and Structure of Materials in Reactive Environments. *Science* **2011**, *331,* 171-174.

37 Zhang, H., Gilbert, B., Huang, F. and Banfield, J. F. Water-driven structure transformation in nanoparticles at room temperature. *Nature* **2003**, *424,* 1025-1029.

38 Ratkovich, A. S. and Penn, R. L. Controlling Nanosized ZnO Growth Kinetics Using Various Zn:OH Concentration Ratios. *The Journal of Physical Chemistry C* **2007**, *111,* 14098-14104.

39 Ribeiro, C., Lee, E. J. H., Longo, E. and Leite, E. R. A Kinetic Model to Describe Nanocrystal Growth by the Oriented Attachment Mechanism. *ChemPhysChem* **2005**, *6,* 690-696.

40 Ocana, M., Garcia-Ramos, J. V. and Serna, C. J. Low-Temperature Nucleation of Rutile Observed by Raman Spectroscopy during Crystallization of TiO_2. *Journal of the American Ceramic Society* **1992**, *75,* 2010-2012.

41 Li, D., Nielsen, M. H., Lee, J. R., Frandsen, C., Banfield, J. F. and De Yoreo, J. J. Direction-specific interactions control crystal growth by oriented attachment. *Science* **2012**, *336,* 1014-1018.

42 Burrows, N. D., Kesselman, E., Sabyrov, K., Stemig, A., Talmon, Y. and Penn, R. L. Crystalline nanoparticle aggregation in non-aqueous solvents. *CrystEngComm* **2014**, *16,* 1472-1481.

43 Yuwono, V. M., Burrows, N. D., Soltis, J. A., Anh Do, T. and Lee Penn, R. Aggregation of ferrihydrite nanoparticles in aqueous systems. *Faraday Discussions* **2012**, *159,* 235-245.

44 Sabyrov, K., Yuwono, V. M. and Penn, R. L. Synthesis of porous rutile nanocrystals under mild conditions. **(in preparation)**.

Chapter 2: References

1 Oskam, G., Nellore, A., Penn, R. L. and Searson, P. C. The growth kinetics of TiO_2 nanoparticles from titanium (IV) alkoxide at high water/titanium ratio. *The Journal of Physical Chemistry B* **2003**, *107,* 1734-1738.

2 Cheng, H., Ma, J., Zhao, Z. and Qi, L. Hydrothermal preparation of uniform nanosize rutile and anatase particles. *Chemistry of Materials* **1995**, *7,* 663-671.

3 Moritz, T., Reiss, J., Diesner, K., Su, D. and Chemseddine, A. Nanostructured crystalline TiO_2 through growth control and stabilization of intermediate structural building units. *The Journal of Physical Chemistry B* **1997**, *101,* 8052-8053.

4 Wang, C. C. and Ying, J. Y. Sol−gel synthesis and hydrothermal processing of anatase and rutile titania nanocrystals. *Chemistry of Materials* **1999**, *11,* 3113-3120.

5 Oskam, G., Hu, Z., Penn, R. L., Pesika, N. and Searson, P. C. Coarsening of metal oxide nanoparticles. *Physical Review E* **2002**, *66,* 011403.

6 Penn, R. L., Banfield, J. F. Oriented attachment and growth, twinning, polytypism, and formation of metastable phases: Insights from nanocrystalline TiO_2. *American Mineralogist* **1998**, *83,* 1077–1082.

7 Lifshitz, I. M. and Slyozov, V. V. The kinetics of precipitation from supersaturated solid solutions. *Journal of Physics and Chemistry of Solids* **1961**, *19,* 35-50.

8 Wagner, C. Theorie der alterung von niederschlägen durch umlösen (Ostwald-Reifung). *Zeitschrift für Elektrochemie, Berichte der Bunsengesellschaft für Physikalische Chemie* **1961**, *65,* 581-591.

9 Hiemenz, P. C., Rajagopalan, R. *Principles of Colloid and Surface Chemistry*. (Marcel Dekker, 1997).

10 Zhang, J., Huang, F. and Lin, Z. Progress of nanocrystalline growth kinetics based on oriented attachment. *Nanoscale* **2010**, *2,* 18-34.

11 Yuwono, V. M., Burrows, N. D., Soltis, J. A. and Penn, R. L. Oriented aggregation: formation and transformation of mesocrystal intermediates revealed. *Journal of the American Chemical Society* **2010**, *132,* 2163-2165.

12 Niederberger, M. and Colfen, H. Oriented attachment and mesocrystals: non-classical crystallization mechanisms based on nanoparticle assembly. *Physical Chemistry Chemical Physics* **2006**, *8,* 3271-3287.

13 Schliehe, C., Juarez, B. H., Pelletier, M., Jander, S., Greshnykh, D., Nagel, M., Meyer, A., Foerster, S., Kornowski, A., Klinke, C. and Weller, H. Ultrathin PbS sheets by two-dimensional oriented attachment. *Science* **2010**, *329,* 550-553.

14 O'Regan, B. and Gratzel, M. A low-cost, high-efficiency solar cell based on dye-sensitized colloidal TiO_2 films. *Nature* **1991**, *353,* 737-740.

15 Quan, X., Yang, S., Ruan, X. and Zhao, H. Preparation of titania nanotubes and their environmental applications as electrode. *Environmental Science & Technology* **2005**, *39,* 3770-3775.

16 Liu, G., Wang, L., Yang, H. G., Cheng, H.-M. and Lu, G. Q. Titania-based photocatalysts-crystal growth, doping and heterostructuring. *Journal of Materials Chemistry* **2010**, *20,* 831-843.

17 Zhang, H. and F. Banfield, J. Thermodynamic analysis of phase stability of nanocrystalline titania. *Journal of Materials Chemistry* **1998**, *8,* 2073-2076.

18 Ranade, M. R., Navrotsky, A., Zhang, H. Z., Banfield, J. F., Elder, S. H., Zaban, A., Borse, P. H., Kulkarni, S. K., Doran, G. S. and Whitfield, H. J. Energetics of nanocrystalline TiO_2. *Proceedings of the National Academy of Sciences of the United States of America* **2002**, *99,* 6476-6481.

19 Smith, S. J., Stevens, R., Liu, S., Li, G., Navrotsky, A., Boerio-Goates, J. and Woodfield, B. F. Heat capacities and thermodynamic functions of TiO_2 anatase and rutile: analysis of phase stability. *American Mineralogist* **2009**, *94,* 236-243.

20 Zhang, H. and Banfield, J. F. Size dependence of the kinetic rate constant for phase transformation in TiO_2 nanoparticles. *Chemistry of Materials* **2005**, *17,* 3421-3425.

21 Zhang, H. and Banfield, J. F. Understanding polymorphic phase transformation behavior during growth of nanocrystalline aggregates: insights from TiO_2. *The Journal of Physical Chemistry B* **2000**, *104,* 3481-3487.

22 Gribb, A. A., Banfield, J. F. Particle size effects on transformation kinetics and phase stability in nanocrystalline TiO_2. *American Mineralogist* **1997**, *82,* 717–728.

23 Isley, S. L., Jordan, D. S. and Penn, R. L. Titanium dioxide nanoparticles: Impact of increasing ionic strength during synthesis, reflux, and hydrothermal aging. *Materials Research Bulletin* **2009**, *44,* 119-125.

24 Isley, S. L. and Penn, R. L. Relative brookite and anatase content in Sol-gel synthesized titanium dioxide nanoparticles. *The Journal of Physical Chemistry B* **2006**, *110,* 15134-15139.

25 Rietveld, H. A profile refinement method for nuclear and magnetic structures. *Journal of applied Crystallography* **1969**, *2,* 65-71.

26 O'Connor, B. and Li, D. Influence of refinement strategies on rietveld phase composition determinations. *Advances in X-ray Analysis* **2000**, *42,* 204-211.

27 Scherrer, P. Estimation of the size and internal structure of colloidal particles by means of röntgen. Nachrichten von der Gesellschaft der Wissenschaften zu Göttingen, Mathematisch-Physikalische Klasse **1918**, *2,* 96-100.

28 Danino, D., Bernheim-Groswasser, A. and Talmon, Y. Digital cryogenic transmission electron microscopy: an advanced tool for direct imaging of complex fluids. *Colloids and Surfaces A: Physicochemical and Engineering Aspects* **2001**, *183-185,* 113-122.

29 *http://rsbweb.nih.gov/ij*.

30 Finnegan, M. P., Zhang, H. and Banfield, J. F. Phase stability and transformation in titania nanoparticles in aqueous solutions dominated by surface energy. *The Journal of Physical Chemistry C* **2007**, *111,* 1962-1968.

31 Sugimoto, T., Zhou, X. P. and Muramatsu, A. Synthesis of uniform anatase TiO_2 nanoparticles by gel-sol method - 1. Solution chemistry of $Ti(OH)_{(n)}^{((4-n)+)}$ complexes. *Journal of Colloid and Interface Science* **2002**, *252,* 339-346.

32 Liberti, A., Chiantella, V. and Corigliano, F. Mononuclear hydrolysis of titanium (IV) from partition equilibria. *Journal of Inorganic and Nuclear Chemistry* **1963**, *25,* 415-427.

33 Suzuki, A. and Kotera, Y. The kinetics of the transition of titanium dioxide. *Bulletin of the Chemical Society of Japan* **1962**, *35,* 1353–1357.

34 Hishita, S., Mutoh, I., Koumoto, K. and Yanagida, H. Inhibition mechanism of the anatase-rutile phase transformation by rare earth oxides. *Ceramics International* **1983**, *9,* 61-67.

35 Zhang, H. and Banfield, J. F. New kinetic model for the nanocrystalline anatase-to-rutile transformation revealing rate dependence on number of particles. *American Mineralogist* **1999**, *84,* 528-535.

36 Stumm, W. and Wollast, R. Coordination chemistry of weathering: kinetics of the surface-controlled dissolution of oxide minerals. *Reviews of Geophysics* **1990**, *28,* 53-69.

37 Penn, R. L. and Banfield, J. F. Formation of rutile nuclei at anatase (112) twin interfaces and the phase transformation mechanism in nanocrystalline titania. *American Mineralogist* **1999**, *84,* 871-876.

38 Cassaignon, S., Koelsch, M. and Jolivet, J. P. Selective synthesis of brookite, anatase and rutile nanoparticles: thermolysis of $TiCl_4$ in aqueous nitric acid. *Journal of Materials Science* **2007**, *42,* 6689-6695.

39 Isley, S. L. and Penn, R. L. Titanium dioxide nanoparticles: effect of sol-gel pH on phase composition, particle size, and particle growth mechanism. *The Journal of Physical Chemistry C* **2008**, *112,* 4469-4474.

40 Gilbert, B., Zhang, H. Z., Huang, F., Finnegan, M. P., Waychunas, G. A. and Banfield, J. F. Special phase transformation and crystal growth pathways observed in nanoparticles. *Geochemical Transactions* **2003**, *4,* 20-27.

41 Winardi, S., Mukti, R. R., Kumar, K.-N. P., Wang, J., Wunderlich, W. and Okubo, T. Critical nuclei size, initial particle size and packing effect on the

phase stability of sol-peptization-gel-derived nanostructured titania. *Langmuir* **2010**, *26,* 4567-4571.

42 Bosworth, W. Strain-induced preferential dissolution of halite. *Tectonophysics* **1981**, *78,* 509-525

Chapter 3: References

1 Banfield, J. F. and Zhang, H. Nanoparticles in the environment. *Reviews in Mineralogy and Geochemistry* **2001**, *44,* 1-58.

2 Ranade, M. R., Navrotsky, A., Zhang, H. Z., Banfield, J. F., Elder, S. H., Zaban, A., Borse, P. H., Kulkarni, S. K., Doran, G. S. and Whitfield, H. J. Energetics of nanocrystalline TiO_2. *Proceedings of the National Academy of Sciences of the United States of America* **2002**, *99,* 6476-6481.

3 Zhang, H. and F. Banfield, J. Thermodynamic analysis of phase stability of nanocrystalline titania. *Journal of Materials Chemistry* **1998**, *8,* 2073-2076.

4 Banfield, J. F., Bischoff, B. L. and Anderson, M. A. TiO_2 accessory minerals: coarsening, and transformation kinetics in pure and doped synthetic nanocrystalline materials. *Chemical Geology* **1993**, *110,* 211-231.

5 Gribb, A. A. and Banfield, J. F. Particle size effects on transformation kinetics and phase stability in nanocrystalline TiO_2. *American Mineralogist* **1997**, *82,* 717-728.

6 Sabyrov, K., Burrows, N. D. and Penn, R. L. Size-dependent anatase to rutile phase transformation and particle growth. *Chemistry of Materials* **2012**, *25,* 1408-1415.

7 Finnegan, M. P., Zhang, H. and Banfield, J. F. Phase stability and transformation in titania nanoparticles in aqueous solutions dominated by

surface energy. *The Journal of Physical Chemistry C* **2007**, *111,* 1962-1968.

8 Banfield, J. F., Welch, S. A., Zhang, H., Ebert, T. T. and Penn, R. L. Aggregation-based crystal growth and microstructure development in natural iron oxyhydroxide biomineralization products. *Science* **2000**, *289,* 751-754.

9 Smith, S. J., Stevens, R., Liu, S., Li, G., Navrotsky, A., Boerio-Goates, J. and Woodfield, B. F. Heat capacities and thermodynamic functions of TiO_2 anatase and rutile: Analysis of phase stability. *American Mineralogist* **2009**, *94,* 236-243.

10 Zhang, H. and Banfield, J. F. Phase transformation of nanocrystalline anatase-to-rutile via combined interface and surface nucleation. *Journal of Materials Research* **2000**, *15,* 437-448.

11 Zhang, H. and Banfield, J. F. New kinetic model for the nanocrystalline anatase-to-rutile transformation revealing rate dependence on number of particles. *American Mineralogist* **1999**, *84,* 528-535.

12 Winardi, S., Mukti, R. R., Kumar, K.-N. P., Wang, J., Wunderlich, W. and Okubo, T. Critical nuclei size, initial particle size and packing effect on the phase stability of sol-peptization-gel-derived nanostructured titania. *Langmuir* **2010**, *26,* 4567-4571.

13 Zhang, H. and Banfield, J. F. Size dependence of the kinetic rate constant for phase transformation in TiO_2 nanoparticles. *Chemistry of Materials* **2005**, *17,* 3421-3425.

14 Penn, R. L. and Banfield, J. F. Formation of rutile nuclei at anatase (112) twin interfaces and the phase transformation mechanism in nanocrystalline titania. *American Mineralogist* **1999**, *84,* 871-876.

15 Hanaor, D. H. and Sorrell, C. Review of the anatase to rutile phase transformation. *Journal of Materials Science* **2011**, *46,* 855-874.

16 Isley, S. L., Jordan, D. S. and Penn, R. L. Titanium dioxide nanoparticles: Impact of increasing ionic strength during synthesis, reflux, and hydrothermal aging. *Materials Research Bulletin* **2009**, *44,* 119-125.

17 Gilbert, B., Ono, R. K., Ching, K. A. and Kim, C. S. The effects of nanoparticle aggregation processes on aggregate structure and metal uptake. *Journal of Colloid and Interface Science* **2009**, *339,* 285-295.

18 Huang, F., Gilbert, B., Zhang, H. and Banfield, J. F. Reversible, Surface-controlled structure transformation in nanoparticles induced by an aggregation state. *Physical Review Letters* **2004**, *92,* 155501.

19 Isley, S. L. and Penn, R. L. Relative brookite and anatase content in sol-gel synthesized titanium dioxide nanoparticles. *The Journal of Physical Chemistry B* **2006**, *110,* 15134-15139.

20 Rietveld, H. A profile refinement method for nuclear and magnetic structures. *Journal of Applied Crystallography* **1969**, *2,* 65-71.

21 Scherrer, P. Estimation of the size and internal structure of colloidal particles by means of röntgen. Nachrichten von der Gesellschaft der Wissenschaften zu Göttingen, Mathematisch-Physikalische Klasse **1918**, *2,* 96-100.

22 Penn, R. L. and Banfield, J. F. Oriented attachment and growth, twinning, polytypism, and formation of metastable phases; insights from nanocrystalline TiO_2. *American Mineralogist* **1998**, *83,* 1077-1082.

23 Lu, K. Nanocrystalline metals crystallized from amorphous solids: nanocrystallization, structure, and properties. *Materials Science and Engineering: R: Reports* **1996**, *16,* 161-221.

24 Yin, S., Huang, F., Zhang, J., Zheng, J. and Lin, Z. The effects of particle concentration and surface charge on the oriented attachment growth kinetics of CdTe nanocrystals in H_2O. *The Journal of Physical Chemistry C* **2011**, *115,* 10357-10364.

25 Burrows, N. D., Hale, C. R. H. and Penn, R. L. Effect of ionic strength on the kinetics of crystal growth by oriented aggregation. *Crystal Growth & Design* **2012**, *12,* 4787-4797.

26 Huang, F., Zhang, H. and Banfield, J. F. Two-stage crystal-growth kinetics observed during hydrothermal coarsening of nanocrystalline ZnS. *Nano Letters* **2003**, *3,* 373-378.

27 Lee Penn, R., Tanaka, K. and Erbs, J. Size dependent kinetics of oriented aggregation. *Journal of Crystal Growth* **2007**, *309,* 97-102.

28 Ribeiro, C., Lee, E. J. H., Longo, E. and Leite, E. R. A kinetic model to describe nanocrystal growth by the oriented attachment mechanism. *ChemPhysChem* **2005**, *6,* 690-696.

29 Li, D., Nielsen, M. H., Lee, J. R. I., Frandsen, C., Banfield, J. F. and De Yoreo, J. J. Direction-specific interactions control crystal growth by oriented attachment. *Science* **2012**, *336,* 1014-1018.

Chapter 4: References

1 Scanlon, D. O., Dunnill, C. W., Buckeridge, J., Shevlin, S. A., Logsdail, A. J., Woodley, S. M., Catlow, C. R. A., Powell, M. J., Palgrave, R. G. and Parkin, I. P. Band alignment of rutile and anatase TiO_2. *Nature Materials* **2013**, *12,* 798-801.

2 Hurum, D. C., Agrios, A. G., Gray, K. A., Rajh, T. and Thurnauer, M. C. Explaining the enhanced photocatalytic activity of Degussa P25 mixed-phase TiO_2 using EPR. *The Journal of Physical Chemistry B* **2003**, *107,* 4545-4549.

3 Sabyrov, K., Burrows, N. D. and Penn, R. L. Size-dependent anatase to rutile phase transformation and particle growth. *Chemistry of Materials* **2012**, *25,* 1408-1415.

4 Sabyrov, K., Adamson, V. and Penn, R. L. Two-step phase transformation of anatase to rutile in aqueous suspension. *CrystEngComm* **2014**, *16,* 1488-1495.

5 Zhang, H. and Banfield, J. F. Phase transformation of nanocrystalline anatase-to-rutile via combined interface and surface nucleation. *Journal of Materials Research* **2000**, *15,* 437-448.

6 Huang, F., Zhang, H. and Banfield, J. F. Two-stage crystal-growth kinetics observed during hydrothermal coarsening of nanocrystalline ZnS. *Nano Letters* **2003**, *3,* 373-378.

7 Zhang, H. and Banfield, J. F. New kinetic model for the nanocrystalline anatase-to-rutile transformation revealing rate dependence on number of particles. *American Mineralogist* **1999**, *84,* 528-535.

8 Zhang, H. and Banfield, J. F. Size dependence of the kinetic rate constant for phase transformation in TiO_2 nanoparticles. *Chemistry of Materials* **2005**, *17,* 3421-3425.

9 Penn, R. L. and Banfield, J. F. Formation of rutile nuclei at anatase (112) twin interfaces and the phase transformation mechanism in nanocrystalline titania. *American Mineralogist* **1999**, *84,* 871-876.

10 Scherrer, P. Estimation of the size and internal structure of colloidal particles by means of röntgen. *Nachr. Ges. Wiss. Göttingen* **1918**, *2,* 96-100.

11 Gilbert, B., Zhang, H., Huang, F., Finnegan, M. P., Waychunas, G. A. and Banfield, J. F. Special phase transformation and crystal growth pathways observed in nanoparticles. *Geochemical Transactions* **2003**, *4,* 20-27.

12 Burrows, N. D., Hale, C. R. H. and Penn, R. L. Effect of pH on the kinetics of crystal growth by oriented aggregation. *Crystal Growth & Design* **2013**, *13,* 3396-3403.

13 Burrows, N. D., Hale, C. R. H. and Penn, R. L. Effect of ionic strength on the kinetics of crystal growth by oriented aggregation. *Crystal Growth & Design* **2012**, *12,* 4787-4797.

14 Lee Penn, R., Tanaka, K. and Erbs, J. Size dependent kinetics of oriented aggregation. *Journal of Crystal Growth* **2007**, *309,* 97-102.

15 Penn, R. L. and Banfield, J. F. Imperfect oriented attachment: dislocation generation in defect-free nanocrystals. *Science* **1998**, *281,* 969-971.

16 Banfield, J. F., Welch, S. A., Zhang, H., Ebert, T. T. and Penn, R. L. Aggregation-based crystal growth and microstructure development in natural iron oxyhydroxide biomineralization products. *Science* **2000**, *289,* 751-754.

Chapter 5: References

1 Ranade, M., Navrotsky, A., Zhang, H., Banfield, J., Elder, S., Zaban, A., Borse, P., Kulkarni, S., Doran, G. and Whitfield, H. Energetics of nanocrystalline TiO_2. *Proceedings of the National Academy of Sciences* **2002**, *99,* 6476-6481.

2 Zhang, H. and Banfield, J. F. Understanding polymorphic phase transformation behavior during growth of nanocrystalline aggregates: insights from TiO_2. *The Journal of Physical Chemistry B* **2000**, *104,* 3481-3487.

3 Sabyrov, K., Adamson, V. and Penn, R. L. Two-step phase transformation of anatase to rutile in aqueous suspension. *CrystEngComm* **2014**, *16,* 1488-1495.

4 Voorhees, P. W. The theory of Ostwald ripening. *Journal of Statistical Physics* **1985**, *38,* 231-252.

5 Zhang, H. and Banfield, J. F. Size dependence of the kinetic rate constant for phase transformation in TiO_2 nanoparticles. *Chemistry of Materials* **2005**, *17,* 3421-3425.

6 Gribb, A. A. and Banfield, J. F. Particle size effects on transformation kinetics and phase stability in nanocrystalline TiO_2. *American Mineralogist* **1997**, *82,* 717-728.

7 Sabyrov, K., Burrows, N. D. and Penn, R. L. Size-dependent anatase to rutile phase transformation and particle growth. *Chemistry of Materials* **2012**, *25,* 1408-1415.

8 Penn, R. L. and Banfield, J. F. Formation of rutile nuclei at anatase {112} twin interfaces and the phase transformation mechanism in nanocrystalline titania. *American Mineralogist* **1999**, *84,* 871-876.

9 Penn, R. L. and Banfield, J. F. Oriented attachment and growth, twinning, polytypism, and formation of metastable phases: Insights from nanocrystalline TiO_2. *American Mineralogist* **1998**, *83,* 1077-1082.

10 Yuwono, V. M., Burrows, N. D., Soltis, J. A. and Penn, R. L. Oriented aggregation: formation and transformation of mesocrystal intermediates revealed. *Journal of the American Chemical Society* **2010**, *132,* 2163-2165.

11 Yuwono, V. M., Burrows, N. D., Soltis, J. A., Do, T. A. and Penn, R. L. Aggregation of ferrihydrite nanoparticles in aqueous systems. *Faraday Discussions* **2012**, *159,* 235-245.

12 Isley, S. L. and Penn, R. L. Titanium dioxide nanoparticles: effect of sol-gel pH on phase composition, particle size, and particle growth mechanism. *The Journal of Physical Chemistry C* **2008**, *112,* 4469-4474.

13 Scherrer, P. Estimation of the size and internal structure of colloidal particles by means of röntgen. *Nachr. Ges. Wiss. Göttingen* **1918**, *2,* 96-100.

14 Dunphy Guzman, K. A., Finnegan, M. P. and Banfield, J. F. Influence of surface potential on aggregation and transport of titania nanoparticles. *Environmental Science & Technology* **2006**, *40,* 7688-7693.

15 French, R. A., Jacobson, A. R., Kim, B., Isley, S. L., Penn, R. L. and Baveye, P. C. Influence of ionic strength, pH, and cation valence on aggregation kinetics of titanium dioxide nanoparticles. *Environmental Science & Technology* **2009**, *43,* 1354-1359.

16 Penn, R. L. and Soltis, J. A. Characterizing crystal growth by oriented aggregation. *CrystEngComm* **2014**, *16,* 1409-1418.

17 Burleson, D. J. and Penn, R. L. Two-step growth of goethite from ferrihydrite. *Langmuir* **2005**, *22,* 402-409.

18 Li, D., Soberanis, F., Fu, J., Hou, W., Wu, J. and Kisailus, D. Growth mechanism of highly branched titanium dioxide nanowires via oriented attachment. *Crystal Growth & Design* **2013**, *13,* 422-428.

19 Frandsen, C., Legg, B. A., Comolli, L. R., Zhang, H., Gilbert, B., Johnson, E. and Banfield, J. F. Aggregation-induced growth and transformation of β-FeOOH nanorods to micron-sized α-Fe_2O_3 spindles. *CrystEngComm* **2014**, *16,* 1451-1458.

Appendices

Appendix A: Chapter 3 supporting information

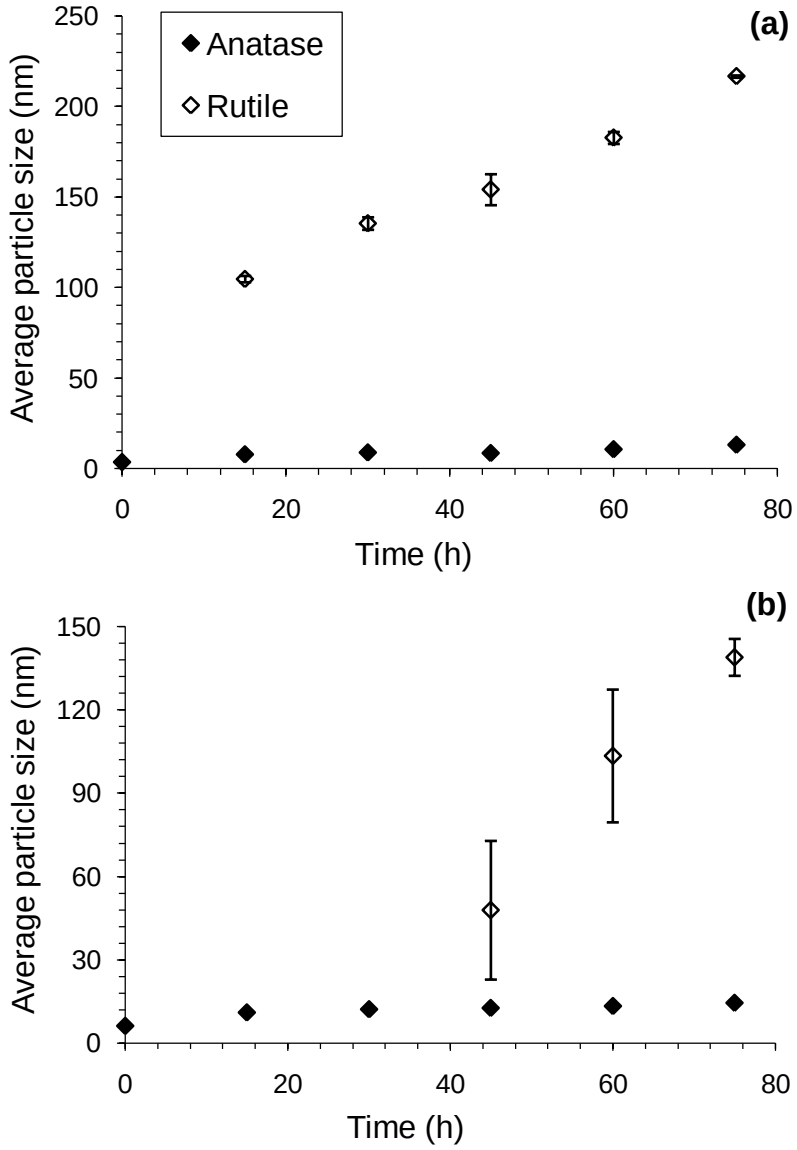

Figure A.1 Plots showing average anatase and rutile sizes as a function of aging time for the samples initially containing 3.7 nm (a) and 6.0 nm (b) anatase. The

sizes were determined by XRD peak broadening analysis using Scherrer equation.

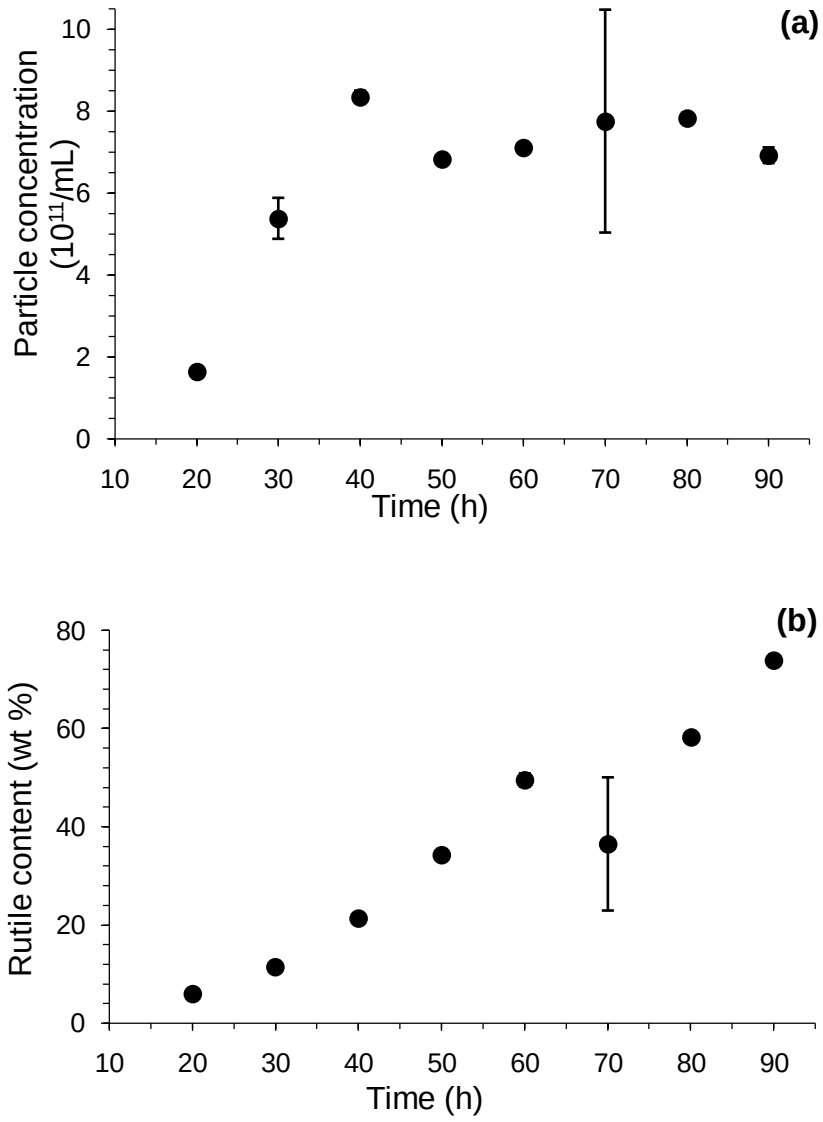

Figure A.2 Plots showing number of rutile nanocrystals per mL of suspension (a) and rutile content (b) as a function of aging time for the sample initially containing 3.7 nm anatase. It should be noted that the calculated rutile number concentration is a rough estimate as it was calculated assuming rutile nanocrystals as spheres even though different shaped rutile nanocrystals were observed, including rod-shaped ones.

Appendix B: Chapter 4 supporting information

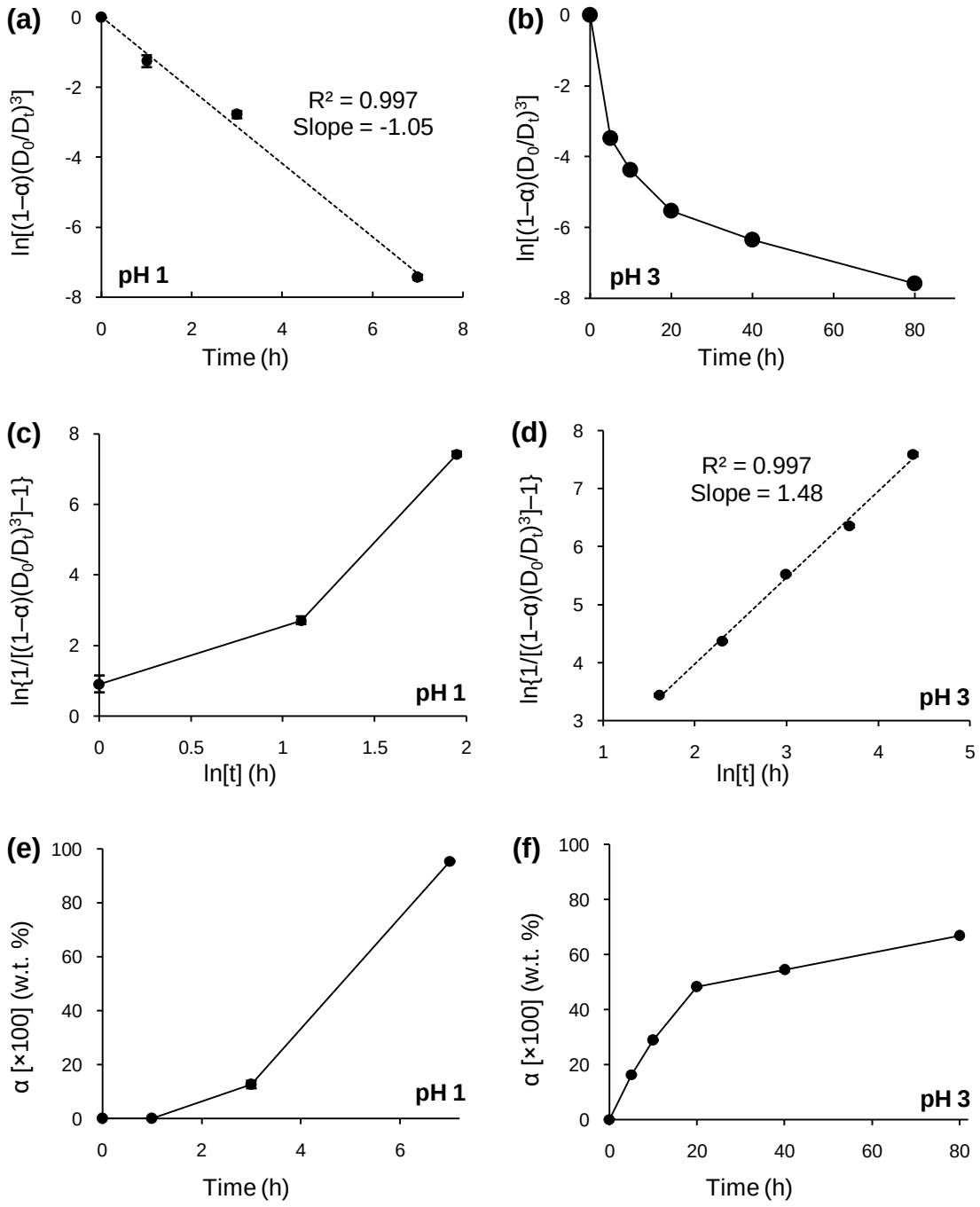

Figure B.1 Anatase to rutile phase transformation data were fitted with DP (a, b) and IN (c, d) models at 250 °C and pH 1, 3. (e, f) presents the corresponding weight percentage transformation as a function of aging time at pH 1 and 3. The

dashed lines represent the linear regression fit of the equations on the experimental data, whereas the black connecting lines help guide the eye.

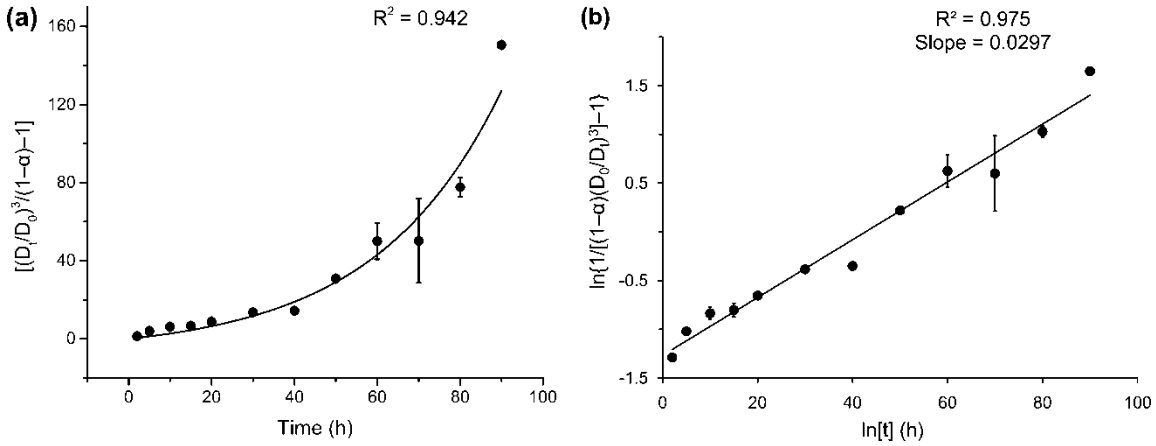

Figure B.2 Plots presenting the application of combined kinetic model on anatase to rutile phase transformation at 200 °C and pH 1. Non-linear (a) and linear (b) regression curve fit performed on the experimental data using Equations 5 and 4, respectively. R^2 values are shown to indicate how well the data points fitted the equations.